# A NITRIDE-BASED REACTION FOR THE FORMATION OF A THREE-PHASE MOLYDENUM–SILICON-BORON INTERMETALLIC ALLOY

A Thesis
Presented to
The Academic Faculty

By

Michael R. Middlemas

In Partial Fulfillment
Of the Requirements of the Degree
Master of Science in the
School of Materials Science and Engineering

Georgia Institute of Technology
August 2005

A NITRIDE-BASED REACTION FOR THE FORMATION OF A THREE-PHASE MOLYDENUM–SILICON-BORON INTERMETALLIC ALLOY

Approved by:

Dr. Joe K. Cochran, Advisor
School of Materials Science and Engineering
*Georgia Institute of Technology*

Dr. Thomas H. Sanders
School of Materials Science and Engineering
*Georgia Institute of Technology*

Dr. Ken H. Sandhage
School of Materials Science and Engineering
*Georgia Institute of Technology*

Date Approved: July 18, 2005

ACKNOWLEDGEMENTS

I would first like to thank my thesis committee members Dr. Sanders and Dr. Sandhage. I would also like to thank all the people who helped me with experimental setup and advice, especially Jim Lee, Richard Schaeffer and Tammy McCoy. I am especially grateful to my advisor Dr. Cochran for all the help and advice he has given throughout this project. It has been a pleasure working with him and I am looking forward to continuing onto my doctorate with him.

TABLE OF CONTENTS

LIST OF TABLES

LIST OF FIGURES

## SUMMARY

Mo-Si-B alloys may have the fracture toughness and high-temperature oxidation resistance required for use as jet turbine engine blades. Mo-3Si-1B (wt%) forms a three-phase mixture of $\alpha$-$Mo_{ss}$, A15 ($Mo_3Si$) and T2 ($Mo_5SiB_2$). It has been observed that at high-temperature, A15 and T2 form a protective borosilicate glass layer preventing oxidation of the otherwise easily oxidized molybdenum. In order to achieve the proper combination of mechanical and thermal properties, the material must have a continuous molybdenum matrix with a fine dispersion of intermetallics to produce a consistent protective layer. Previous research has focused on melt-based processing and sintering of pre-alloyed powders. These methods produce undesirable microstructures that cannot be improved by annealing due to slow kinetics.

In this research project, reactive sintering of molybdenum, $Si_3N_4$ and BN powders was used to create a semi-continuous molybdenum matrix with a fine dispersion of the A15 and T2 intermetallics. Sintering of the materials was further enhanced by the use of submicron-sized reactants. Commercially available powders and simple experimental methods such as ball milling and spray drying were used, making the process applicable to large scale production.

X-ray diffraction analysis was used to study the reactions that form the desired phases. It was determined that formation of the A15 intermetallic phases begins as low as 1200ºC and formation of T2 begins at 1300ºC. The reactions are complete by 1400ºC.

The XRD experiments show this process is reproducible and does not produce any unexpected phases.

A variety of starting material grades and processing methods were explored. Samples with bulk densities as high as 95% of theoretical were produced. Scanning electron microscopy was used to study the dispersion of the intermetallic phases. The micrographs show dispersed intermetallics in a semi-continuous molybdenum matrix with grain sizes on the order of 1-4μm. It was found that by varying parameters such as mixing method and heating rates, it is possible to engineer the final microstructure, changing the level of dispersion of the intermetallics and continuity of the matrix.

# CHAPTER I

## INTRODUCTION

Much research has been conducted to raise the operating temperature of turbine engines in order to increase engine performance. The power output and efficiency of jet engines are determined by the rotor inlet temperature of the turbine.[1] Modern jet engine turbine blade technology is based on the nickel superalloy materials developed in the 1950's. These alloys have allowed for much advancement in jet engine performance due their high temperature mechanical properties. Current jet turbine engines expose superalloys to their maximum operating temperature, nearing 1150ºC, but by utilizing technologies such as thermal barrier coatings and elaborate cooling schemes, the rotor inlet temperature for the engines can be pushed as high as 1500ºC.[2] More horsepower could be gained by running the engines even hotter, but as more elaborate systems are employed to cool the superalloy airfoils, the efficiency of the engines decreases. In order for continued advancement of jet turbine engine technology, there is a need for new, higher temperature structural materials.

Mo-Si-B intermetallic alloys have the potential of possessing both the oxidation resistance and fracture toughness required to meet the strict requirements for turbine blades. These alloys gain their oxidation resistance from a borosilicate surface scale formed by the oxidation of silicon and boron. The area of interest in this project is the alloy P&W which has a composition of Mo-3Si-1B (wt%). This alloy forms a three-

phase mixture of $Mo_{ss}$ and the intermetallics A15 ($Mo_3Si$) and T2 ($Mo_5SiB_2$). In order to achieve the necessary fracture toughness and oxidation resistance, the intermetallic phases must be present as fine dispersoids in a continuous molybdenum matrix. Previous research has focused mainly on melt casting and sintering of pre-alloyed powders. These methods produce coarse grained microstructures with discontinuous molybdenum dispersions.

In a new process developed at the Georgia Institute of Technology, synthesis of A15 and T2 as fine, uniform dispersoids in a semi-continuous $\alpha$-Mo matrix was achieved using powder metallurgical methods. In this process, $Si_3N_4$ and BN are used as silicon and boron precursors. Reaction of molybdenum and the nitride powders to form the desired phases was confirmed using x-ray diffraction analysis. This method is able to produce alloys of near theoretical density with a fine grain structure on the order of 1-4μm. While no testing of physical properties was completed, with further refinement, this process appears capable of producing Mo-Si-B intermetallic alloys with the properties required for the next generation of turbine blades.

This thesis begins with a review of previous research in the Mo-Si-B field. The new proposed reaction synthesis method and the potential reaction sequences are discussed. The experimental chapter details the materials selected and the processes used to prepare, sinter and characterize the samples. In the results and discussion section, the phase content, densities and microstructures are evaluated for samples prepared from different starting material grades and preparation methods. The microstructures of the samples produced in this project are also compared to those from other researchers. Finally conclusions and recommendations for further research will be made.

# CHAPTER II

# LITERATURE SURVEY

The relevant literature pertaining to Mo-Si-B alloys research is reviewed in this chapter. The properties of these alloys, the evolution of this field and the results of past research are discussed. The next section provides evidence that the proposed reaction of molybdenum, $Si_3N_4$ and BN is a viable method for the formation of the A15 and T2 intermetallic phases. The project plan and possible reaction sequences are also introduced.

## 2.1 Molybdenum Silicides Background

Efforts have been focused on finding new high-temperature structural materials. One area of interest has been refractory metals, due to their high melting points and excellent mechanical properties above 1000ºC. One material which has received much attention is molybdenum. With a melting point of 2617ºC, molybdenum shows very little creep below 1400ºC. In addition, it has a high hardness and a density close to that of nickel superalloys. While the mechanical and physical properties of molybdenum are well suited for high temperature applications, its environmental properties are not. In high-temperature oxidizing environments, molybdenum undergoes catastrophic failure due to rapid oxidation of the material. Molybdenum oxide becomes volatile at temperatures as low as 760ºC. Unlike oxide layers of silicon and aluminum, $MoO_3$ forms no barrier against further oxidation.

While molybdenum itself performs poorly in oxidizing environments, intermetallic compounds of molybdenum and silicon have long been known for their excellent oxidation resistance. $MoSi_2$ is commonly used for heating elements able to withstand continuous use in air up to 1700ºC. The oxidation resistance of this material stems from the formation of a protective $SiO_2$ surface scale. Upon heating, molybdenum and silicon are oxidized. The $MoO_3$ evaporates and the $SiO_2$ left behind flows together, creating a continuous passivating layer.[3] After this initial stage, further oxidation of the material is limited by atomic scale diffusion of oxygen through the protective glass layer. Unlike applied environmental coatings, this layer is self healing. When the surface of the material is damaged, the underlying silicon from the bulk material oxidizes, thus repairing the coating. While the oxidation properties of $MoSi_2$ are excellent, it is brittle at low temperatures and has high creep rates at high temperatures. Fracture toughness has been improved by creating $Si_3N_4$ or SiC composites with the material, but the mechanical properties are still not suitable high temperature structural materials.[4]

Other intermetallics in the Mo-Si binary system have been studied extensively as alternatives for $MoSi_2$. Because of its more complicated crystal structure, $Mo_5Si_3$ (T1) has creep rates an order of magnitude lower than $MoSi_2$, but has poor oxidation resistance by comparison. Akinc and Meyer found that small additions of boron (1-3wt%) increase the oxidation resistance of $Mo_5Si_3$ up to five orders of magnitude, bringing it close to that of $MoSi_2$.[5] In their experiments, doping the T1 phase with 1.24wt% boron reduced the oxide scale thickness from several hundred microns to less than 10μm. Boron addition improves the system by creating a borosilicate glass which is more oxidation resistant and by lowering the viscosity of the glass, allowing for better surface coverage.

The Mo-Si-B ternary phase diagram was developed by Nowotny in 1957. The 1600ºC isothermal section of diagram is shown in Figure 2.1. The three elements form a number of intermetallics with melting points above 2000ºC, including the molybdenum solid solution. The regions of the phase diagrams are relatively stable through cooling and the deep eutectics commonly found with Si and B intermetallics are not present in this system.[6] While this stability lends itself to long term use in high temperature conditions, it makes it difficult to optimize the microstructure. Without precipitation reactions and phase transformations, there is little opportunity to modify the microstructure of a material. In addition, the slow diffusion rates ($D<10^{-16}$ $m^2/s$) which give the material its creep resistance and high temperature stability make annealing of the microstructure difficult. Perepezko likens this system to ceramics in that the final microstructure of the material is highly dependent on its initial forming methods.

2.1.1 A15-T1-T2 Phase Region

Work in the Mo-Si-B system has been focused primarily in two regions of the phase diagram. Akinc and Meyer's research has been centered on the $Mo_5Si_3$ (T1)-$Mo_5SiB_2$ (T2)-$Mo_3Si$ (A15) region of the phase diagram. Materials in this region form a three-phase intermetallic mixture. Ingots of these materials are typically formed by arc melting of the pure elements. They have been shown to have steady state oxidation rates as low as $5.0*10^{-5}$ $mg/(cm^2h)$. While the three intermetallics in this system offer better mechanical properties and creep resistance than $MoSi_2$, low temperature brittleness still makes these materials poor candidates for the high stress environment of turbine engine blades.

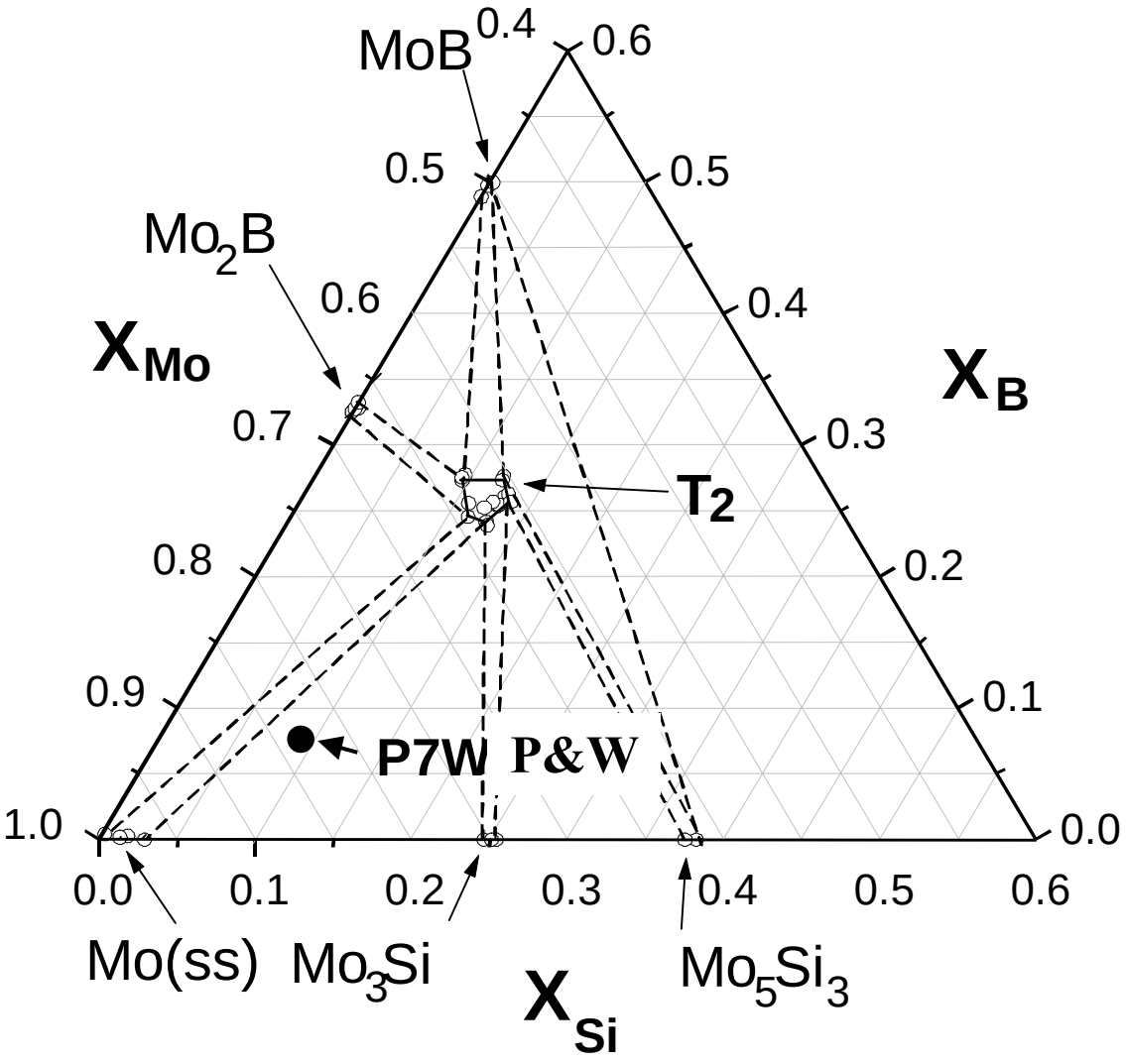


Figure 2.1: Isothermal section of the Mo-rich portion of Mo-Si-B phase diagram at 1600 °C.[1]

### 2.1.2 $Mo_{ss}$-A15-T2 Phase Region

The alloy of interest for this project is a composition called P&W which is made up of Mo-3Si-1B (wt%) or Mo-8.9Si-7.7B (at%). This alloy lies in the region of the phase diagram containing $Mo_{ss}$ and the intermetallics A15 ($Mo_3Si$) and T2 ($Mo_5SiB_2$). The crystal structures of the constituent phases are listed in Table 2.1 and shown in Figure 2.2. The coefficients of thermal expansion (CTE) of the three materials are similar, preventing stresses from thermal shock[7,8]. Using the lever rule, Jéhanno et al. calculated the phase content of this composition to be 55% $Mo_{ss}$, 15% $Mo_3Si$ and 30% T2 by volume with a theoretical density (TD) of 9.62 g/cc.[9] Their calculated theoretical density incorporates some error as they assumed pure, stoichiometric phases. Molybdenum is known to form a solid solution with 3at% silicon. Also, the chemical formula of T2 is not stoichiometric due to boron substitution at the silicon site and has been determined to be $Mo_5Si_{0.89}B_{2.11}$.[10] For the purposes of this project, the theoretical density will be assumed to be 9.6g/cc.

Research on this portion of the phase diagram was pioneered by Berczik who holds patents on compositions of molybdenum with of 1.6-15.2 at% Si and 0.0-39.4 at% B.[11,12] The fracture toughness of the alloys in this composition range is improved by the presence of the ductile molybdenum phase. Many of these alloys have been produced by melt casting methods. Electron backscatter images of as-cast alloys developed by Nunes et al. are shown in Figure 2.3. Due to its higher average atomic number, molybdenum appears lighter than the intermetallic phases. The micrographs show that liquid phase fabrication (arc melting) of this system results in coarse segregation of non-equilibrium phases. Even by annealing, these alloys cannot be homogenized into a fine grained, equilibrium microstructure. This is evident in Figure 2.4 which shows the microstructure of cast alloys which have been annealed for 24 hours at 1600ºC. The resulting microstructures are typically a matrix of

Table 2.1: Mo-A15-T2 crystal structure data. [7,8,]

| Phase | Mo | A15 | T2 |
|---|---|---|---|
| **Crystal Structure** | BCC | Cubic | Tetragonal |
| **Lattice Parameters (Å) - a** | 3.1453 | 4.893 | 6.029 |
| **c** | | | 11.079 |
| **Theoretical Density (g/cc)** | 10.27 | 8.98 | 8.76 |
| **CTE (10-6/°C) - a** | 6 | 7.17 ± 0.46 | 7.9 ± 0.1 |
| **c** | | | 7.5 ± 0.2 |

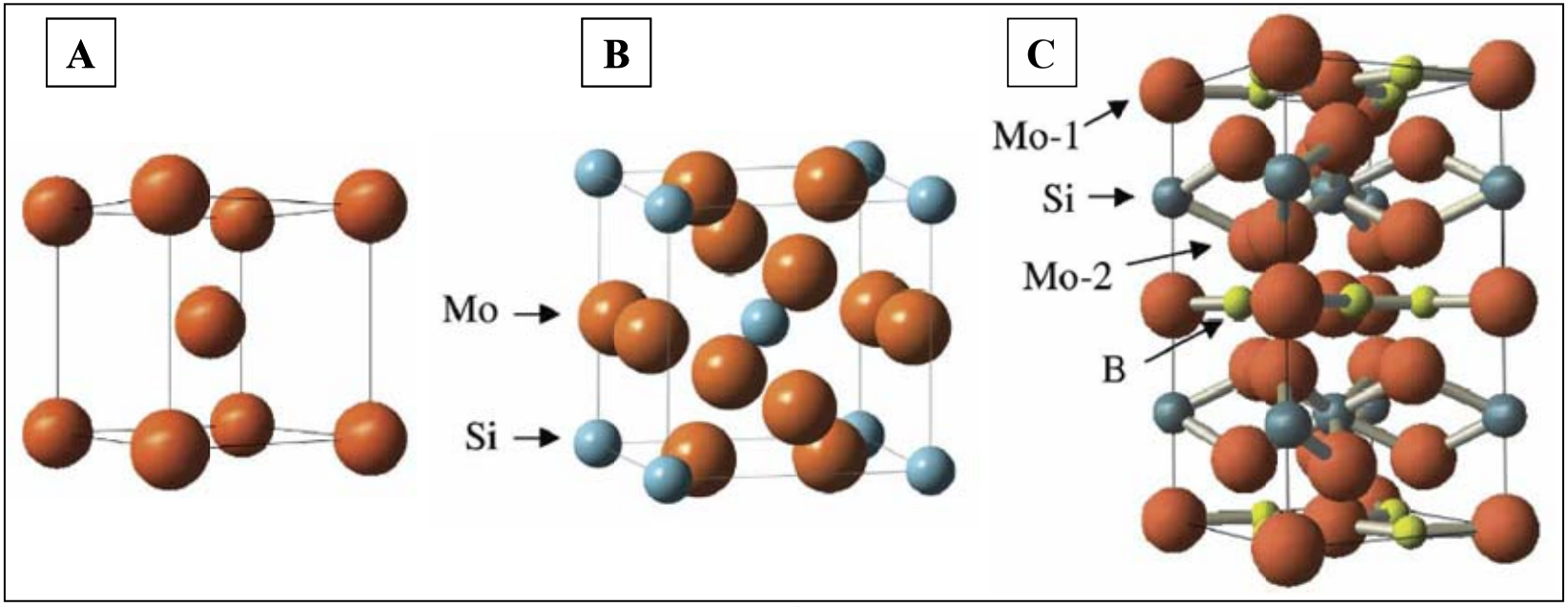


Figure 2.2: Crystal structures of Mo (A), A15 (B) and T2 (C).[1]

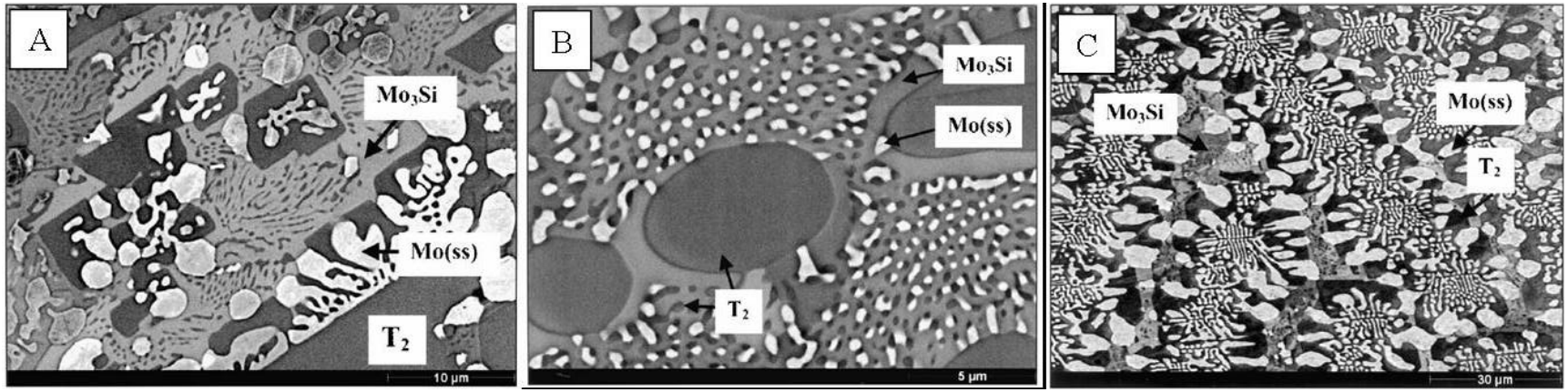


Figure 2.3: BS images of as-cast alloys: (A) Mo-16Si-12B, (B) Mo-13Si-15B and (C) Mo-9.6Si-14.2B (at%).[6]



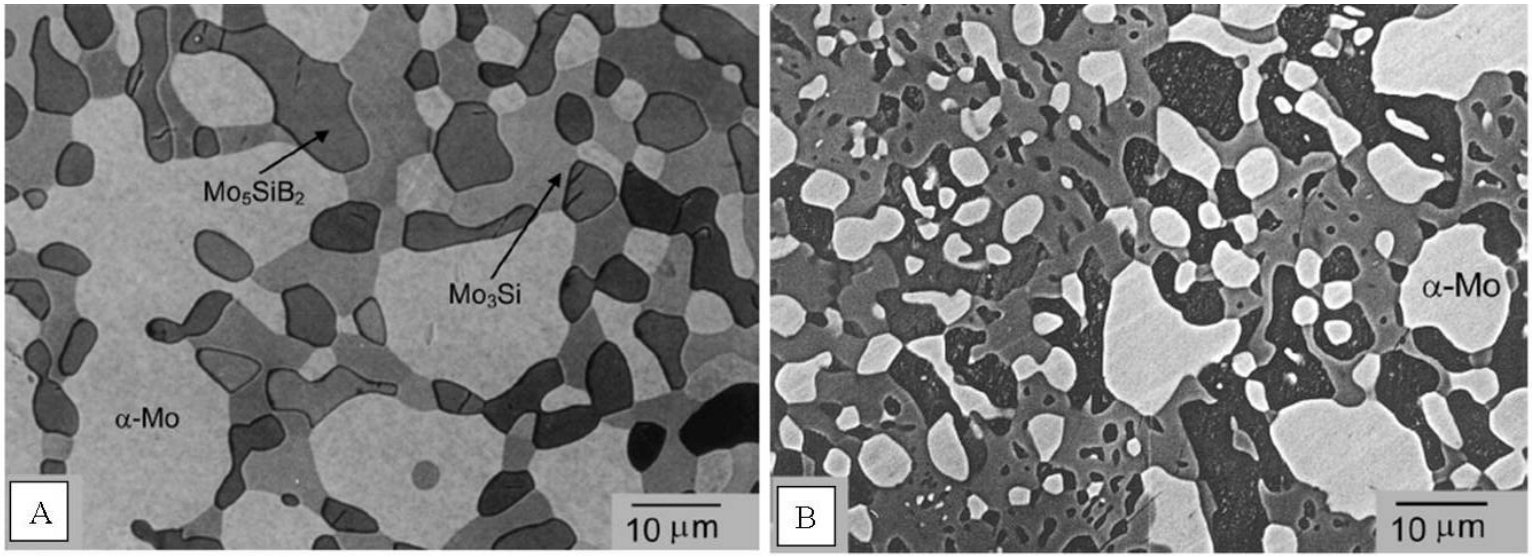


Figure 2.4: BS images of cast and annealed alloys: (A) Mo-12Si-8.5B and (B) Mo-12Si-10Nb-8.5B (at%).[13]

intermetallic phases with dispersed molybdenum grains. The toughness of these materials comes from ductile phase toughening.

While the presence of isolated molybdenum particles helps improve the fracture toughness of the material, for significant improvement Berczik concluded that these alloys need to be processed in such a way that molybdenum is present as a continuous network. In his patents, two possible paths for achieve this microstructure are suggested: "1) blending molybdenum powder with either a prealloyed intermetallic powder (such as molybdenum borosilicide) or boron and silicon powder, followed by consolidating the powder at a temperature below the melting temperature of the alloy; or 2) rapidly solidifying a melt containing molybdenum, silicon and boron, followed by consolidating the rapidly solidified material at a temperature below the melting temperature."

The methods suggested by Berczik have been demonstrated by a number of researchers. Figure 2.5 shows the microstructure of a material prepared by Jéhanno et al. In their method, a Mo-Si-B alloy prepared by arc melting and casting was formed into a powder by inert gas atomization. The powder was then sintered using a Hot Isostatic Press (HIP). Choe, et al. have prepared alloys in a similar manner.[13] A cast alloy was crushed into a powder which was then consolidated by HIPing. In an attempt to produce an intermetallic alloy with a continuous molybdenum matrix, a mixture of the alloyed powder and pure molybdenum powder was also HIPed. The resulting microstructures are shown in Figure 2.6. Examining the micrographs, it does not appear that these methods will produce microstructures with a continuous molybdenum matrix. Due to the connected intermetallic phases, these materials are likely to have low fracture toughness.

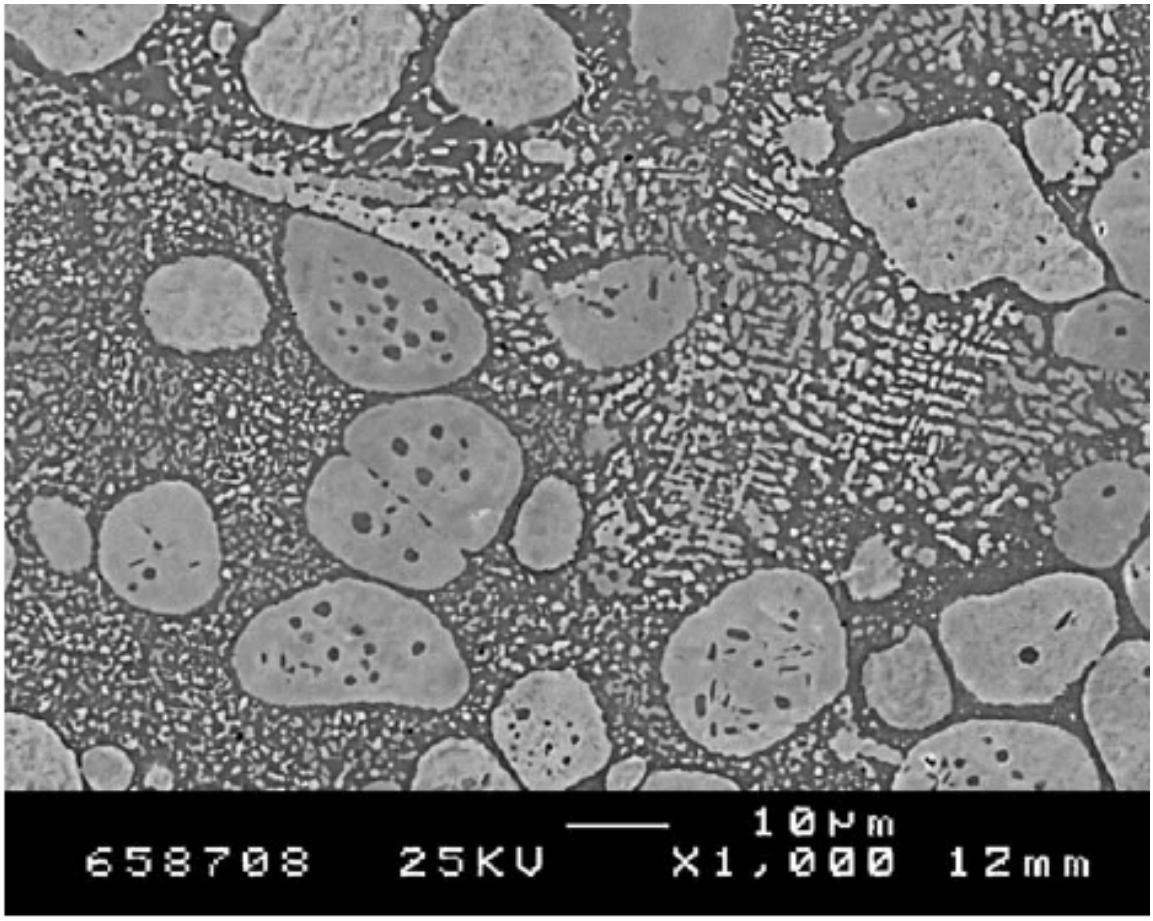


Figure 2.5: Pre-alloyed powder consolidated by HIPing - Mo-8.9Si-7.7B (at%).[9]

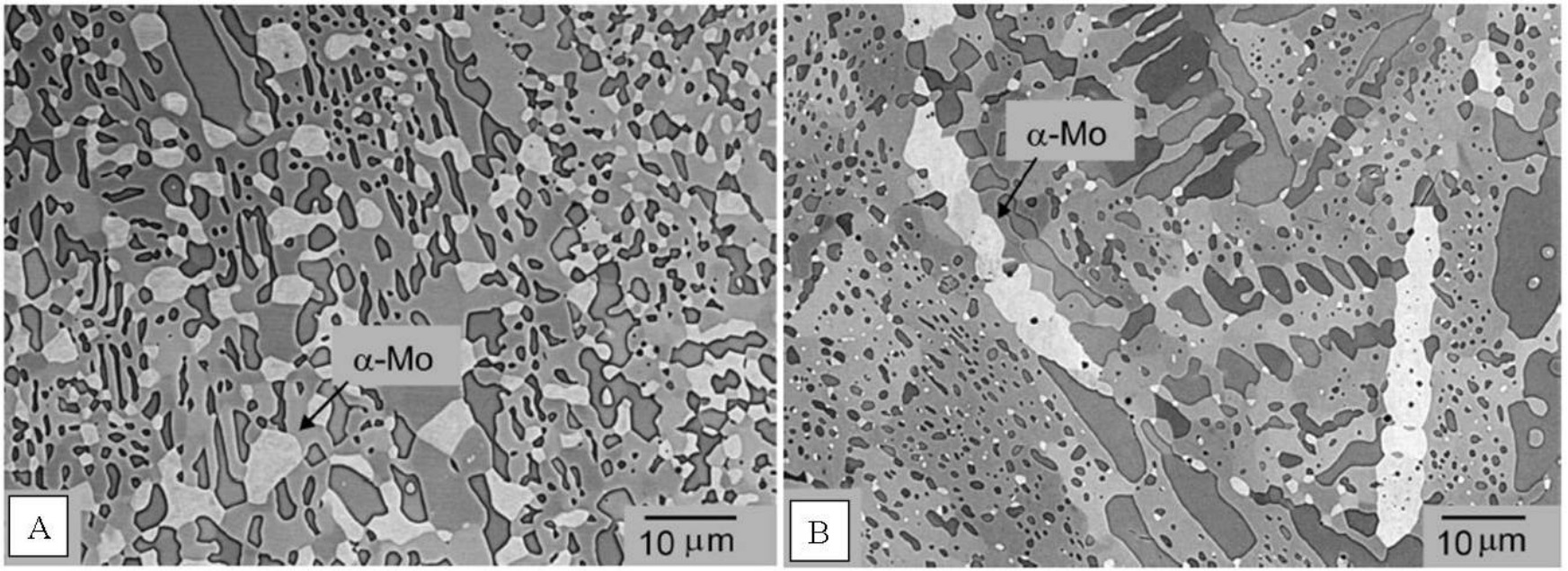


Figure 2.6: BS images of alloys processed by HIPing: (A) Mo-16.8Si-8.4B powders and (B) Mo-20Si-10B and Mo powders (at%).[13]

Schneibel et al. have developed powder metallurgy methods for producing Mo-A15-T2 alloys with a continuous molybdenum matrix.[14,15,16] In the first method, A15 and T2 formed by arc melting were crushed into powders. The intermetallic powders were then mixed with molybdenum powder and consolidated by hot isostatic pressing. The resulting microstructure is shown in Figure 2.7. In another technique, an intermetallic alloy produced by arc melting is crushed into a powder. Vacuum annealing is used to remove silicon from the surface of the powder particles, leaving a molybdenum metal surface layer. The annealed powder is then HIPed. The resulting microstructure, Figure 2.8, has a continuous molybdenum matrix with dispersed intermetallic particles. The fracture toughness of this material (with 49vol% molybdenum matrix) was been reported to be 21MPa√m. While these results bode well for being able to engineer a Mo-Si-B alloy with good mechanical properties, examining the microstructures, it does not appear that these materials would have adequate oxidation resistance. While no oxidation properties were reported, with grain sizes on the order of 100μm it is unlikely that the materials would form a continuous protective borosilicate layer. While these methods produce the desired Mo-matrix, they are not able to do so on a fine scale because the pre-alloyed materials were crushed to a coarse size of 50-230μm. The materials used in these procedures do not lend themselves to fine powder metallurgy because fine powders are prone to oxidation due to their large specific surface area. In the process of creating fine powder of silicon, boron or the molybdenum silicides, oxidation of the raw materials becomes a problem. Once formed, boron oxide and silicon oxide cannot be easily reduced and will be carried into the final microstructure.

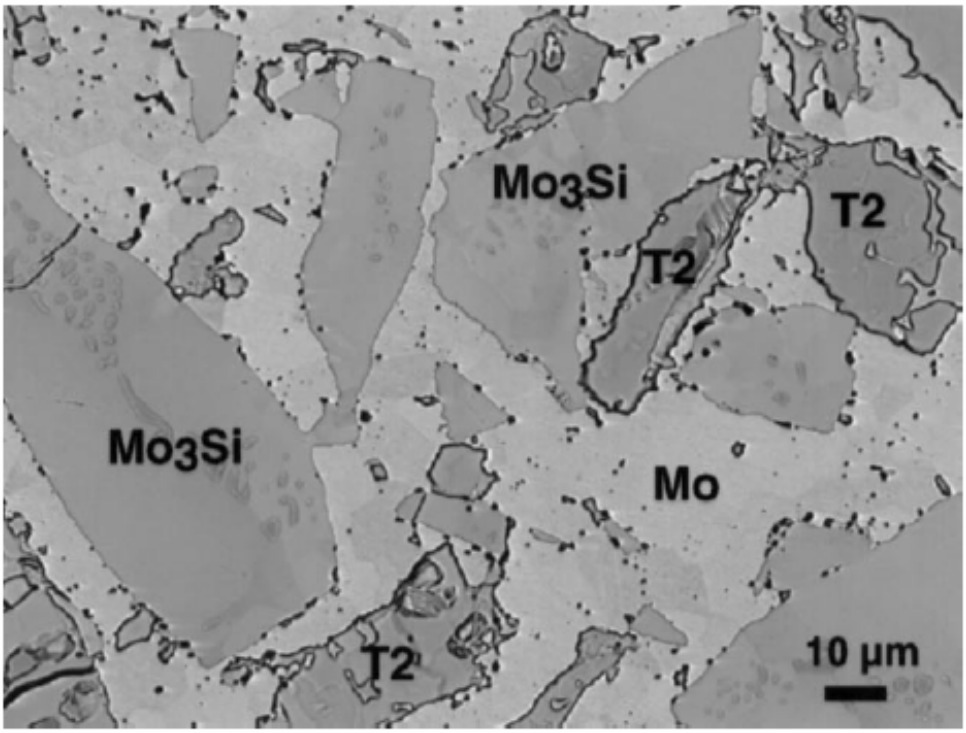

Figure 2.7: BS image of and alloy formed by HIPing Mo, A15 and T2 powders.[14]

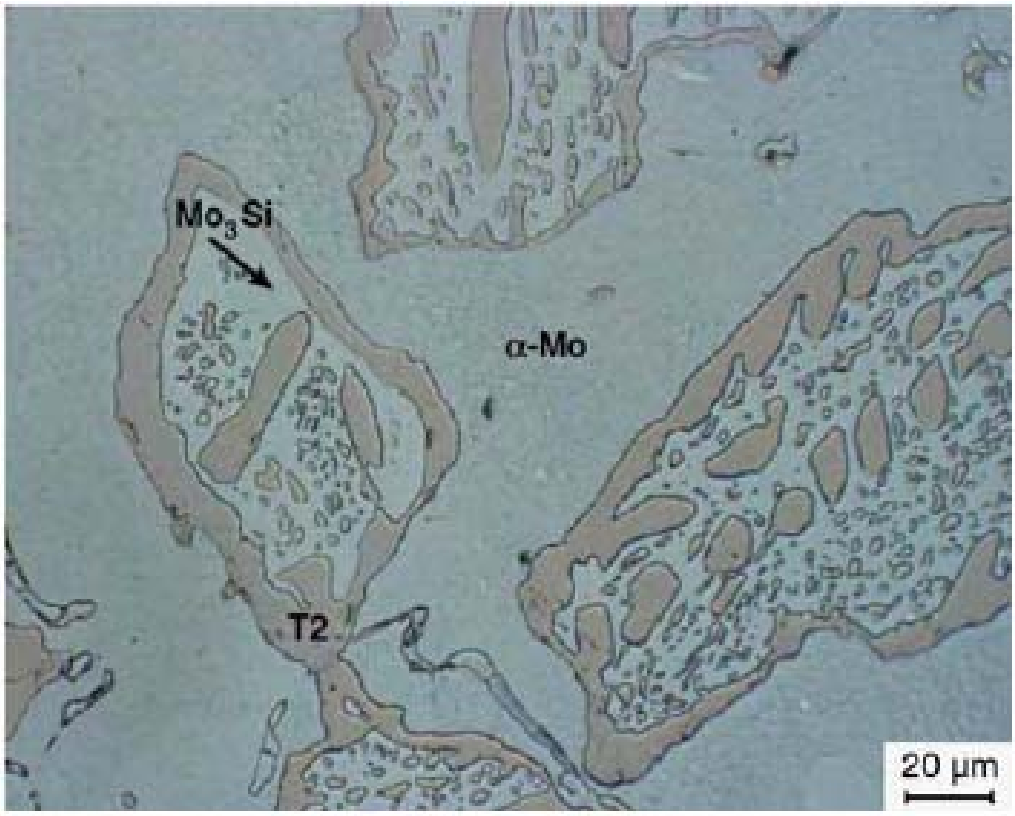

Figure 2.8: Optical image of an alloy formed by HIPing vacuum annealed powders.[16]

In a recent advancement Jéhanno et al. have demonstrated a continuous molybdenum matrix alloy with grain sizes of 10μm or less, as seen in Figure 2.9. This microstructure is formed by hot extrusion of the alloy shown in Figure 2.5. While many authors have reported on the mechanical properties of Mo-Si-B alloys, none of the research has been conducted on materials with the continuous Mo-matrix and fine grained microstructure necessary for both strength and oxidation resistance. Figures 2.10 and 2.11 compare the tensile strength and elongation to failure of this new alloy to that of the unextruded alloy, pure molybdenum and a Ni-based single crystal material. By changing the microstructure from an intermetallic matrix to a molybdenum matrix, the tensile strength is greatly improved and the ductile-to-brittle transition temperature decreases approximately 200ºC. While this is an improvement, below 1000ºC, the extruded alloy has near zero ductility. Although the low temperature properties of this material trail behind the Ni-based alloy, at 1000ºC the strength and ductility of the conventional single crystal material are crossed over by that of the extruded alloy. While the environmental properties of this material were not reported, the mechanical properties illustrate the promise of Mo-Si-B alloys for higher temperature turbine blade applications.

## 2.2 Proposed Nitride-Based Reaction Method

The main objective of this project is to investigate the viability of the synthesis and control of A15 and T2 phases as fine, uniform dispersoids in a continuous α-Mo matrix using powder metallurgical methods. This will be achieved by using raw materials with micron to submicron sized particles which are protected from atmospheric contamination by a temporary passivating agent. Covalent compounds of Si and B with nitrogen are very stable in oxidizing environment up to 1000ºC, allowing fine particle

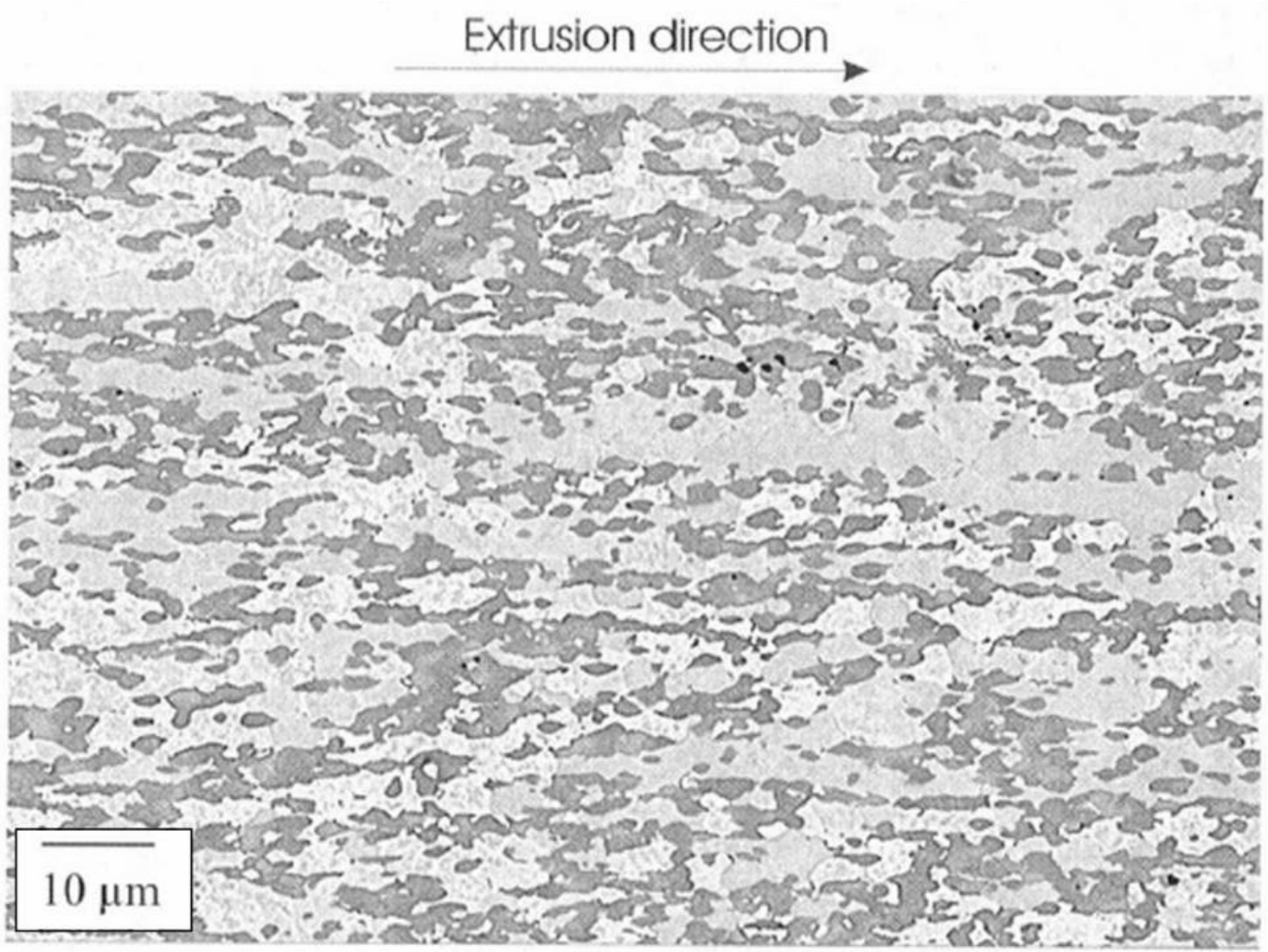


Figure 2.9: BS image of an alloy formed by HIPing of pre-alloyed powders followed by hot extrusion - Mo-8.9Si-7.7B (at%).[2]

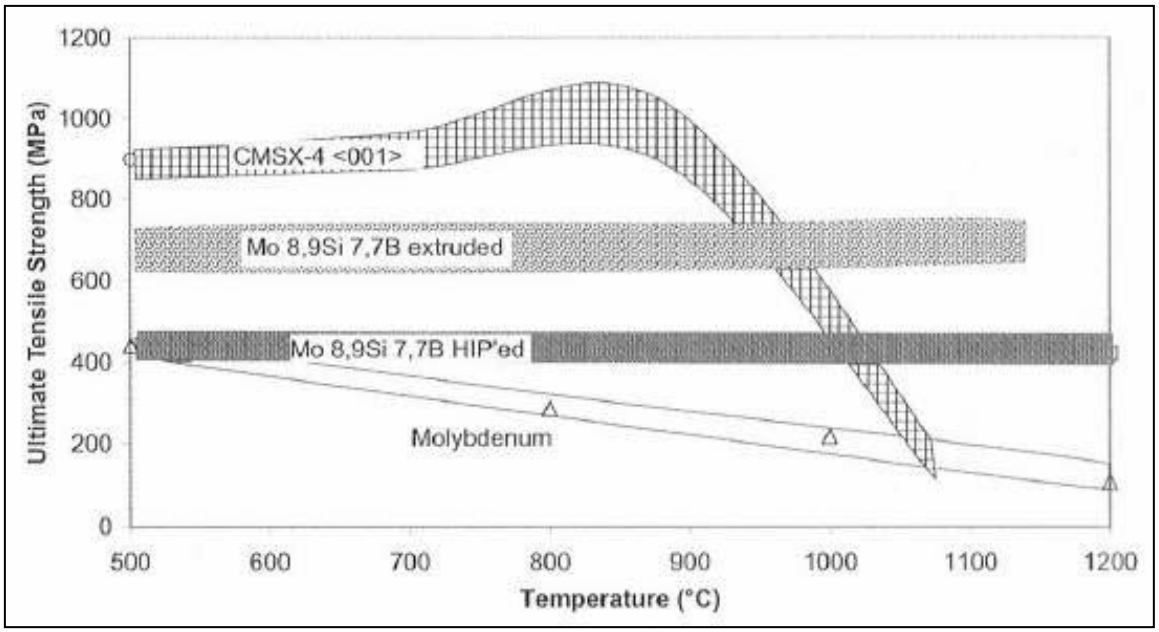


Figure 2.10: Tensile strength of Mo-alloys compared to Ni-based single crystals.[2]

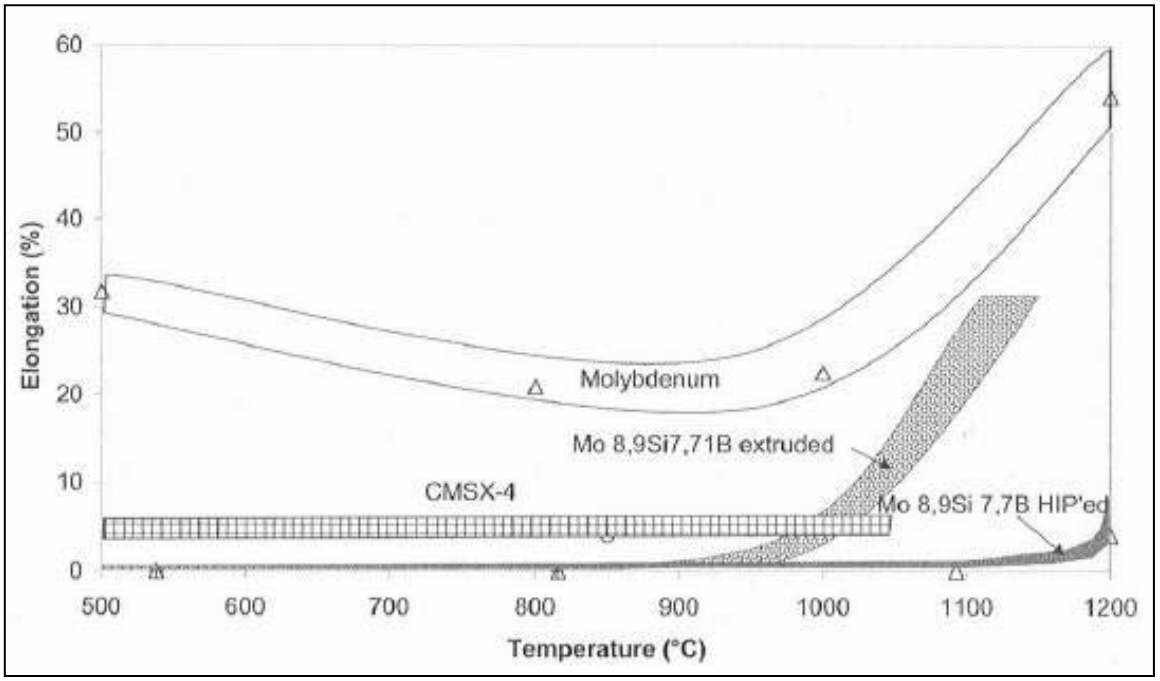


Figure 2.11: Elongation to rupture of Mo-alloys compared to Ni-based single crystals.[2]

processing without formation of silicon and boron oxides. In this process, $Si_3N_4$ and BN will be used as silicon and boron precursors. These nitrides are commercially available in fine powder sizes with low oxygen content. The molybdenum source will be from commercially available molybdenum and molybdenum oxide powders. Nitride powders mixed with either molybdenum or molybdenum oxide powders will be fired in a reducing atmosphere, reacting to form A15 and T2. $MoO_3$ is known to reduce at 700ºC, well below the temperature at which the nitrides will oxidize. For the $MoO_3$-based samples, reduction of the oxide will occur by the following reaction:

$$MoO_3 + 3H_2 \rightarrow Mo + 3H_2O \quad (1)$$

During reduction, the already fine $MoO_3$ will be converted into an even finer sized molybdenum powder.

The first goal of this project will be to demonstrate that this process is capable of producing the desired A15 and T2 intermetallic compounds. Molybdenum silicides are known to form at the interfaces of Mo-$Si_3N_4$ joints and Krishnarao et al. have used the reaction of molybdenum and $Si_3N_4$ to form $MoSi_2$ composites.[17,18] Both nitrides have high equilibrium nitrogen partial pressures and small free energies to promote formation of T2 and A15. The decomposition reactions of the nitrides are presented in Equations 2 and 3. The equilibrium nitrogen partial pressures can be calculated from Equations 4 and 5:

$$Si_3N_4 \rightarrow 3Si + 2N_2 \quad (2)$$

$$BN \rightarrow B + \tfrac{1}{2} N_2 \quad (3)$$

$$\Delta G_{Si_3N_4} = -RT \ln(P_{N_2}^{\ 2}) \quad (4)$$

$$\Delta G_{BN} = -RT \ln(P_{N_2}^{\ 1/2}) \quad (5)$$

The nitrogen partial pressures and Gibbs free energies at various temperatures are listed in Table 2.2 and plotted in Figures 2.12 and 2.13.

Table 2.2: Thermochemical data for $Si_3N_4$ and BN.[19,20]

| Temperature (°C) | $Si_3N_4$ | | BN | |
|---|---|---|---|---|
| | ΔG (kcal/mol) | $P_{eq}N_2$ (atm) | ΔG (kcal/mol) | $P_{eq}N_2$ (atm) |
| 1418 | 46.3 | 1.02E-03 | 25.1 | 3.00E-07 |
| 1523 | 34.6 | 7.80E-03 | 21.4 | 6.30E-06 |
| 1723 | 15.4 | 1.40E-01 | 15.1 | 4.40E-04 |
| 1886 | 0.0 | 1.00E+00 | 10.0 | 1.00E-02 |

Also of interest in this project will be the steps that occur to form these phases. The reactions between the starting materials are proposed to occur by two possible sequences, or a combination of both. In the first proposed sequence, upon heating to the 1600-1700ºC range decomposition of the nitrides will occur, leaving elemental Si and B to react with the molybdenum powder. The reaction to form the intermetallic phase T2 could occur in a number of ways. One possibility is that both silicides form by direct reactions:

$$3Mo + Si \rightarrow Mo_3Si \quad (6)$$

$$5Mo + Si + 2B \rightarrow Mo_5SiB_2 \quad (7)$$

The reaction to form T2 could also occur by a stepped reaction:

$$3Mo + Si \rightarrow Mo_3Si \quad (8)$$

$$2Mo + Mo_3Si + 2B \rightarrow Mo_5SiB_2 \quad (9)$$

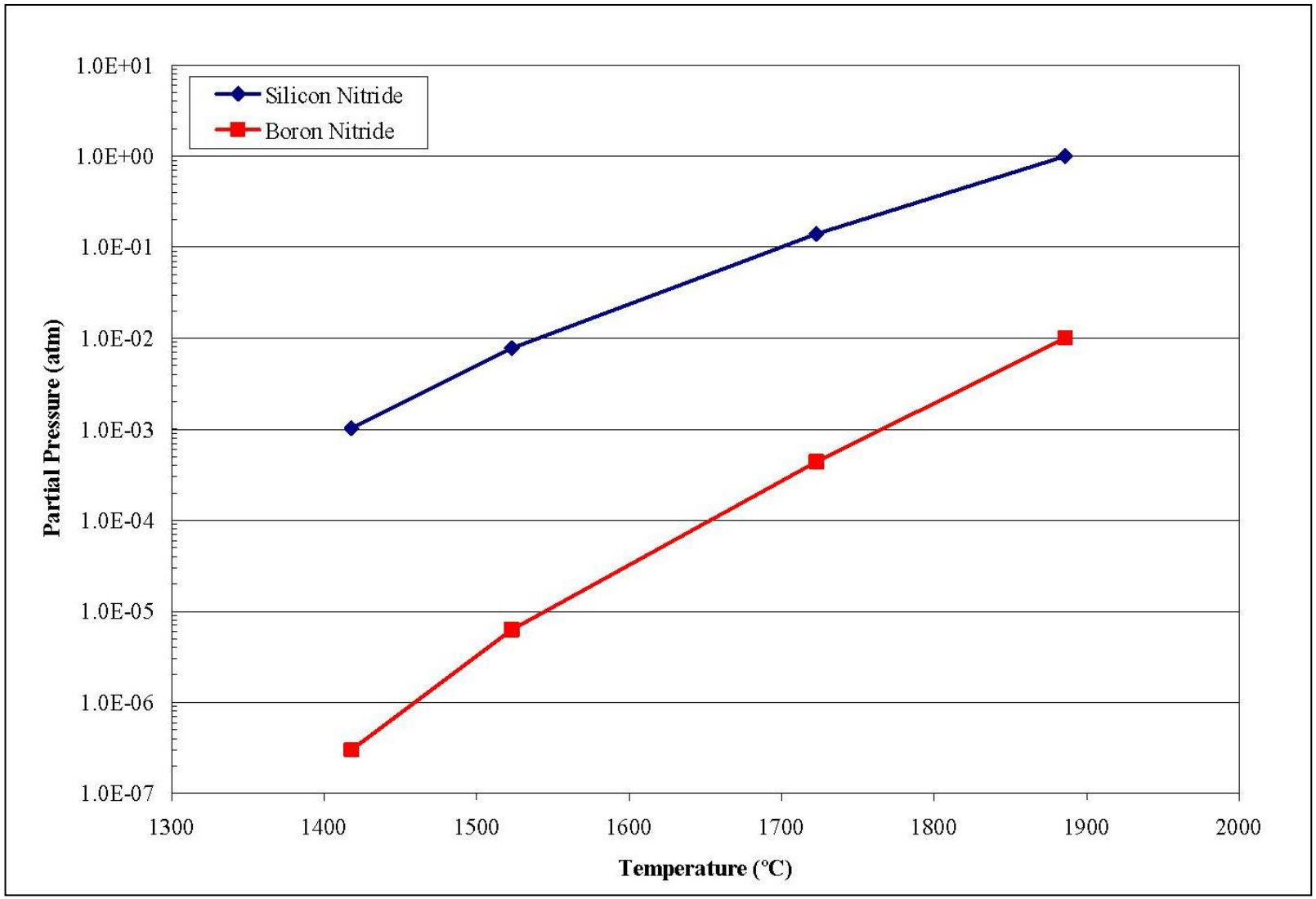


Figure 2.12: Nitrogen partial pressure of $Si_3N_4$ and BN as a function of temperature.

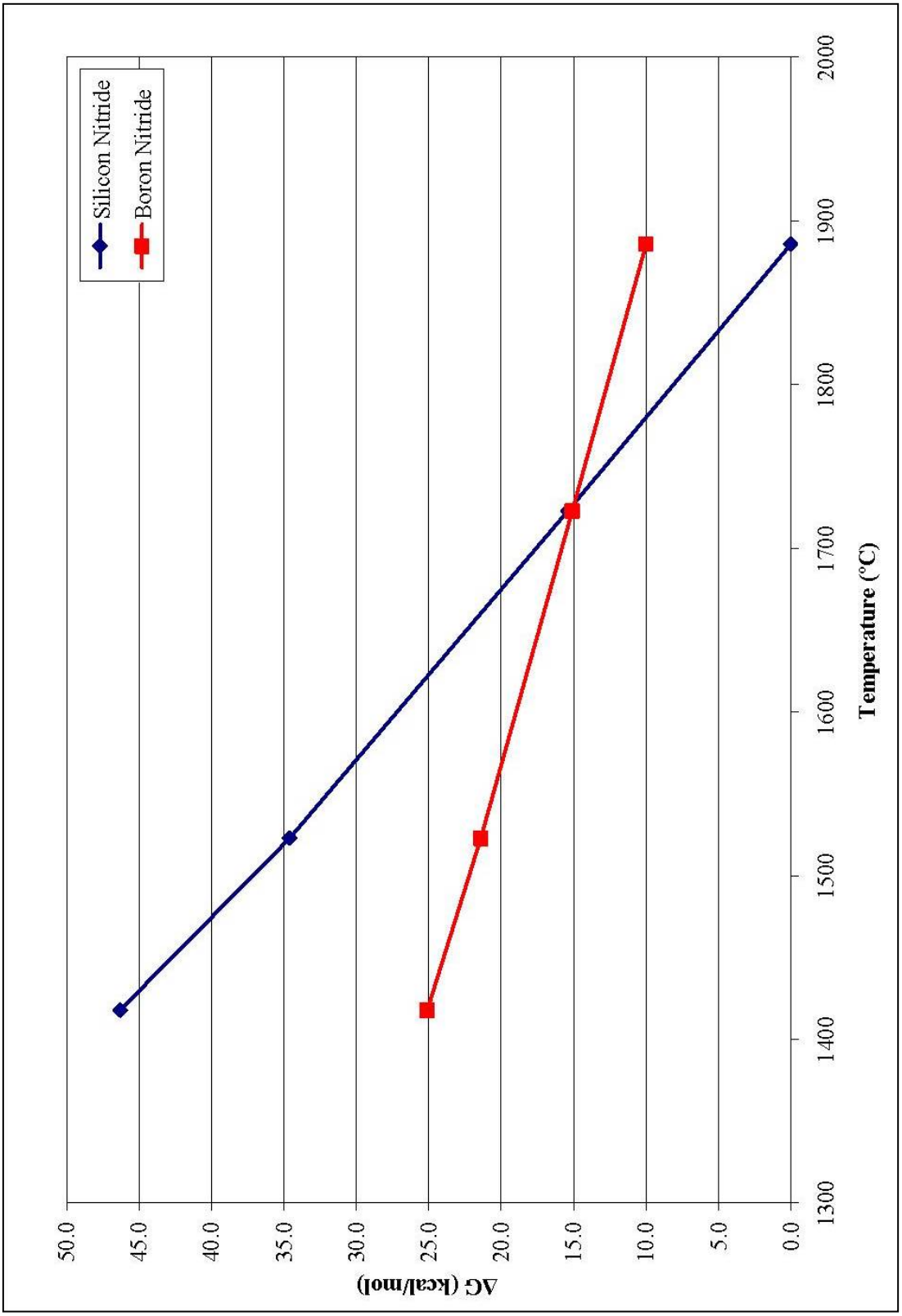


Figure 2.13: Gibbs free energy of $Si_3N_4$ and BN as a function of temperature.

It is also possible that the formation of T2 could occur by way of an intermediate boride, as observed with its formation from the liquid state:

$$2Mo + B \rightarrow Mo_2B \quad (10)$$

$$2Mo_2B + Mo + Si \rightarrow Mo_5SiB_2 \quad (11)$$

or

$$2Mo_2B + Mo_3Si \rightarrow Mo_5SiB_2 + 2Mo \quad (12)$$

If decomposition of the nitrides occurs prior to reaction with molybdenum, sintering will likely be enhanced by the formation of a transient liquid phase. This is because $Si_3N_4$ decomposes well above the melting point of silicon (1412ºC).

It is also possible that Mo will react directly with the nitrides because of the small nitride free energies and probable much more negative energies for T2 and A15. In this case, reaction to form A15 would occur by the following process:

$$3\ Mo + 1/3\ Si_3N_4 \rightarrow Mo_3Si + 2/3\ N_2 \quad (13)$$

Formation of the T2 phase could then occur in a number of ways, such as by a direct reaction:

$$5\ Mo + 1/3\ Si_3N_4 + 2BN \rightarrow Mo_5SiB_2 + 5/3\ N_2 \quad (14)$$

a stepped reaction:

$$2Mo + Mo_3Si + 2BN \rightarrow Mo_5SiB_2 + N_2 \quad (15)$$

or by formation of intermediates:

$$Mo + 2BN \rightarrow MoB_2 + N_2 \quad (16)$$

$$MoB_2 + Mo + Mo_3Si \rightarrow Mo_5SiB_2 \quad (17)$$

X-Ray Diffraction (XRD) analysis will be used to study the reactions. By identifying the phases present in the samples at different temperatures stages throughout

the sintering process, it will be possible to determine the actual reaction sequence. Evaluation of this data will also help determine whether the formation of transient liquid silicon is occurring.

# CHAPTER III

# EXPERIMENTAL PROCEDURE

In this chapter, the techniques and apparatus used to prepare and characterize the samples are discussed. Different starting materials were selected to explore the effects of surface area and particle size on the reaction and sintering behavior of the materials. A variety of powder processing methods were tried to improve the phase distribution and densities of the fired samples. Characterization of the samples was done using density measurements, x-ray diffraction analysis and electron microscopy.

## 3.1 Materials Selection

A variety of high-purity starting materials were used. In addition to the data supplied by the manufacturers, further characterization of the materials was performed. The possible presence of any impurity phases in the materials was examined using a Phillips PW1800 x-ray diffractometer. The surface areas of the powders were determined using a Coulter SA3100 BET surface area analyzer. The measured surface areas and other supplied properties are listed in Table 3.1. Two differently sized molybdenum powders were chosen. The first supplied by Atlantic Equipment Engineers (AEE) has a particle size distribution in the 1-2μm range and the second supplied by Climax Engineered Materials has a 100-500nm particle size distribution, as reported by the manufacturers. SEM images of these powders in Figure 3.1 verify the values reported by the manufacturers. XRD analysis confirms both powders contain only pure α-Mo.

Table 3.1: Properties of raw material powders.

| **Molybdenum** | **Grade** | **Purity** | **Particle Size** | **Surface Area ($m^2/g$)** | **Oxygen Content** |
|---|---|---|---|---|---|
| AEE | MO-100 | 99.98% | 1-2 μm | 0.5 | N/A |
| Climax | Ultrafine | 99.95% | 100-500 nm | 3.3 | 0.8 wt% |
| | | | | | |
| **Silicon Nitride** | **Grade** | **Purity** | **Particle Size** | **Surface Area ($m^2/g$)** | **Oxygen Content** |
| UBE Industries | SN-E03 | 99% | ~0.5 μm (APS) | 4 | 0.82 wt% |
| UBE Industries | SN-E10 | 99% | ~0.5 μm (APS) | 12.0 | 1.45 wt% |
| | | | | | |
| **Boron Nitride** | **Grade** | **Purity** | **Particle Size** | **Surface Area ($m^2/g$)** | **Oxygen Content** |
| Sigma-Aldrich | 255475 | 99% | ~ 1 μm | N/A | N/A |
| Cerac | B-1084 | 99.5% | 0.73 μm (APS) | 6.7 | N/A |
| AEE | BO-501 | 99.9% | 0.3-0.7 μm | 11.6 | < 1.5 wt% |

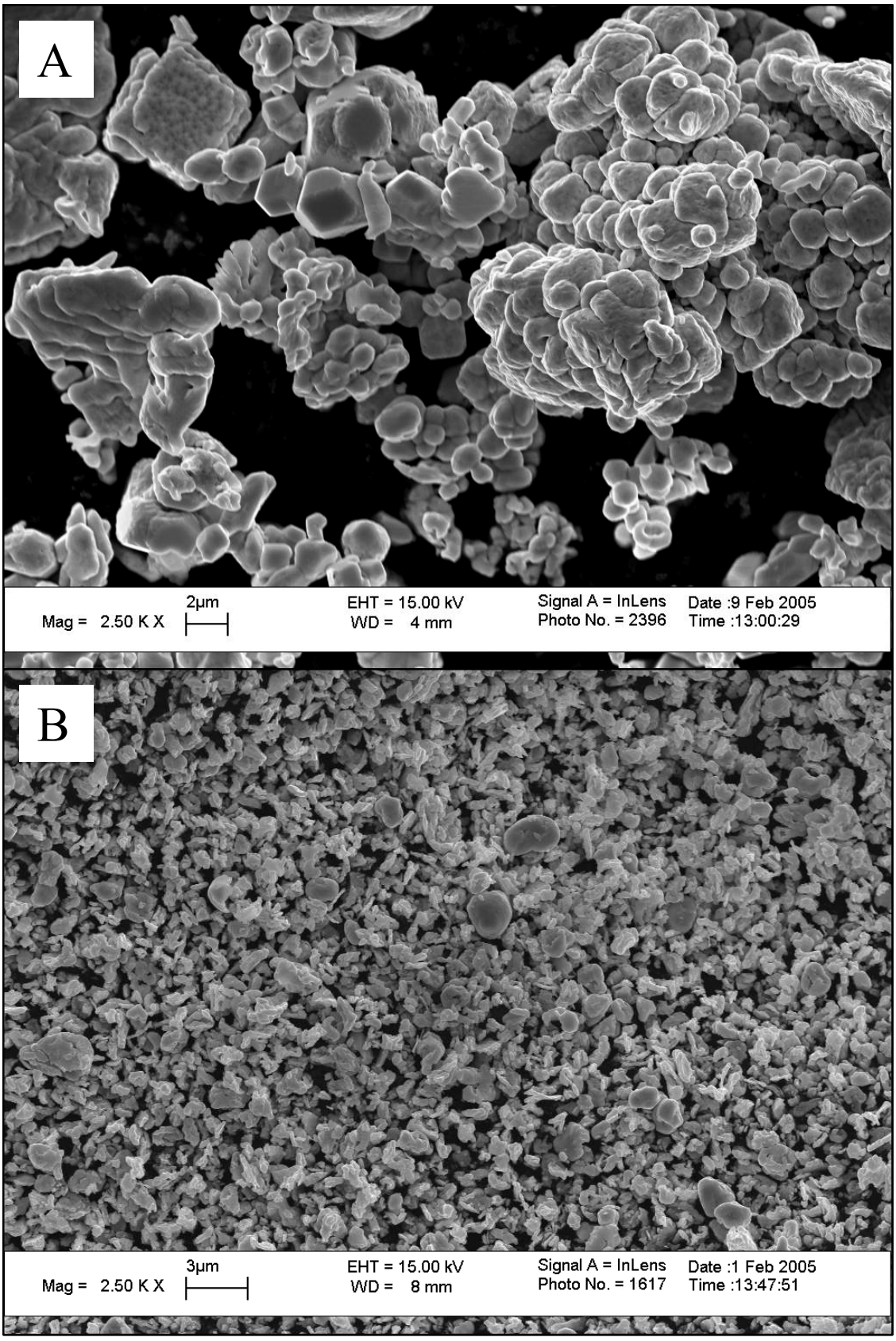


Figure 3.1: Comparison of molybdenum powders: AEE (A) and Climax (B).

Two grades of α-silicon nitride were used, both produced by UBE Industries. These two powders have the same mean particle size and vary mainly in the particle size distribution and surface area of the powder. The SNE03 grade powder has a wider size distribution and lower surface area than the SNE10 grade powder[21]. Conversely, the SNE10 powder has higher oxygen impurity content. No impurity phases were found by XRD analysis. Three grades of hexagonal boron nitride were selected with increasing particle fineness. Again, XRD analysis showed no anomalous phases.

## 3.2 Powder Preparation

Four molybdenum based powder combinations were prepared to examine the effects of particle size and surface area of the starting materials on the densification and final microstructure of the alloy. These mixtures are listed in Table 3.2 with their approximate surface area. The amount of starting powders needed to maintain the desired 96Mo-3Si-1B weight percentages after decomposition of the nitrides was calculated to be 92.94wt% Mo, 4.84wt% $Si_3N_4$ and 2.22wt% BN. Various methods of mixing were explored to determine powder preparation effects on the final microstructure. Another mixture was prepared to evaluate molybdenum oxide as the molybdenum source in the process. The powder ratio necessary to keep the desired composition after

Table 3.2: Composition and approximate net surface area of powder batches.

| Batches | Raw Materials | SA, $m^2/g$ |
|---|---|---|
| **1.** **A**EE | AEE Mo, UBE-SN-E03, Sigma BN | < 0.8 |
| **2.** **C**limax, **C**oarse | Climax Mo, UBE-SN-E03, Cerac BN | ~ 3.4 |
| **3.** **C**limax, **F**ine | Climax Mo, UBE-SN-E10, AEE BN | ~ 3.9 |
| **4.** **A**EE, **F**ine | AEE Mo, UBE-SN-E10, AEE BN | ~ 1.3 |
| 5. $MoO_3$-Based | $MoO_3$, UBE-SN-E03, Sigma BN | - |

reduction of the oxide and decomposition of the nitrides was 95.24wt% $MoO_3$, 3.30wt% $Si_3N_4$ and 1.45wt% BN. In all cases, the ratios of molybdenum, silicon and boron were kept constant. Throughout the project, the powder preparation methods were refined to improve powder dispersion and the green density of the samples. The methods used are discussed below.

### 3.2.1 Ball Milling

Ball milling was used to prepare powder mixtures of the AEE, Climax-Coarse, Climax-Fine and $MoO_3$-based mixtures. The powders were milled in acetone with 3mm $ZrO_2$ media (Performance Ceramics) inside 250cc polyethylene (Nalgene) bottles for 24 hours. After milling, the slurries were stirred by hand until all of the acetone had evaporated to prevent differential settling due to the different densities of the starting materials. Large agglomerates were crushed using a mortar and pestle and the powders were screened using a 100-mesh sieve.

### 3.2.2 High Energy Milling

To improve dispersion of the starting powders and break up powder agglomerates, a higher energy milling process was employed. The powders were mixed using a commercial paint shaker for 15 minutes. Two batches of the Climax-Coarse mixture were made to evaluate the effect of different sized milling media. In the first batch, the powder was mixed using the 3mm $ZrO_2$ media. In the second, 6mm $Al_2O_3$ media (Performance Ceramics) was used. Both batches were mixed in acetone inside polyethylene bottles. The mixtures were stirred until dried and screened with a 100-mesh sieve.

### 3.2.3 Spray Drying

A Climax-Coarse batch was prepared by ball milling, with 0.5wt% stearic acid added to the mix to serve as a lubricant to reduce density gradients in the pressed pellets. Addition of the stearic acid led to poor greenbody strength. To eliminate this problem, a new batch was made using 1wt% polymethyl methacrylate (PMMA 2008, Ineos Acrylics) added as a binder in addition to the 0.5wt% stearic acid. In addition, PMMA acts as a powder dispersant to help prevent agglomeration of the starting materials after the high energy dispersion. The slurry was mixed in acetone using a paint shaker and 6mm $Al_2O_3$ media. To ensure the PMMA did not separate from the powder mixture, after milling the dispersed dilute slurry (~10vol% solids) was sprayed or atomized with an airbrush into a large container to provide rapid drying or "spray drying". This process was also used to prepare spray dried powders of the Climax-Fine and AEE-Fine mixtures. For the Climax powders, this process produces spherical particle aggregates. Even the fines are aggregates of particles, as seen in the SEM images of the final powder mixtures shown in Figure 3.2. The AEE molybdenum powder is too coarse to make spheres from the atomized spray of the airbrush, but the process still creates fine aggregates of particles. Compare this to the stir-dried Climax-Coarse powder which shows large, hard agglomerates with a wide size distribution. By refining parameters such as the slurry feed rate and air flow of the airbrush, it should be possible to produce spherules from the AEE mixtures and improve the overall process to produce a higher volume of spheres with a narrower size distribution.

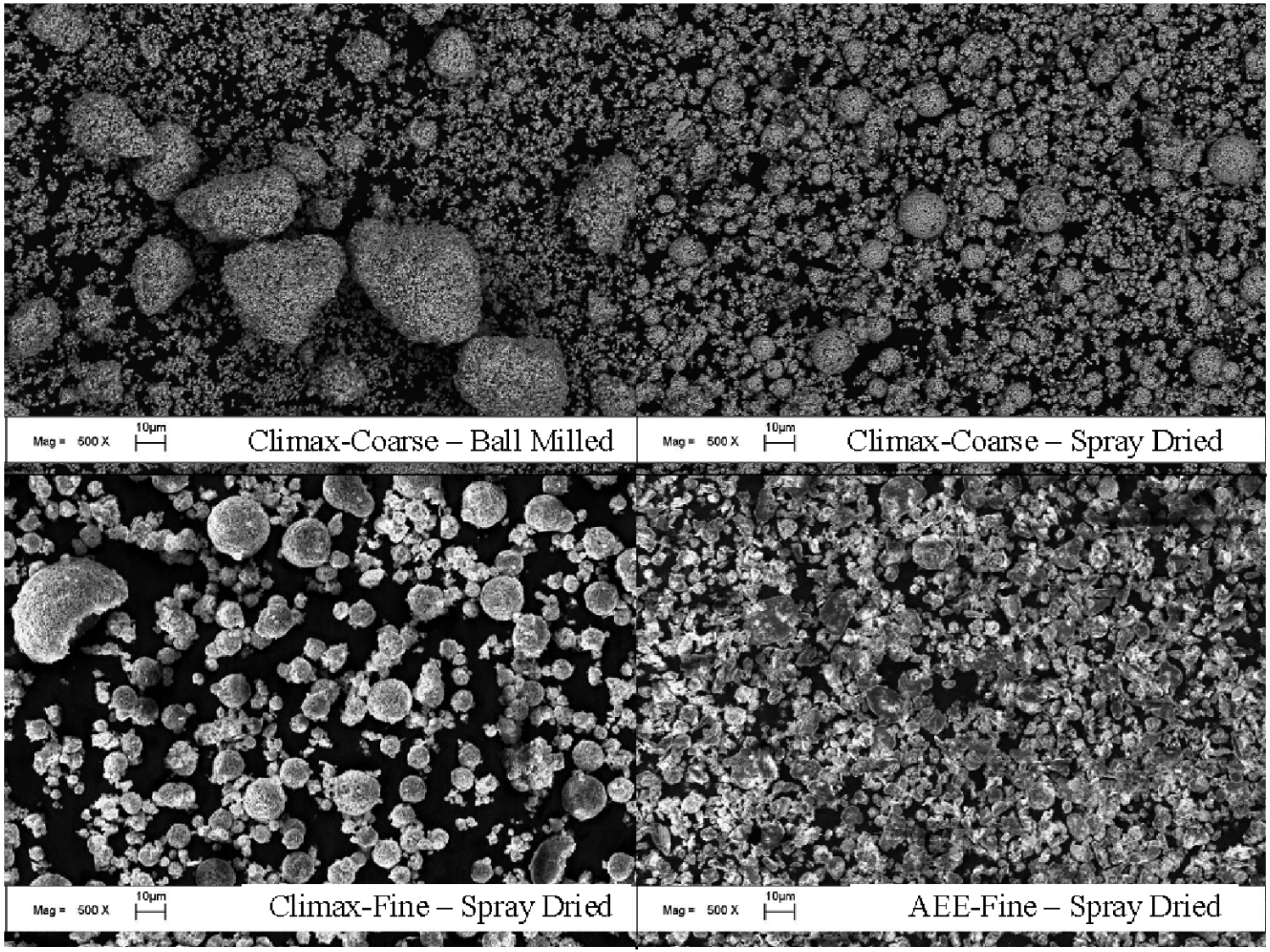


Figure 3.2: Comparison of spray dried and ball milled powders.

## 3.3 Sample Preparation

For this project, simple and easily reproducible sample preparation methods were used. Powders were pressed into cylindrical pellets and fired by conventional sintering. In future efforts, the same reactant mixtures could be applied to net-shape fabrication techniques which are more compatible with the complex geometry of turbine blades, such as gel casting or injection molding.

### 3.3.1 Powder Pressing

Powder pellets were uniaxially pressed using a 3/8" cylindrical die. A study to improve the green density of the pellets was conducted on the Climax-Coarse powder. The mixtures prepared by ball milling, both dry and with 0.5wt% addition of stearic acid were compared to the powder prepared by spray drying. Figure 3.3 compares the green densities of the pellets as a function of pressure. While the ball milled powder with stearic acid achieved the highest density, at pressures over 30ksi hairline fractures due to density gradients appeared. The same problem sometimes occurred for the ball milled powder over 40ksi. No cracking was found in the pellets pressed from the spray dried powder, making them the highest green density pellets pressed without flaws.

### 3.3.2 Sintering

Samples were placed in high-purity alumina boats (Vesuvius) and sintered in a 24" tube furnace (Lindbergh Blue) with a 9/16" alumina tube (Vesuvius). The furnace temperature was computer controlled and was monitored by a thermocouple placed directly above the center of the tube. The difference between the temperature measured by the control thermocouple (Omega) and a thermocouple placed inside the tube varied less than 5ºC. The temperature measured across the four inch zone in the center of the

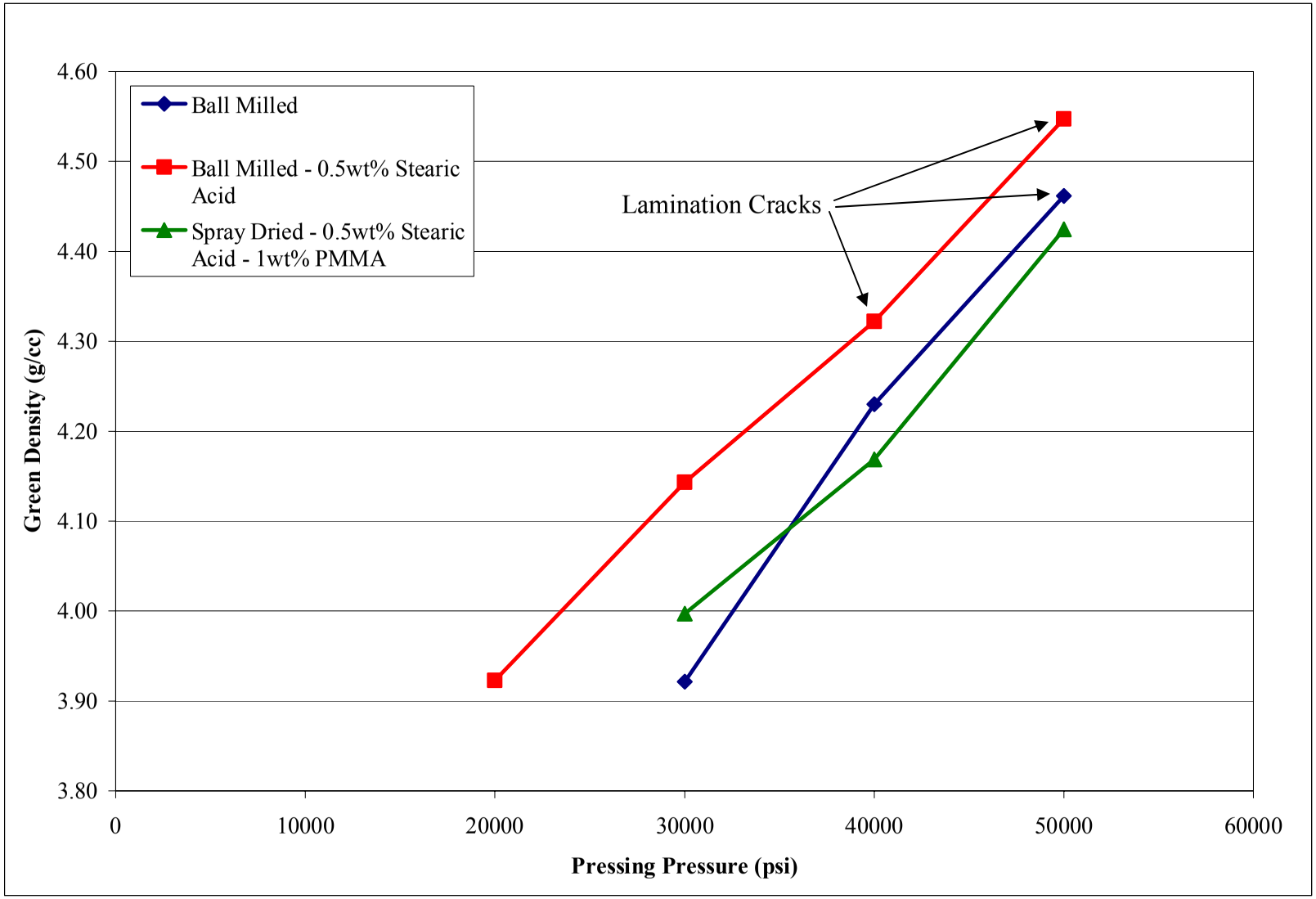


Figure 3.3: Comparison of the green densities for Climax-Coarse powders prepared by different methods.

furnace tube fluctuates less than 2ºC at 1500ºC. The furnace tube was sealed to prevent sample oxidation and contamination. The atmosphere inside the tube was controlled using two rotometers (Cole-Parmer) to maintain the desired ratios of the inlet gases. All samples were fired in a 10:1 mixture of either $N_2/H_2$ or $He/H_2$ Ultra-High Purity grade gases (Airgas Products) with a total gas flow of approximately 150cc/min. Prior to firing, the furnace tube was evacuated and flushed three times. To prevent backflow of oxygen in the system, the exhaust was bubbled through an airlock.

The furnace used is not able to maintain high ramp rates without sustaining damage. For tests conducted at a heating rate of 30ºC/min, the samples were pushed from the edge of the furnace tube into the hot zone using an alumina push rod (Vesuvius). The samples were pushed in at ¼" increments at timed intervals which corresponded to the desired heating rate. A gas tight seal was maintained using the apparatus shown in Figure 3.4. Samples prepared with a lubricant or binder underwent a burnout period, heating at 1ºC/min to 300ºC with a one hour hold to slowly remove the organics.

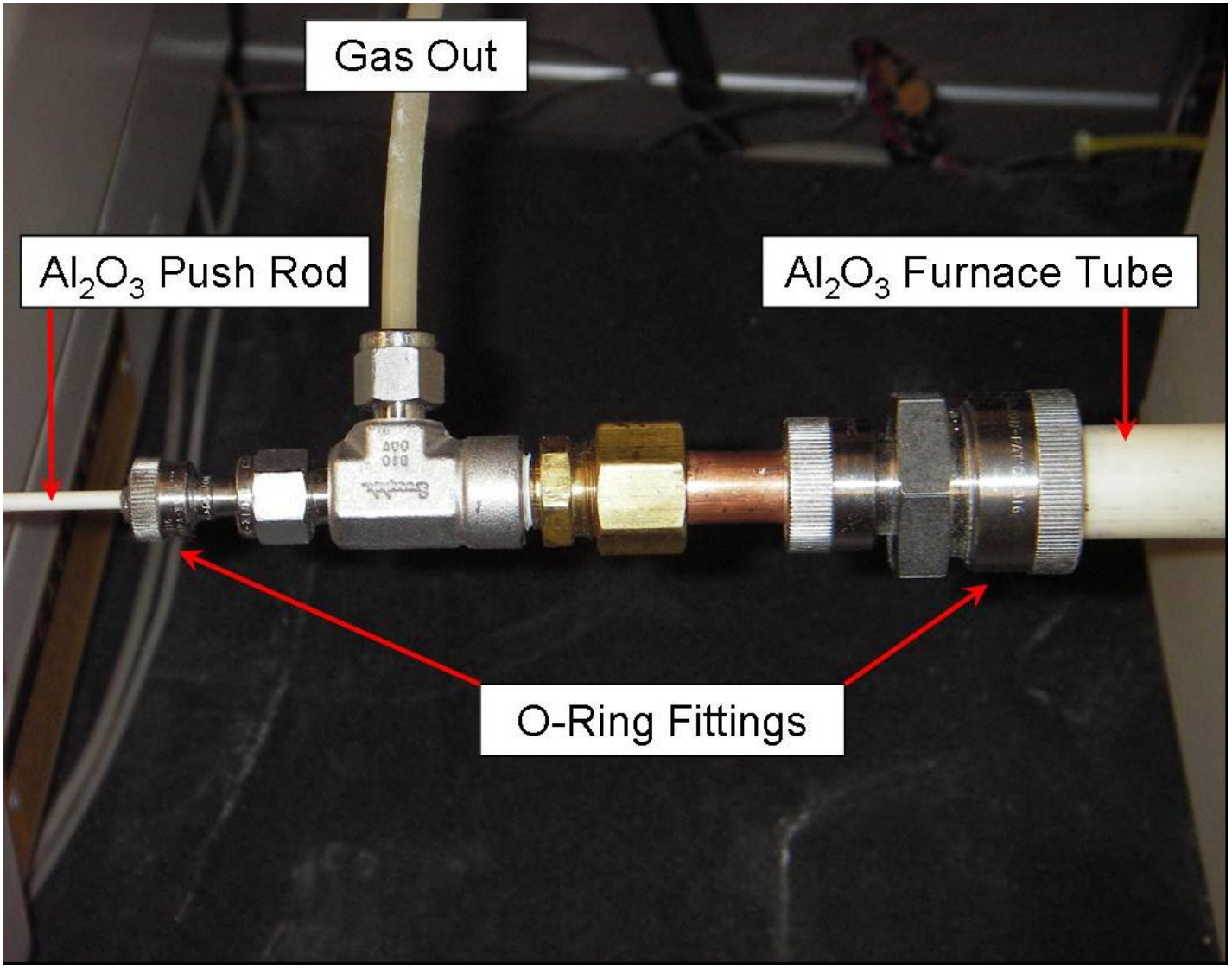


Figure 3.4: Pushrod apparatus used for high heating rates.

## 3.4 Characterization

Sample characterization techniques were used to observe the reactions steps involved with the formation of the desired intermetallic phases, the sintering behavior of the different powder mixtures and the final phase distribution of the samples.

### 3.4.1 Density Measurement

The densities of the samples were measured using two methods. Post-sintering dimensional measurements were taken for all the samples and used to calculate the bulk densities by the following equation:

$$\rho_{Bulk} = M / V \tag{1}$$

where M is the mass of the pellet and V is the volume. Inaccuracies in the measured volume can occur due to cupping and warping of the fired pellets. More accurate values are obtained using Archimedes method, which compares the samples dry weight ($W_{Dry}$) and its weight both suspended ($W_{Susp}$) in and saturated ($W_{Sat}$) with water:

$$\rho_{Bulk} = \frac{W_{Dry}}{W_{Sat} - W_{Susp}} \tag{2}$$

To ensure all open porosity was saturated, samples were placed in boiling water for 20 minutes. The percentage of open porosity of the sample is calculated as:

$$\%O.P. = \frac{W_{Sat} - W_{Dry}}{W_{Sat} - W_{Susp}} * 100 \tag{3}$$

Only the densities of the samples prepared in the latter half of the project were measured using Archimedes method. In all cases, this method calculated a higher density than that measured from dimensional measurements. For consistency, any comparisons of densities between different samples are made using values measured by the same technique, which will be noted in the discussion.

### 3.4.2 Phase Analysis

X-ray diffraction analysis was conducted to determine the phases formed at various temperatures. Samples were fired at the desired temperature with a 6 to 24 hour hold. To eliminate any surface oxidation, fired pellets were ground to the center and polished flat prior to XRD analysis. Measurements were made with a Phillips PW1800 diffractometer using $Cu_{K\alpha}$ radiation with a scan speed of 0.008º2θ/sec. The phases present in the samples were identified using Phillips X'pert phase identification software. All of the reported diffraction scans are plotted by their relative intensity, as compared to the (100) molybdenum peak.

### 3.4.3 Microstructural Analysis

The microstructures of the samples were observed using a Leo 1530 Scanning Electron Microscope operating in backscatter mode. Pellets were ground to the center before polishing to avoid any surface variations in the phase composition. The α-Mo phase appears brighter in the micrographs due to its higher average atomic number. The intermetallic phases appear darker, but there is not enough contrast to distinguish between the A15 and T2 phases. Porosity in the microstructure appears black in the micrographs.

# CHAPTER IV

## RESULTS AND DISCUSSION

In this chapter, the formation and characterization of the Mo-Si-B alloy is discussed. The reactions to form the A15 and T2 intermetallics were studied using x-ray diffraction. Density measurements were used to examine the sintering behavior of the different powder mixtures and electron backscatter microscopy was used to compare the microstructures of the fired samples. Additional topics discussed are the depletion of intermetallic phases on the surface of the samples and whether transient liquid sintering is occurring in this process.

### 4.1 $MoO_3$-Based Samples

Experiments were conducted to evaluate using molybdenum oxide as the molybdenum source for the alloy. The already fine $MoO_3$ powder should yield very fine molybdenum particles after reduction. $MoO_3$, $Si_3N_4$ and BN were mixed in the appropriate proportions to give the desired Mo-3Si-1B (wt %) alloy after reduction of the oxide and decomposition of the nitride starting materials. The powders were ball milled in acetone for 24 hours and stirred until dry to ensure a fine mixture of the powders. The mixture was then dry pressed at 10,000psi into cylindrical pellets. These pellets were fired in a 10:1 mixture of helium to hydrogen. A second set of samples using the original AEE molybdenum powder with the coarsest nitrides (Chapter 3.2) were fired concurrently for comparison. The samples were fired at 3ºC/min to 700ºC with a two

hour hold to allow for reduction of the oxide. The firing schedule was then continued at 3ºC/min to the desired temperature with a four hour hold. During the first two tests, the furnace shut down before reaching the setpoint. These data points are at 828ºC and 1365ºC and have zero hold time at that temperature. The remaining samples were fired at 1500ºC, 1550ºC and 1600ºC with four hour holds. Density values for these samples are listed in Table 4.1 and are plotted in Figure 4.1.

X-ray diffraction analysis of the 1600ºC samples confirmed formation of both the A15 and T2 intermetallic phases. While these phases were present in samples starting with both the molybdenum metal and the oxide, the diffraction peaks for the intermetallics were weaker in the $MoO_3$ samples. Further tests were performed to study the reduction of $MoO_3$. An oxide-based sample was fired at 700ºC for 120 minutes in pure $H_2$. XRD analysis of this sample confirmed that the $MoO_3$ was fully reduced, with the only phases present in the diffraction pattern being BN, $Si_3N_4$ and Mo. In Figure 4.2 the nitride peaks of the reduced $MoO_3$ pellet are smaller than those for an unfired Mo-based pellet, indicating that some oxidation of the BN and $Si_3N_4$ is occurring.

Table 4.1: $MoO_3$ and Mo-based sample densities.

| | **$MoO_3$-Based** | | **Mo-Based** | |
|---|---|---|---|---|
| **Firing Temperature** | **Green Density (g/cc)** | **Fired Density (g/cc)** | **Green Density (g/cc)** | **Fired Density (g/cc)** |
| 828ºC | 2.61 | 2.20 | 4.79 | 4.83 |
| 1365ºC | | 3.55 | | 4.91 |
| 1500ºC 4h | | 6.39 | | 5.48 |
| 1550ºC 4h | | 7.32 | | 6.43 |
| 1600ºC 4h | | 7.64 | | 6.90 |
| 1600ºC 6h – Long Reduction | | 6.84 | | - |

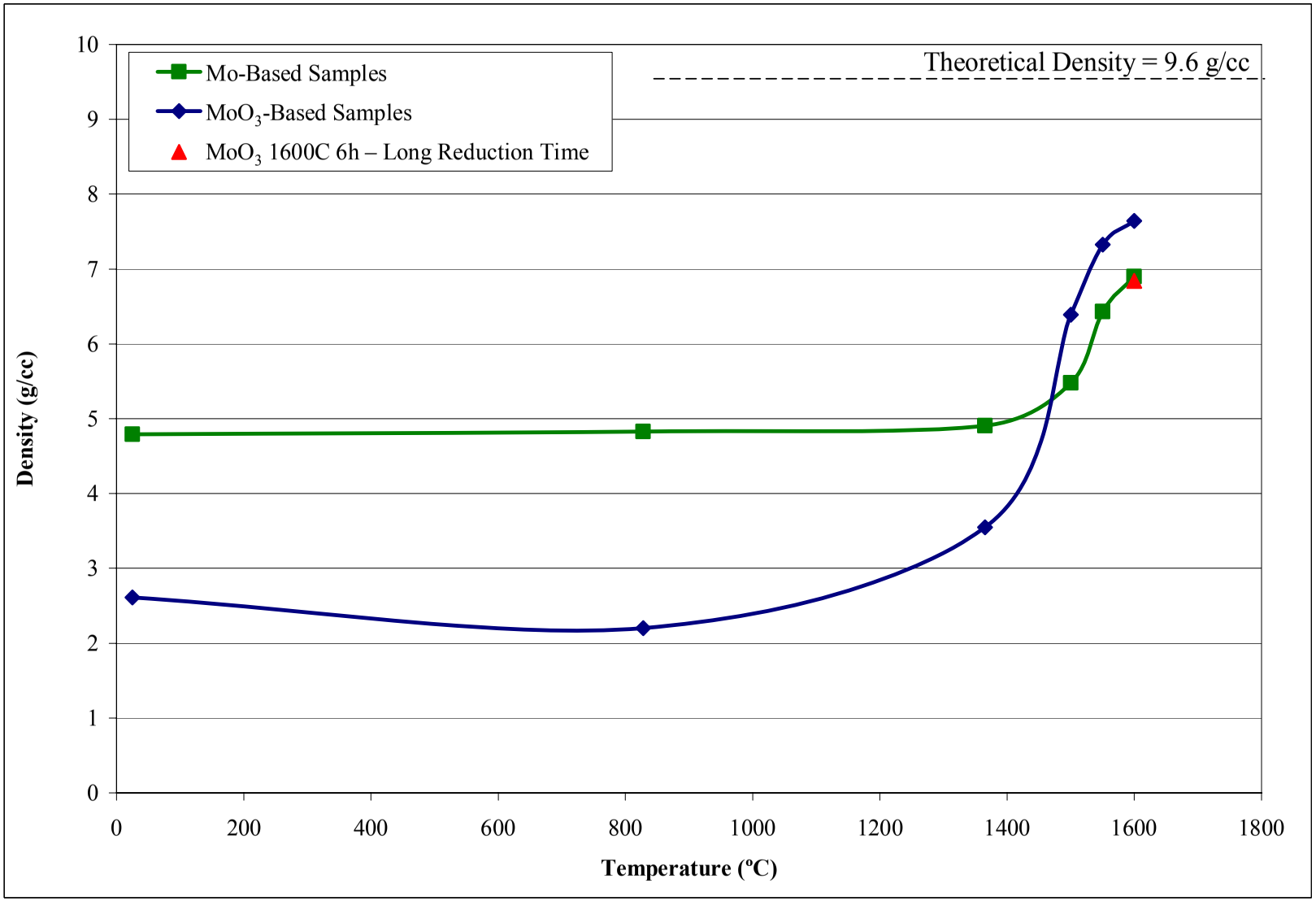


Figure 4.1: Sintering curves for $MoO_3$ and Mo-based samples.

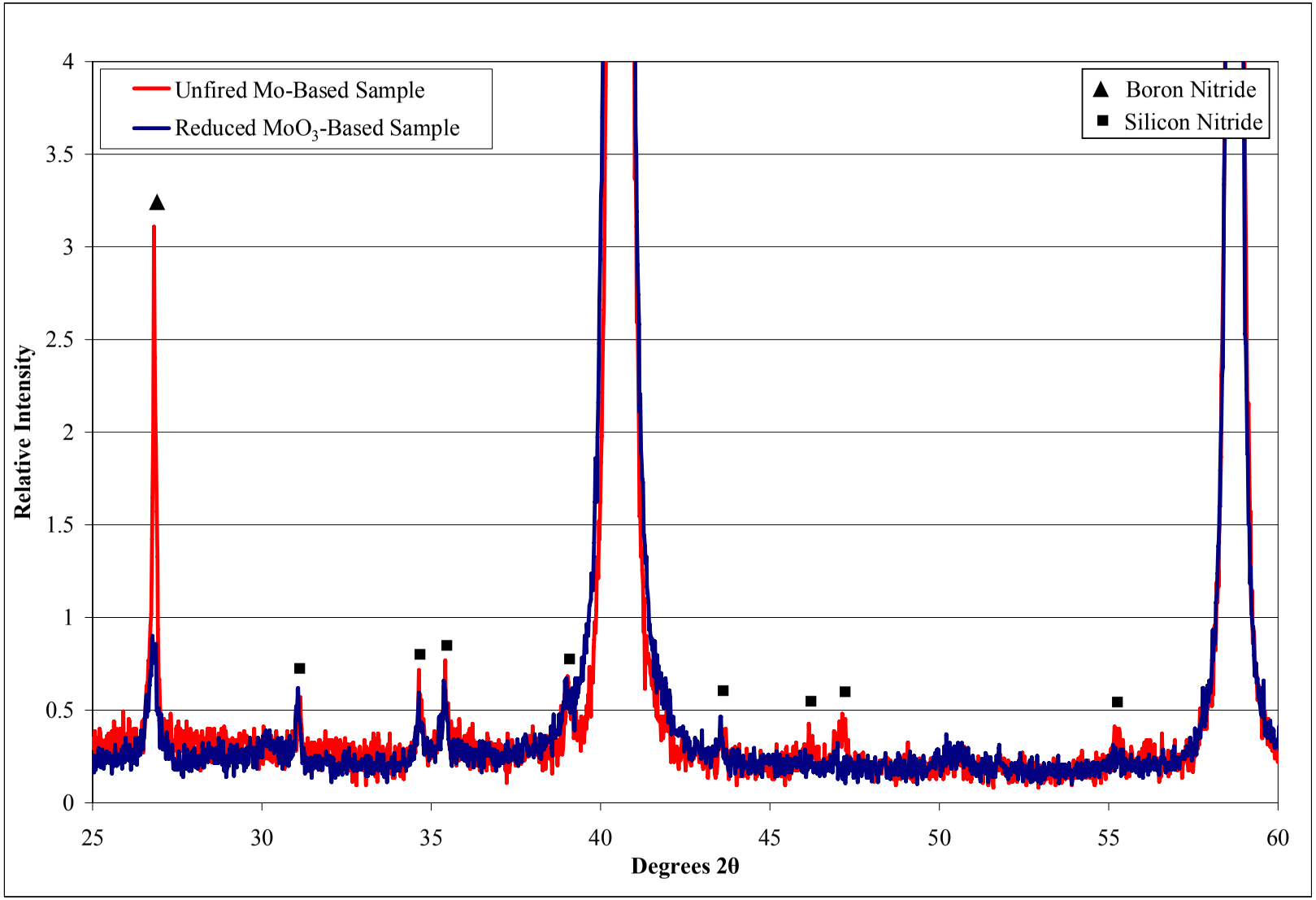


Figure 4.2: XRD comparison of nitride peak heights from the reduced $MoO_3$-based and unfired Mo-based mixtures.

New experiments were completed in an attempt to improve the intermetallic content. A $MoO_3$-based sample was fired at 3ºC/min to 700ºC with a 6 hour hold in pure $H_2$. The hold time was extended from two to six hours to ensure complete removal of oxygen. After the reduction phase, the sample was heated at 3ºC/min to 1600ºC in a 10:1 mixture of $N_2/H_2$ and held for 6 hours before cooling. While this improved the intensities of the intermetallic peaks, they were still lower than that for the molybdenum-based sample fired at the same temperature. It is possible that incomplete removal of oxygen from the center of the sample is leading to oxidation of the BN and $Si_3N_4$ at higher temperatures, forming an amorphous glass that is not detected by XRD analysis. While this glass could be helping densify the material, evidenced by the increased density (8.0g/cc for the $MoO_3$-based sample compared to 6.4g/cc for the Mo-based samples), it would lower the volume fraction of the desired intermetallic phases. This is confirmed in Figure 4.3 by the smaller peaks for the intermetallics in the diffraction patterns as compared to those from a Mo-based mixture. An intergranular glass phase would also negatively affect the mechanical properties of the material.

The experiment was repeated with a longer, lower temperature reduction schedule of 3ºC/min to 650ºC with a 2 hour hold and then 0.5ºC/min to 700ºC with a 2 hour hold. In this sample, the relative intensities of the intermetallics approach that of a later Mo-based sample. In turn the density of this sample was lowered to 7.1g/cc, close to that of the Mo-based sample fired at the same temperature, further evidence of little glass phase formation. This proves that increasing time for the reduction can eliminate the nitride oxidation problem, but large samples would require prohibitively long hold times for complete reduction of their interior. In addition, starting with $MoO_3$ causes problems

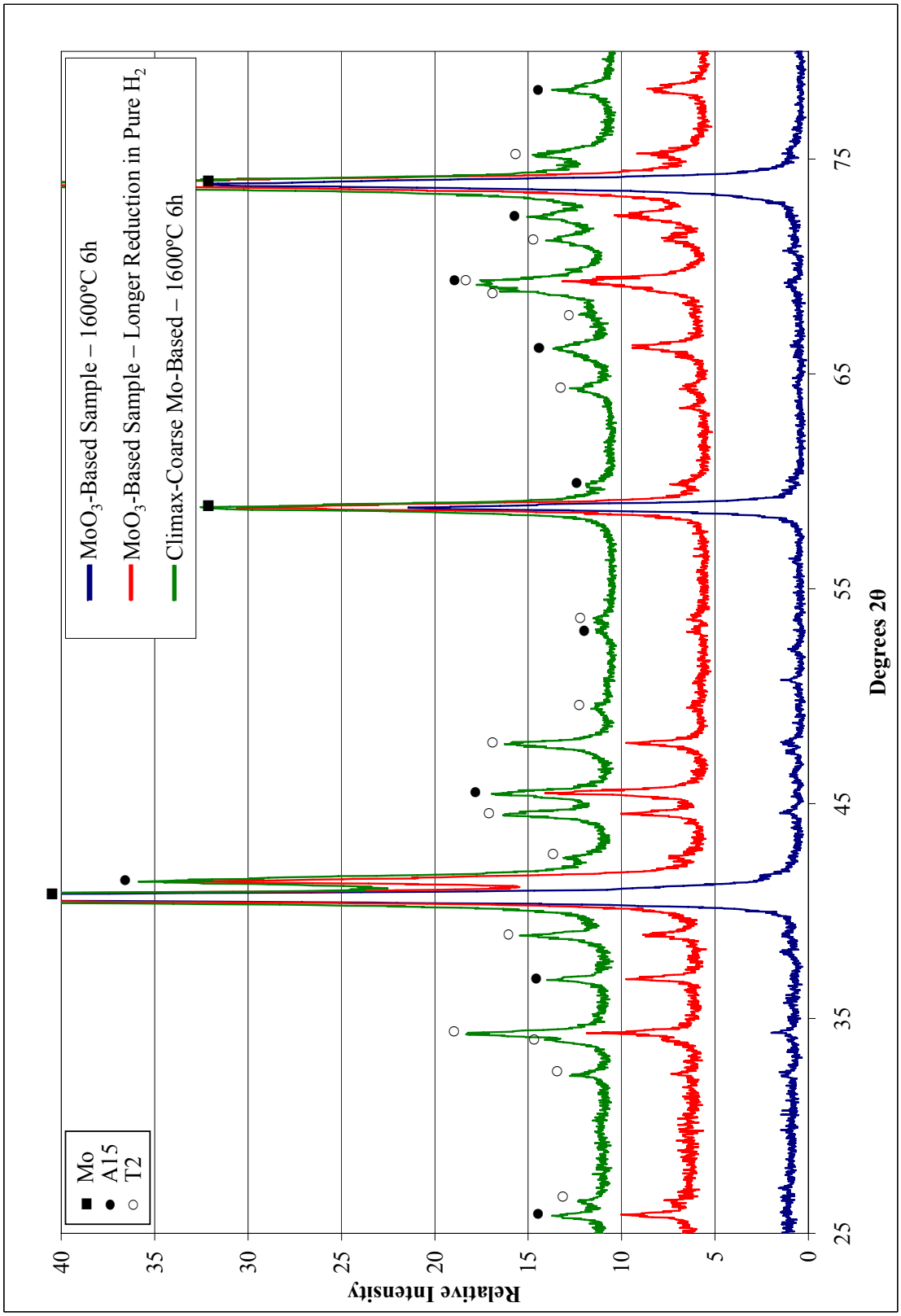


Figure 4.3: Comparison of intermetallic peak heights for $MoO_3$ and Mo-based samples.

with the final densification. After reduction, the sample is close to its original dimensions, but has undergone 35% weight loss, essentially creating a very porous green body. This leads to a large amount of shrinkage in the specimens, on the order of 40-45%. Due to these problems, further study of the $MoO_3$-based samples was abandoned.

## 4.2 Phase Analysis

The initial goal of the project was to prove the viability of reacting molybdenum, $Si_3N_4$ and BN to form the intermetallic phases A15 and T2. XRD phase analysis was used to study these reactions and evaluate the possible reaction sequences listed in Chapter 2. Samples fired at different temperatures were used to pinpoint the start of the reactions and when they had reached completion. Many factors contribute to x-ray diffraction peak intensities in addition to volume fraction of the phase. Because of this, it is difficult to determine the relative phase fractions between measurements. Therefore, all assessments made are qualitative. For better comparison, the diffraction scans are plotted by their relative intensity, as compared to the strongest molybdenum peak.

Experiments were performed on three different powder grade combinations to determine the effects of particle size and surface area in the reactions. Samples were fired in a 10:1 mixture of $N_2/H_2$ at a heating rate of 3ºC/min to temperature with a six hour hold unless otherwise noted. XRD scans taken from the surface of the pellets identify molybdenum as the only phase, likely due to oxidation of the starting nitrides. This would create amorphous $SiO_2$ and $B_2O_3$ phases not detected by XRD. Examination of the cross section of the pellets with an optical microscope confirms the presence of a thin surface layer (<1mm). To ensure the phase identification was representative of the bulk material, the pellets were ground to the center prior to XRD analysis.

4.2.1 AEE – Coarse Nitrides

This combination of powders using the coarsest nitride powders and the AEE molybdenum powder was prepared by ball milling, as discussed in Chapter 3. X-ray diffraction of the 1200ºC sample identifies the starting materials as the only phases present, though their peak intensities are lower compared to an unfired pellet, as seen in Figure 4.4. This probably because changes in the preferred orientation of BN greatly affect its intensity and some silicon may have gone into solution with the molybdenum.

By 1300ºC, the formation of A15 and T2 has started. Although it is difficult to see in Figure 4.4, at 1300ºC faint peaks for the starting nitrides are still present. This observation discounts one of the initial theories that at high temperatures (1600ºC-1700ºC) the nitrides would decompose, leaving elemental Si and B to react with the molybdenum. It is apparent from this experiment that $Si_3N_4$ and BN are reacting directly with the molybdenum to form A15 and T2. By 1400ºC there are no nitrides present and the reaction has neared completion as compared to the sample fired at 1650ºC for 24 hours.

4.2.2 Climax Molybdenum – Coarse Nitrides

This mixture used the Climax molybdenum powder and the intermediately coarse nitrides. The same grade $Si_3N_4$ was used as the AEE mixture but the BN was replaced with a finer powder. This powder mixture was also prepared by ball milling. It is apparent from these experiments that the finer molybdenum powder has increased the reactivity of the mixture. In first scan at 1200ºC (Figure 4.5), the formation of A15 has already begun. While the BN peak at 1200ºC is missing, there is no evidence to suggest the formation of an intermediate boron compound. In the analysis of the pattern, all peaks have been accounted for and are attributed to molybdenum and A15. The BN peak

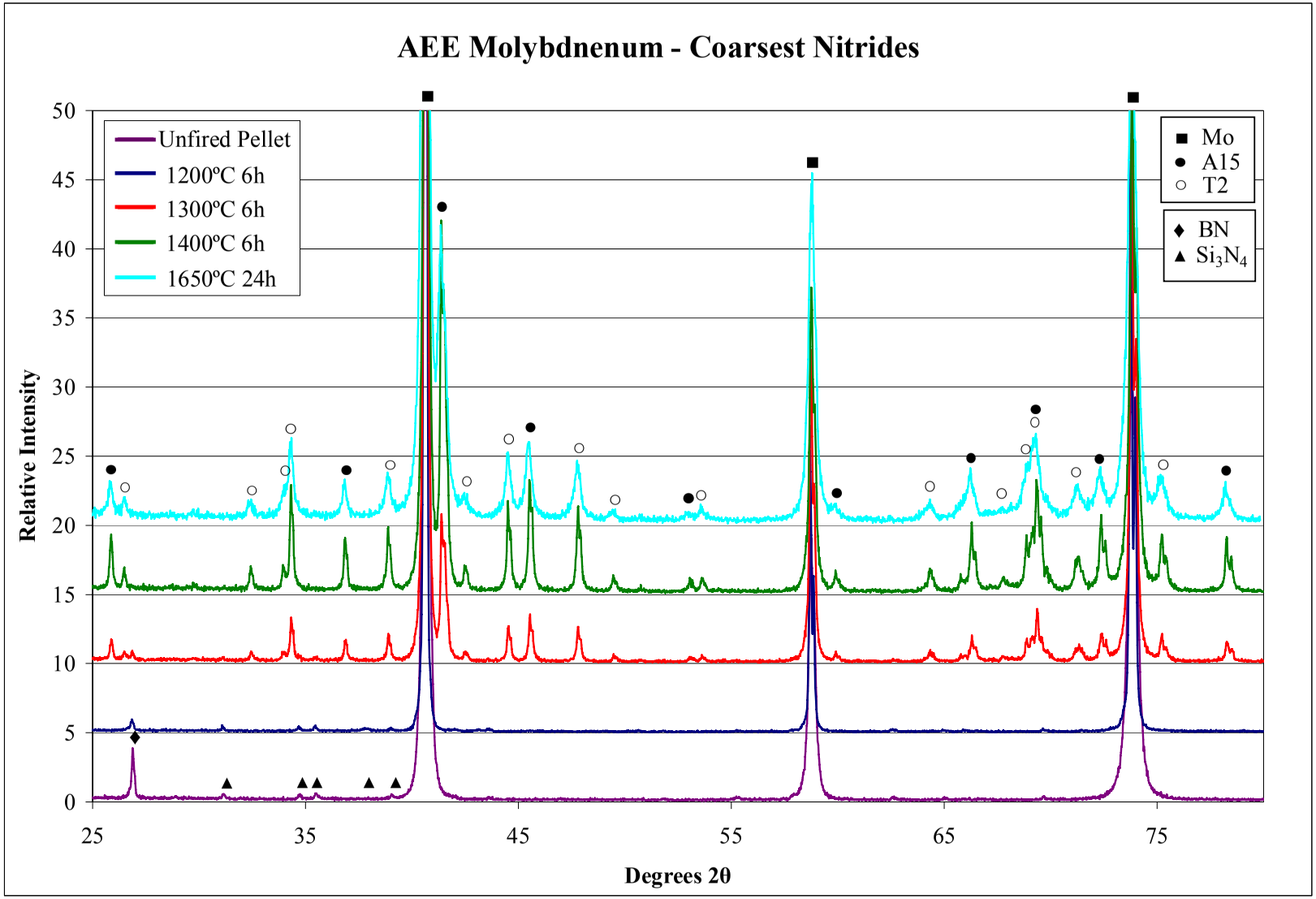


Figure 4.4: XRD pattern identification for AEE samples of increasing heat treatment temperature.

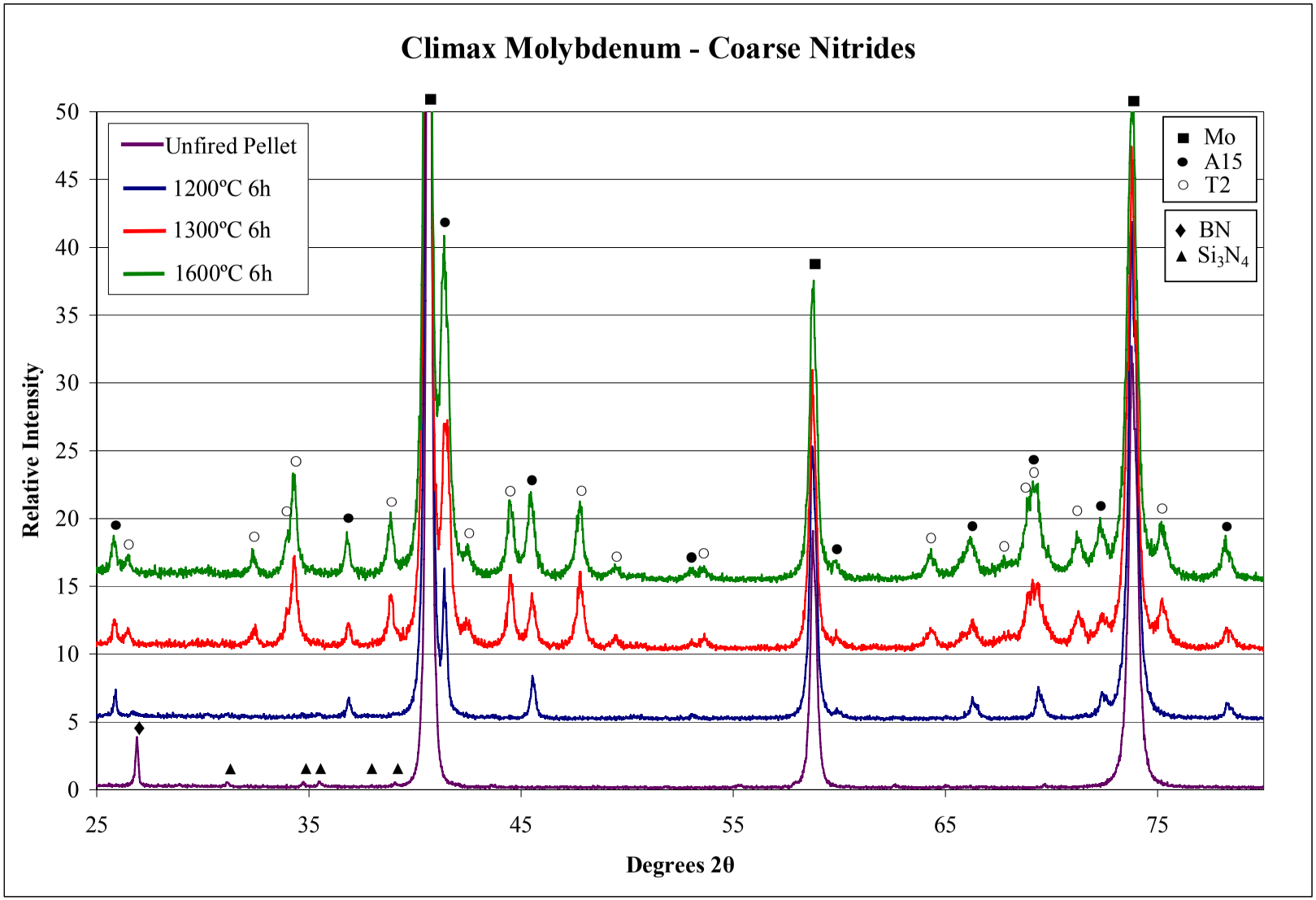


Figure 4.5: XRD pattern identification for Climax-Coarse samples of increasing heat treatment temperature.

intensity for the unfired sample may be exaggerated due to preferred orientation of BN on the surface of the pellet caused by pressing. By 1300ºC the T2 phase has formed and the reactions are near completion, as compared to the sample fired at 1600ºC. The initial reaction step in which A15 forms prior to T2 was not observed with the AEE mixture, probably because it occurs at a temperature between the data taken.

The intermetallics appear to form by direct reaction of molybdenum and the nitrides, as suggested by reaction sequences (13) and (14) presented in Chapter 2.2. Using the standard free energies of formation for the nitrides obtained from published thermodynamic tables, it is possible to estimate the standard free energies of formation for A15 and T2 at the temperatures at which they first appear. Assuming a $\Delta G_{reaction}$ equal to -10 kcal/mol is required to initiate the reaction, the standard free energies of formation of the intermetallics were calculated to be $\Delta G^{o}_{1200^{o}C}$(A15) = -29.2 kcal/mol and $\Delta G^{o}_{1300^{o}C}$(T2) = -102.1 kcal/mol.

An attempt was made to hone in on the exact temperature at which the reaction to form A15 first occurs. A sample was fired at 1100ºC, but an intermediary molybdenum nitride phase was formed. Because the peaks from MoN overlapped with the A15 peaks, it was not possible to determine whether A15 had formed. To avoid formation of the molybdenum nitride, an experiment was conducted in a 10:1 mixture of $He/H_2$ gas. In this atmosphere, T2 was formed at 1100ºC and not A15, as shown in Figure 4.6. In the $N_2/H_2$ atmosphere, only A15 had formed by 1200ºC. This observation of T2 forming before A15 is not directly applicable to those samples fired in the nitrogen atmosphere because by removing nitrogen from the inlet gas, the free energies of the reactions between the nitrides and molybdenum have changed. This finding may be of interest for

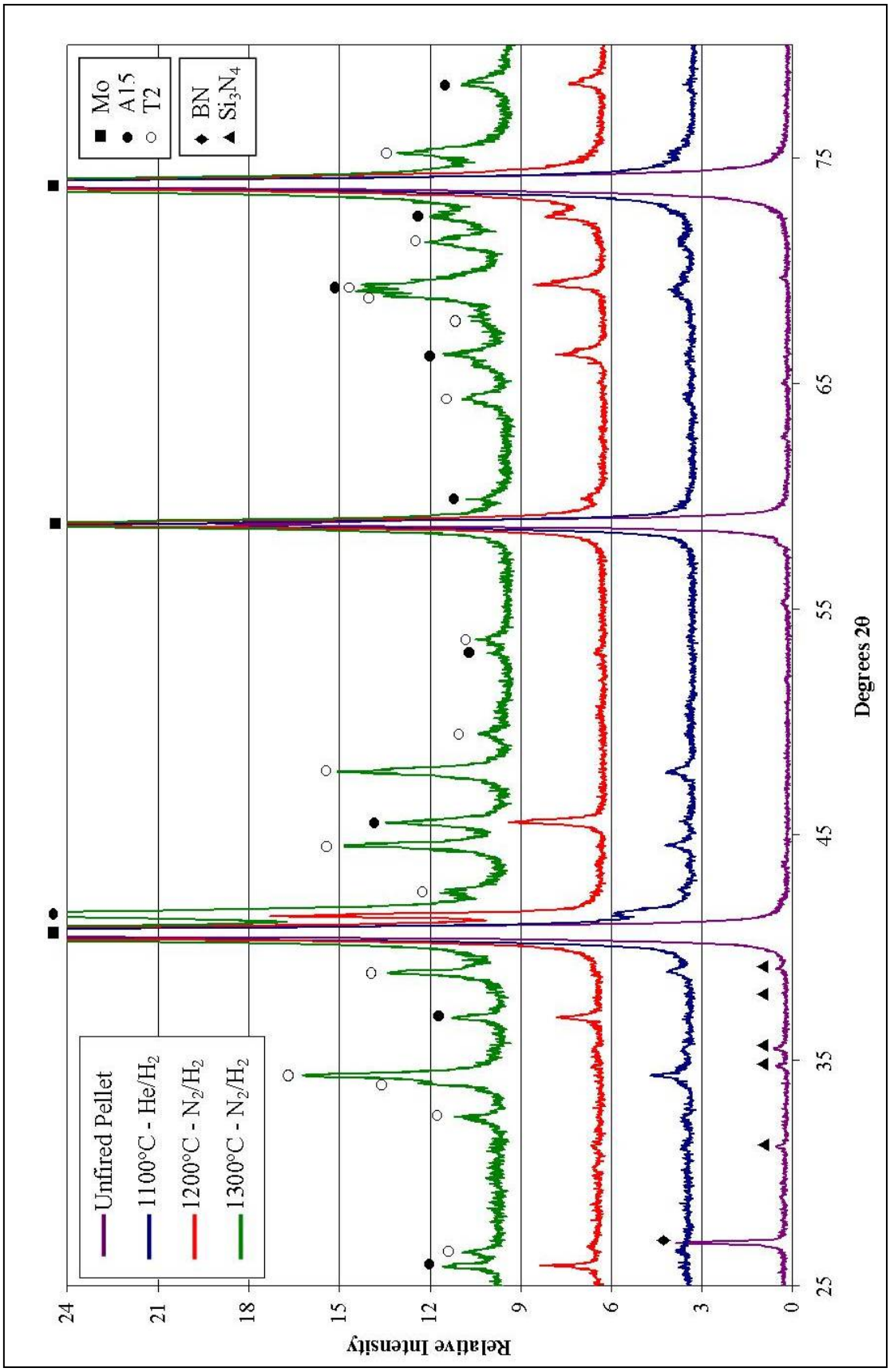


Figure 4.6: XRD comparison illustrating effect of atmosphere on phase formation.

future research, as changing the reaction sequence could alter the morphology of the intermetallics dispersed in the molybdenum matrix.

4.2.3 Climax Molybdenum – Fine Nitrides

This mixture of the Climax molybdenum powder and the finest nitride powders was also prepared by ball milling. There is little variation between the diffraction pattern for this batch at 1200ºC and that of the Climax-Coarse mixture, Figure 4.7. At 1300ºC and 1600ºC, there are no discernable differences in the diffraction patterns between the two batches.

4.2.4 Comparison of Reactions between Starting Materials

Comparisons of the x-ray diffraction patterns for the different materials are shown in Figure 4.8. Judging by the XRD patterns for the two batches using the Climax molybdenum powder, it does not appear that the difference of the nitrides size and surface area has caused any change in the starting temperature or extent of the reactions. Comparing AEE to the Climax molybdenum batches, it is clear that the added reactivity of the sub-micron molybdenum powder plays a greater role in the initial reactions than the size of the nitride powders. At 1300ºC, the nitrides in the AEE batch are still present and the intensities of the intermetallic peaks are smaller than for the Climax-based samples. By 1400ºC, the intermetallic phase content of the AEE equals that of the Climax-based samples and the final reaction quantities are all the same, as illustrated by a comparison of the scans for the high temperature firings.

4.2.5 Effect of Powder Preparation Method on Diffraction Pattern

Because a seemingly adequate understanding of the reaction sequence was determined from the study conducted using the ball milled powders, XRD was not done

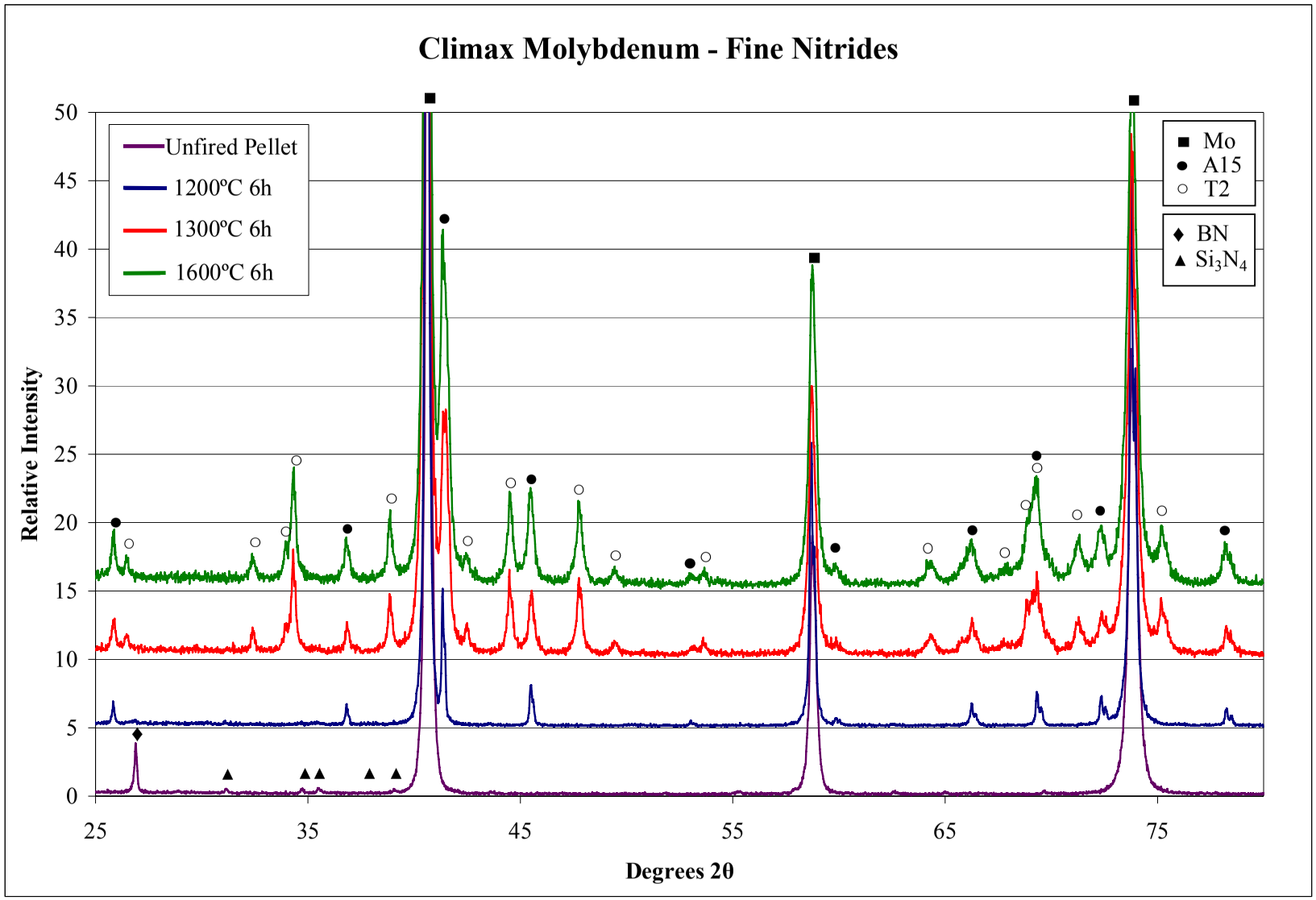


Figure 4.7: XRD pattern identification for Climax-Fine samples of increasing heat treatment temperature.

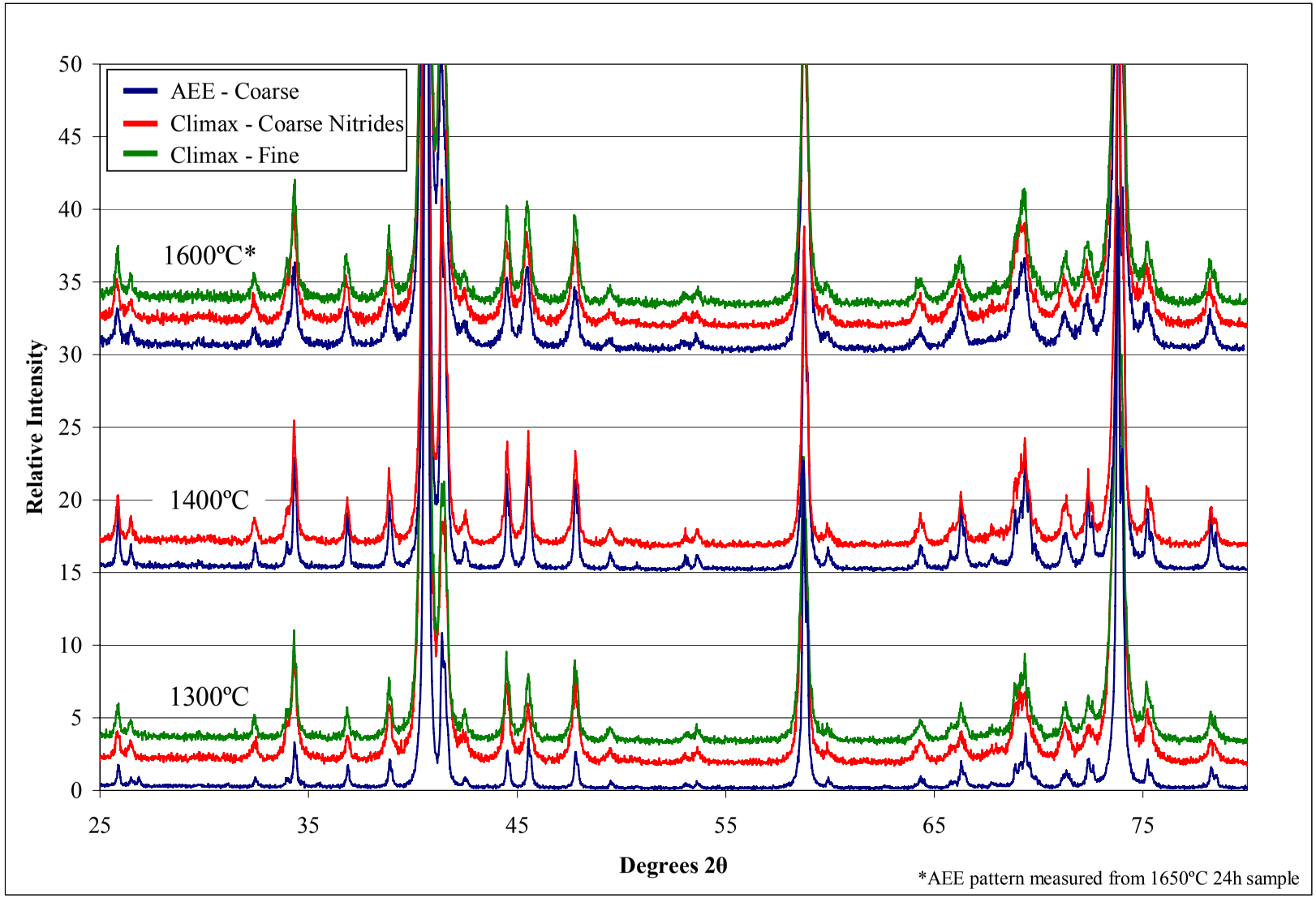


Figure 4.8: Comparison of the XRD patterns at increasing temperatures for the different starting material batches.

for samples pressed from the spray dried powders. Later, to check for differences, a measurement was taken for the Climax-Coarse spray dried sample fired at 1600ºC for 6 hours. Compared to the XRD pattern of the ball milled sample of the same composition (Figure 4.9), the peaks are narrower but taller. Possible differences may arise from the high energy milling or the better dispersion techniques used during the preparation of the spray dried powder. Future work should examine whether the change in powder preparation method has any effect on the final phase composition of the final alloy. Using XRD analysis software, it should be possible to compare the integrated peak intensities of the samples to determine whether the phase fractions in both these samples are equal.

## 4.3 Sintering Behavior

Following the set of experiments comparing Mo-based and $MoO_3$-based powder mixtures, it was decided that using $MoO_3$ increased the probability of oxidizing the starting nitrides and all further work would be carried out using metallic molybdenum powder. Sintering was studied for the four different sized different powder grade combinations, listed in Table 4.2, processed by a variety of methods.

### 4.3.1 Ball Milled Powders

Three different powder combinations were prepared by ball milling in acetone for 24 hours. The slurries were then stirred until dry and screened with a 100-mesh sieve.

Table 4.2: Starting materials of different batches.

| Batches | Raw Materials | SA, $m^2/g$ |
|---|---|---|
| **1.** **A**EE | AEE Mo, UBE-SN-E03, Sigma BN | < 0.8 |
| **2.** **C**limax, **C**oarse | Climax Mo, UBE-SN-E03, Cerac BN | ~ 3.4 |
| **3.** **C**limax, **F**ine | Climax Mo, UBE-SN-E10, AEE BN | ~ 3.9 |
| **4.** **A**EE, **F**ine | AEE Mo, UBE-SN-E10, AEE BN | ~ 1.3 |

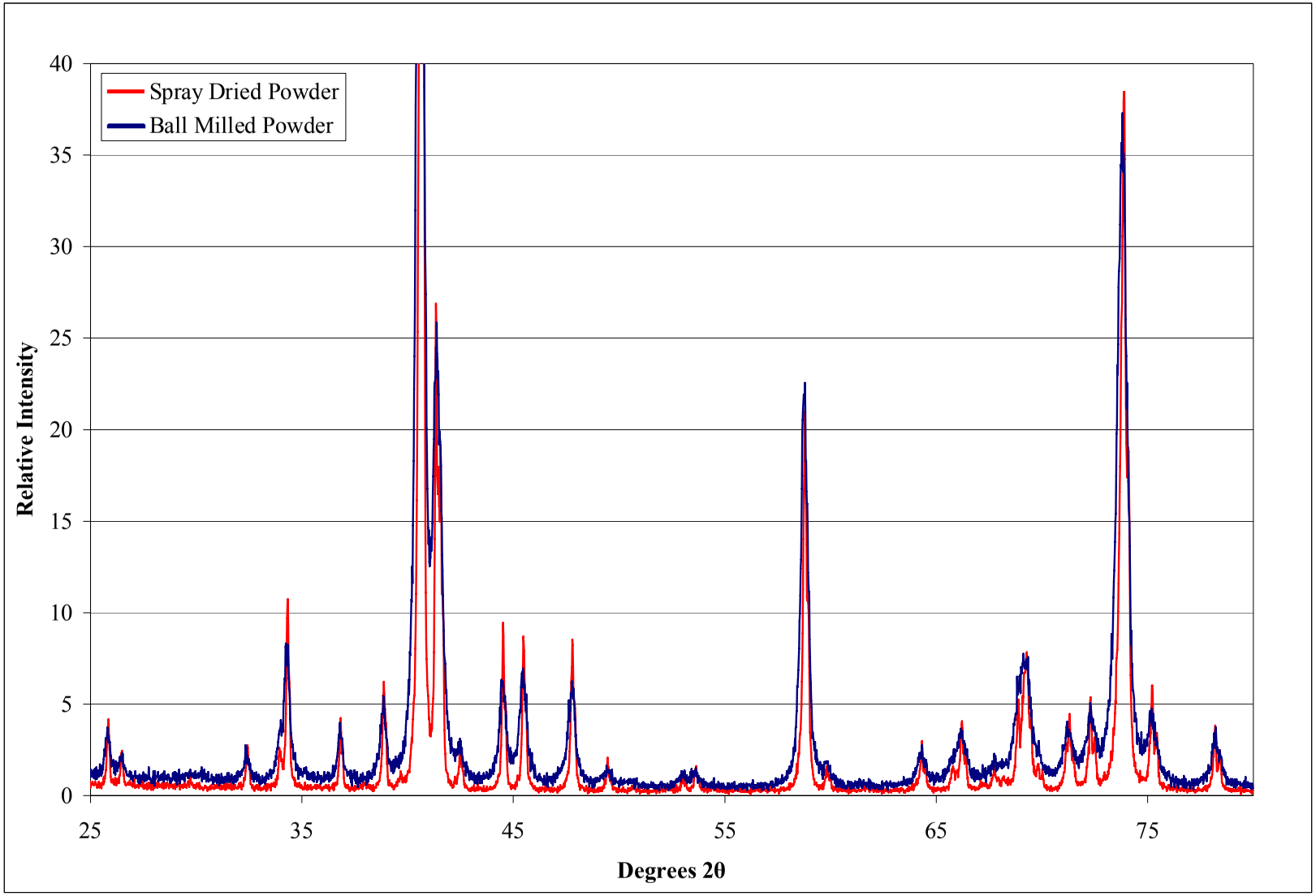


Figure 4.9: Comparison of XRD patterns from 1600ºC 6h firings for Climax-Coarse ball milled and spray dried powders.

The powder mixtures were dry pressed into cylindrical pellets. All pellets were fired in a 10:1 mixture of $N_2/H_2$ with a heating rate of 3ºC/min to temperature with a six hour hold, unless otherwise noted. Sintering data was obtained from the samples prepared for the phase analysis study discussed in Section 4.2. Bulk density values calculated from dimensional measurements are listed in Table 4.3 and plotted in Figure 4.10.

*4.3.1a Climax Molybdenum - Coarse Nitrides – Ball Milled*

In the original study of the AEE powder mixture, Section 4.1, the density achieved at 1600ºC was only 72% of theoretical. While the sintering curve had not flattened out by 1600ºC, firing at higher temperatures may lead to excessive grain growth. In an attempt to maintain a low sintering temperature, a sub-micron molybdenum powder was procured. The Climax molybdenum powder manufacturer reports the particle size as 100-500nm as compared to 1-2μm reported by AEE for their powder. Mixtures were prepared in two batches. The first, described in this section, used the coarser nitrides as described in Section 3.1. Pellets made from this mixture were pressed at 40ksi.

A rapid increase in density is observed beginning at 1200ºC. From the diffraction data it is known that this is the temperature range when the starting materials begin to react, forming A15. The intermetallic reaction forming T2 at 1300ºC appears to add additional energy to the system, causing an even faster increase in the density. This steep increase tapers off at 1400ºC where XRD analysis shows that the reactions are near completion. After this, the densities continue to increase at a slower rate due to sintering of molybdenum and the intermetallics. Another sample was fired at 1650ºC for 24 hours to observe the effect of extended hold time. The longer hold only increased the density 2% compared to a 9% increase for the AEE mixture.

Table 4.3: Density values and phase composition of samples prepared from ball milled powders.

| Sample | Firing Temperature | Green Density (g/cc) | Fired Density (g/cc) | Phases Present |
|---|---|---|---|---|
| Atlantic Engineers Coarsest Nitrides | 1200ºC 6h | 5.11 | 5.00 | Mo, $Si_3N_4$, BN |
| | 1300ºC 6h | | 5.45 | Mo, $Si_3N_4$, BN, A15, T2 |
| | 1400ºC 6h | | 5.44 | Mo, A15, T2 |
| | 1500ºC 6h | | 5.88 | - |
| | 1600ºC 6h | | 6.60 | - |
| | 1650ºC 6h | | 7.96 | - |
| | 1650ºC 24h | | 8.70 | Mo, A15, T2 |
| | | | | |
| Climax Molybdenum Coarse Nitrides | 1200ºC 6h | 4.27 | 5.12 | Mo, A15 |
| | 1300ºC 6h | | 6.76 | Mo, A15, T2 |
| | 1400ºC 6h | | 7.45 | Mo, A15, T2 |
| | 1500ºC 6h | | 7.62 | - |
| | 1600ºC 6h | | 8.03 | Mo, A15, T2 |
| | 1650ºC 6h | | 8.32 | Mo, A15, T2 |
| | 1650ºC 24h | | 8.48 | Mo, A15, T2 |
| | | | | |
| Climax Molybdenum Fine Nitrides | 1200ºC 6h | 3.52 | 4.49 | Mo, A15 |
| | 1300ºC 6h | | 6.16 | Mo, A15, T2 |
| | 1400ºC 6h | | 6.75 | - |
| | 1500ºC 6h | | 7.01 | - |
| | 1600ºC 6h | | 7.34 | Mo, A15, T2 |
| | 1650ºC 6h | | 7.62 | Mo, A15, T2 |
| | 1650ºC 24h | | 7.89 | - |

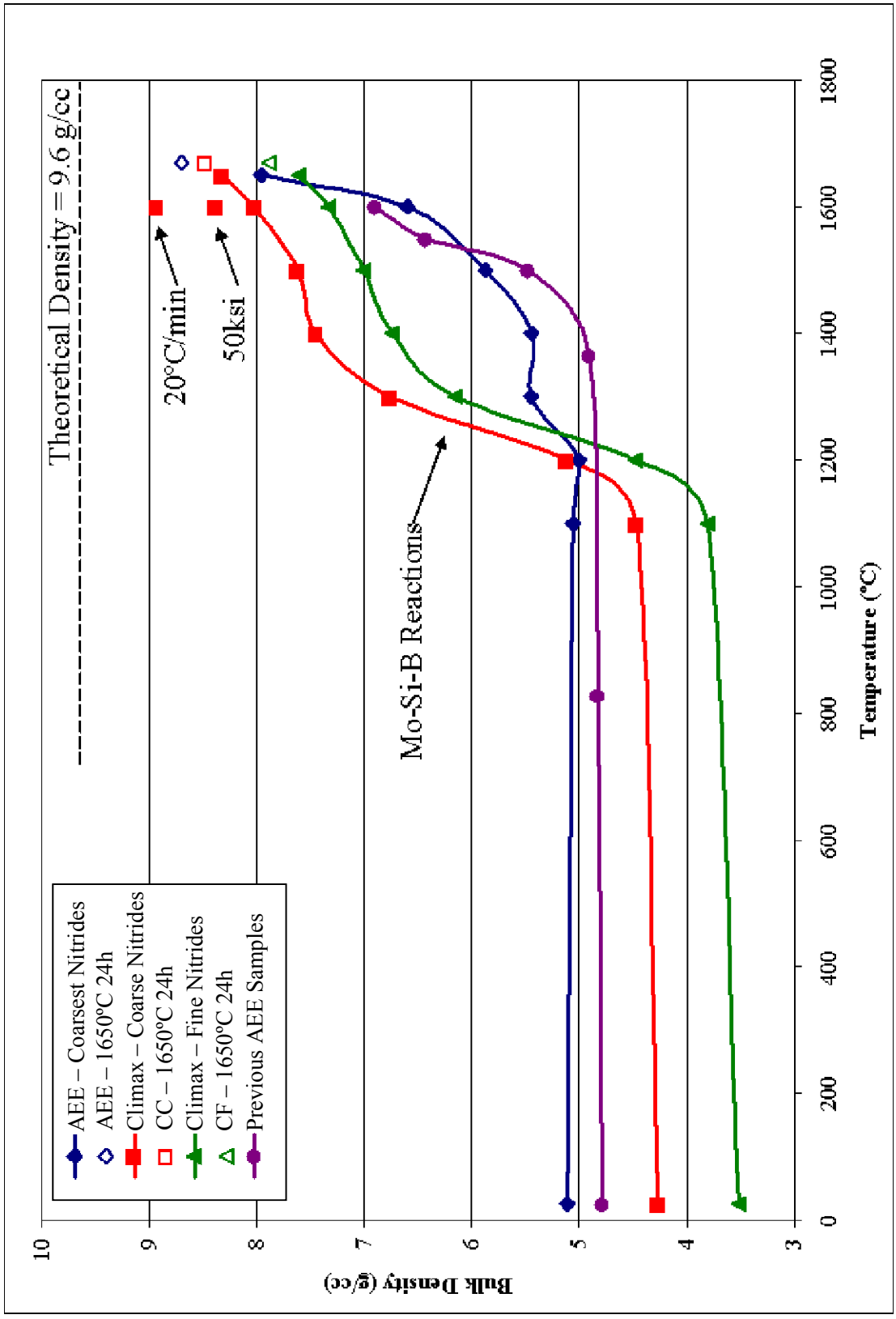


Figure 4.10: Sintering curves for samples of different starting materials prepared by ball milling.

From the data at 1650ºC-6h, it initially does not appear that using the finer molybdenum powder significantly increases the final density, as compared to the AEE samples. This is due to the lower starting green density of the Climax samples. Comparing the change from the green state to 1650ºC-6h, there was a 95% increase in density for the Climax-Coarse samples while the AEE samples only increased 56%. Increasing the green density of the Climax-Coarse pellets further increased the final density 5%, as illustrated by the sample pressed at 50ksi and fired to 1600ºC-6h.

At the 3ºC/min heating rate, it was doubtful that transient liquid sintering was occurring. The diffraction patterns show that the reactions between $Si_3N_4$ and molybdenum are nearly complete well below melting temperature of silicon (1412ºC). An attempt was made to promote the formation of liquid silicon by heating the sample faster to force the $Si_3N_4$/molybdenum reaction to a higher temperature. The heating rate of the furnace was increased from 3ºC/min to 20ºC/min to 1600ºC. This led to an increase in density from 8.03 to 8.93 g/cc or 93% TD, possibly due to the formation of transient liquid silicon.

*4.3.1b Climax Molybdenum - Fine Nitrides – Ball Milled*

Pellets made from this mixture were only pressed at 15ksi due to cracking of the green pellets at higher pressures. This is likely due to the increase in total surface area of the powder mixture caused by the finer nitrides. The sintering behavior of this powder mixture closely follows that of the Climax-Coarse batch. The sintering curves for these two batches are displaced by the difference in the green densities of the samples.

*4.3.1c AEE Molybdenum – Coarsest Nitrides – Ball Milled*

These firings were done to reproduce the initial experiments discussed in Section 4.1. This powder mixture used the coarse AEE molybdenum powder, the coarser grade of $Si_3N_4$ and the coarsest BN powder (Sigma-Aldrich). The new pellets differed from the original experiments in that they were pressed at 40ksi.

Like the Climax-Coarse powder, the AEE mixture has an increase in the rate of densification at the temperatures when A15 and T2 begin to form. In this case, the increase has been displaced to a higher temperature due to the larger particle size of the molybdenum powder. Examination of the x-ray diffraction patterns shows that formation of the intermetallics is not complete by 1300ºC, so it is not fully clear why between 1300ºC to 1400ºC the densification curve flattens out. It is probable that the reaction between the starting materials causes coarsening of the particles. These particles are likely too coarse to sinter in the temperature region between 1300ºC and 1400ºC. After 1400ºC the density continues to increase because the temperature is high enough to sinter the molybdenum and intermetallics. Evidence of this is also present in the Climax-Coarse curve which shows a similar densification slow down between 1400ºC and 1500ºC, after reaction completion.

By lengthening the hold time at 1650ºC for the AEE mixture from 6 to 24 hours, the density was increased from 7.96 to 8.70 g/cc. This was the most gain observed for the 24 hour hold in the three powder combinations, demonstrating the densification of this mixture could further be improved by higher temperatures and extended hold times.

The density measurements from the original AEE samples have been plotted for comparison. The increased rate of densification is not observed in this curve. This is

likely because the data taken at 1365ºC had zero hold time. The first sample in this data series fired with a hold time was the sample at 1500ºC-4h, which was past the observed reaction temperature.

4.3.2 High Energy Milling and Lubricant Addition – Climax-Coarse

An attempt was made to increase green densities by milling the raw materials with much higher energy to promote better deagglomeration of the molybdenum and to improve dispersion of the nitrides. In all studies up to this point, powders were mixed by low energy ball milling. Higher energy milling was achieved by mixing the samples using a commercial paint shaker. This method was tested using the Climax molybdenum with the coarse nitrides. Two approaches were made, one using 3mm spherical $ZrO_2$ media and the other using 6mm spherical $Al_2O_3$ media. The powders were mixed in acetone for 15 minutes in the paint shaker and then stirred until dry to prevent separation. These pellets were pressed at 40ksi.

Another ball milled batch was prepared with 0.5wt% stearic acid added as a lubricant to increase green density. Stearic acid was chosen because it would dissolve in acetone during milling and coat the powder particles during stir drying. Due to cracking at higher pressures, this powder mixture was only pressed at 30ksi and did not lead to any increase in initial density. The pellets were fired in a 10:1 mixture of $N_2/H_2$ at 1ºC/min to 300ºC, with a one hour hold for binder burnout. Firing was continued at 3ºC/min to 1600ºC with a 6 hour hold. The samples were fired together with a sample pressed from the original Climax-Coarse ball milled powder for comparison.

Bulk densities for the samples were measured using dimensional measurements and are listed in Table 4.4. Addition of the stearic acid as a lubricant did not help either

Table 4.4: Densities of samples prepared with lubricant and by high energy milling.

| **Powder Preparation Method** | **Green Density (g/cc)** | **Fired Density (g/cc)** |
|---|---|---|
| **Ball Milled 24h - 1mm $ZrO_2$ media**<br>1ºC/min → 300ºC - 1h hold<br>3ºC/min → 1600ºC - 6h hold | 4.14 | 7.78 |
| | | |
| **Paint Shaker - 1mm $ZrO_2$ media**<br>1ºC/min → 300ºC - 1h hold<br>3ºC/min → 1600ºC - 6h hold | 4.23 | 8.34 |
| | | |
| **Paint Shaker - 6mm $Al_2O_3$ media**<br>1ºC/min → 300ºC - 1h hold<br>3ºC/min → 1600ºC - 6h hold | 4.13 | 8.37 |
| | | |
| **Ball Milled 24h - 1mm $ZrO_2$ media with 0.5wt% Stearic Acid**<br>1ºC/min → 300ºC - 1h hold<br>3ºC/min → 1600ºC - 6h hold | 4.2 | 7.85 |

the starting or final density. While the higher energy milling did not improve the green density, it does lead to an improvement of the final density, increasing the density from 81% for the ball milled sample to 87% for the samples mixed on the paint shaker. The higher energy milling process likely decreases porosity trapped by hard powder agglomerates. The choice of media used for mixing did not cause any difference in the densities. Micrographs of the materials will be needed to determine if there are any microstructural differences.

4.3.3 Spray Dried Powders

While addition of stearic acid to the powder should have increased the green density, the reduction of green strength did not allow high pressing pressure. An attempt at eliminating pressing laminations was made, this time adding 1wt% PMMA (2008) as a binder in addition to the stearic acid. In addition to acting as a binder, PMMA is a commonly used dispersant which should help maintain a fine dispersion of the nitride powders. Based on the density increase observed for the samples prepared using powders mixed by high energy milling, the new batches of powders were also mixed using the paint shaker. To avoid separation of the binder from the powder during drying, the spray drying process discussed in Section 3.2.3 was used to quickly dry the slurry. Spray drying of the powder should give the added benefit of preventing differential settling due to density differences in the starting powders. Pressing of the powder spheres formed by spray drying will also help ensure uniformity by reducing large voids in the green pellets.

4.3.4 Heating Rate and Composition Studies with Spray Dried Powders

Based on the drastic density gain encountered by increasing the heating rate of the sample, as discussed in Section 4.3.1a, a study was conducted to examine the effect of

heating rates on the final densities of the samples. Experiments were conducted on three powder mixtures prepared by spray drying: Climax-Coarse, Climax-Fine and AEE-Fine. The first two mixtures used the same starting powders previously discussed. The AEE-Fine mixture used the AEE molybdenum powder with the finest grades of the nitrides. It was determined in the green density study discussed in Section 3.3.1 that the spray dried powder mixtures could be pressed at 50ksi without resulting in cracked pellets. Climax-Coarse ball milled powder pellets pressed at 50ksi were fired for comparison to earlier findings. Binder burnout was achieved by heating the samples at 1ºC/min to 300ºC with a one hour hold. All samples were fired in a 10:1 mixture of $N_2/H_2$ and held at temperature for 6h before cooling. The densities measured by Archimedes method are listed in Table 4.5. The relative bulk densities and the amount of open porosity measured for each sample are plotted in Figure 4.11.

Climax-Coarse spray dried and ball milled samples were fired to 1600ºC at three different heating rates; 1ºC/min, 3ºC/min and 30ºC/min. Samples were also fired to 1650ºC at 3ºC/min and 30ºC/min. During the 1600ºC firing at 30ºC/min, the ball milled sample became severely distorted from a large void which had formed in the pellet. The density value for this data point was taken from the sample fired at 20ºC/min discussed in Section 4.3.1a. This void likely formed because the fast heating rate caused a rapid expansion of air trapped in the powder compact. No problems were encountered with any of the other samples fired at 30ºC/min. In all cases it is apparent that increasing the heating rate of the samples leads to a higher density, with some samples higher than 95% of the theoretical density. At this point, post-sintering methods such as hot isostatic

Table 4.5: Spray dried sample density comparison.

| **Sample** | **Firing Temperature** | **Heating Rate** | **Green Density (g/cc)** | **Fired Density (g/cc)** |
|---|---|---|---|---|
| Climax Molybdenum Coarse Nitrides Ball Milled | 1600ºC 6h | 1ºC/min | 4.42 | 8.12 |
| | 1600ºC 6h | 3ºC/min | | 8.54 |
| | 1600ºC 6h | 20ºC/min | | 9.30 |
| | 1650ºC 6h | 3ºC/min | | 8.81 |
| | 1650ºC 6h | 30ºC/min | | 8.91 |
| | | | | |
| Climax Molybdenum Coarse Nitrides Spray Dried | 1600ºC 6h | 1ºC/min | 4.40 | 8.23 |
| | 1600ºC 6h | 3ºC/min | | 8.38 |
| | 1600ºC 6h | 30ºC/min | | 9.09 |
| | 1650ºC 6h | 3ºC/min | | 8.73 |
| | 1650ºC 6h | 30ºC/min | | 9.11 |
| | | | | |
| Climax Molybdenum Fine Nitrides Spray Dried | 1600ºC 6h | 3ºC/min | 4.46 | 7.75 |
| | 1600ºC 6h | 30ºC/min | | 8.84 |
| | 1650ºC 6h | 3ºC/min | | 8.16 |
| | 1650ºC 6h | 30ºC/min | | 9.06 |
| | | | | |
| Atlantic Engineers Fine Nitrides Spray Dried | 1600ºC 6h | 3ºC/min | 5.75 | 7.74 |
| | 1600ºC 6h | 30ºC/min | | 7.50 |
| | 1650ºC 6h | 3ºC/min | | 8.22 |
| | 1650ºC 6h | 30ºC/min | | 8.51 |

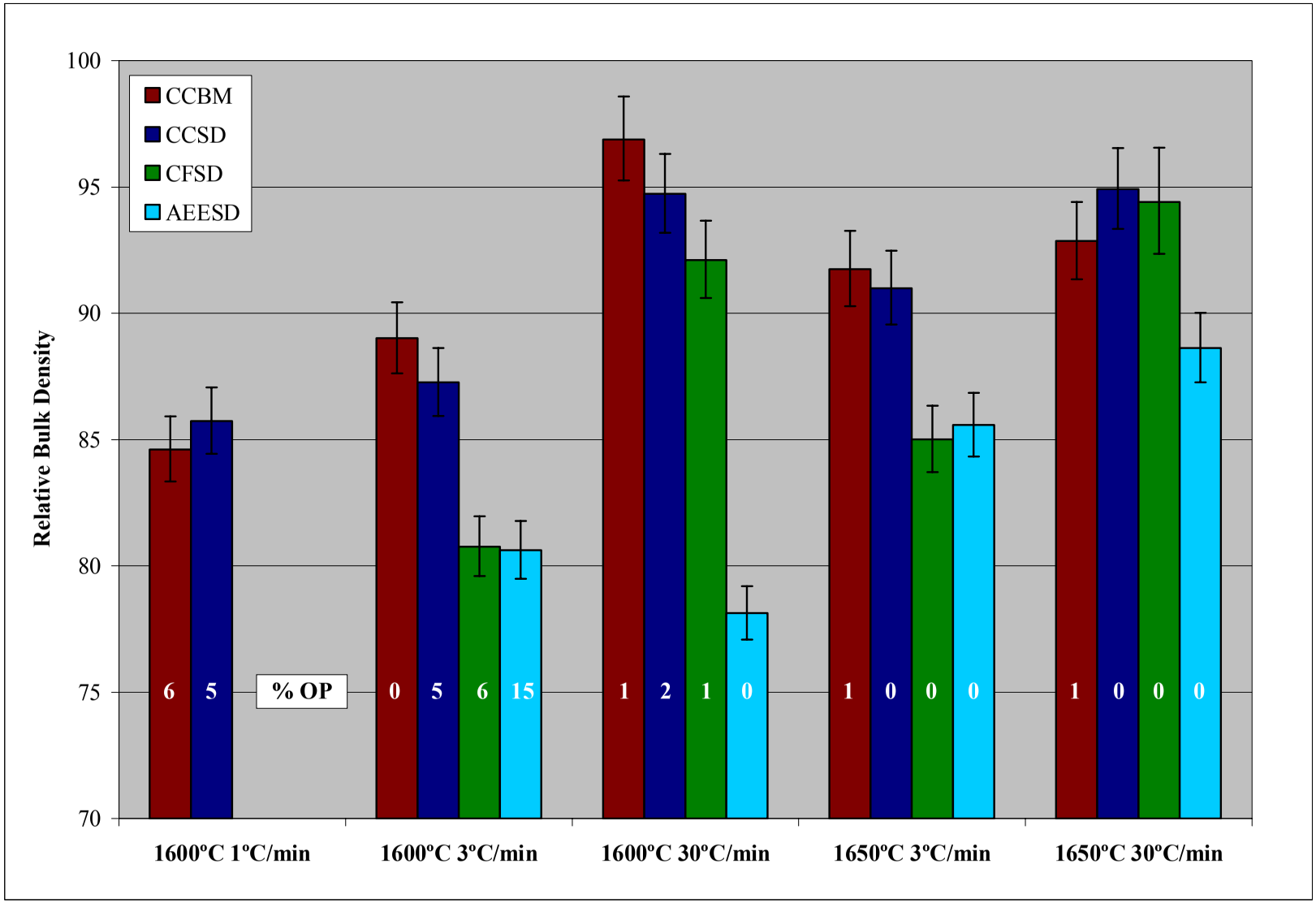


Figure 4.11: Comparison of heating rates and temperature on spray dried powder sample densities.

pressing could be used to remove any remaining closed porosity and bring the material to its theoretical density.

Climax-Fine spray dried powder samples were fired at 3ºC/min and 30ºC/min to 1600ºC and 1650ºC. In both cases the faster heating rate caused a large density increase, showing the most effect of the four powder mixtures. It is not clear why the Climax-Fine samples have such a low density compared to the Climax-Coarse samples fired at 3ºC/min since the green densities of the pellets are comparable. It is possible that the increased amount of oxygen impurity in the finer nitride powders hinders sintering. SEM analysis will determine if this powder combination creates a microstructure worth pursuing, in which case this problem will require further investigation.

The densities measured for the AEE-Fine spray dried powder samples gave mixed results. For 1600ºC, increasing the firing rate from 3ºC/min to 30ºC/min caused a slight decrease in the density, although the difference is close to the amount of error in the measurement. For the samples fired at 3ºC/min and 30ºC/min to 1650ºC, there was a small increase in density associated with the faster heating rate, but the change was not as significant as seen with the Climax molybdenum samples. Compared to the previous AEE batch, no significant change in density was observed due to the finer nitrides. While the densities measured for the AEE-Fine samples were higher, that change can be credited to the increased green density of the pellets pressed from the spray dried powder.

For the most part, increasing the heating rate has resulted in a density gains. While these initial results are promising, it is not apparent how they will translate to larger parts. For samples of larger dimensions, heat flow through the sample will limit the heating rate. Differential heating rates in samples could cause problems with warping.

More examination will be needed to determine a feasible heating rate for the fabrication of actual parts.

## 4.4 Microstructural Analysis

Electron backscatter microscopy was used to investigate the microstructures of the fired samples. To avoid any surface variations, the pellets were ground to the center before polishing. While the images do not distinguish between A15 and T2, due to its higher average atomic number molybdenum appears lighter than the intermetallic phases. These images show that this process is able to produce an alloy with finely dispersed molybdenum and intermetallic phases. While it is not possible to make definitive statements regarding the properties of the material based from the SEM images, qualitative comparison of the phase distribution, grain size and porosity distribution can be made. These images provide evidence that by varying the starting materials and processing conditions, the microstructure of the alloy made by this process can be engineered.

### 4.4.1 High Energy Milling and Lubricant Addition – Climax-Coarse

Two Climax-Coarse powder batches were mixed using a paint shaker with different sized media and another was prepared with a powder lubricant by ball milling. The samples were pressed at 40ksi and fired at 3ºC/min to 1600ºC with a 6 hour hold. In Figure 4.12 these samples are compared to a similar sample pressed from the Climax-Coarse ball milled powder. Comparing the micrographs, it does not appear that difference in milling method significantly affects the phase distribution of the samples. Comparing the ball milled samples, it does not appear that the addition of stearic acid changed the presence of very fine porosity, but it seems to have eliminated the pores in

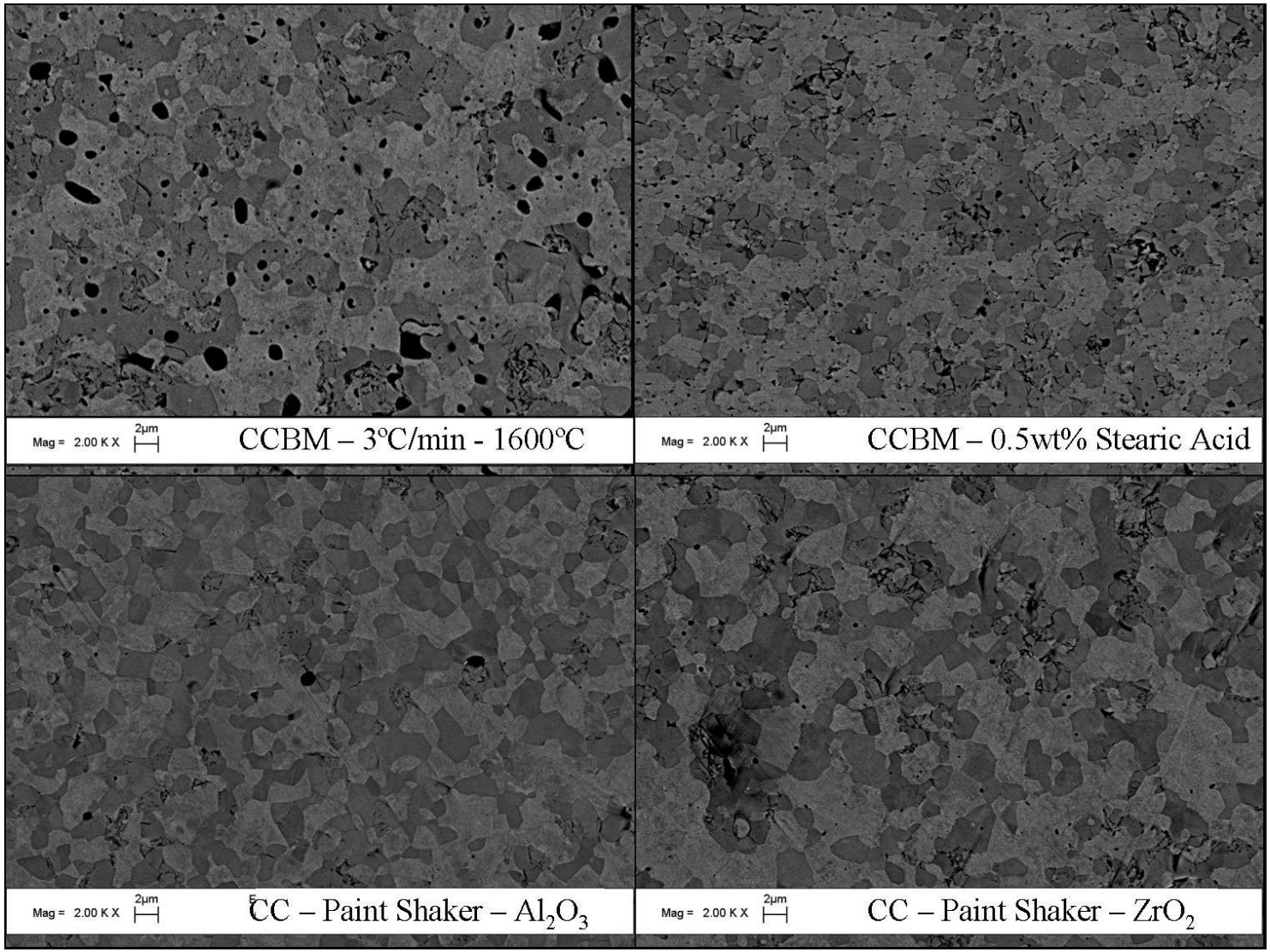


Figure 4.12: Microstructures of samples prepared by different powder preparation methods; fired at 3ºC/min to 1600ºC 6h.

the 1-2μm range. The density gain observed with high energy milling is due to the elimination of the fine porosity present in the ball milled samples. This is likely due to the breaking up of hard powder agglomerates which trap porosity. In this study, parameters such as time and intensity of milling have not been quantified for effects on the microstructure. Better understanding could help in further defect reduction.

4.4.2 Climax Molybdenum - Coarse Nitrides – Ball Milled and Spray Dried

SEM images were taken to evaluate the microstructures of the samples prepared using the Climax-Coarse ball milled powder. Figure 4.13 compares the microstructures achieved by firing the samples at different heating rates. The finer porosity associated with the lower energy ball milling is present in these samples. The large porosity found in the 20ºC/min sample is probably due to the fact that this sample was only pressed at 40ksi, while the rest of the samples were pressed at 50ksi. It is appears from the images that for this powder batch, increasing the heating rate lead to a finer dispersion of the intermetallic phases. Even after heating to 1650ºC, the grain sizes for the molybdenum and intermetallics are kept as low as 2-4μm.

Figure 4.14 compares the Climax-Coarse samples fired at different heating rates for 1600ºC and 1650ºC. At 1ºC/min to 1600ºC, the intermetallic phases are less well dispersed than they are in the rest of the samples. The samples fired at higher heating rates appear dense and have well dispersed intermetallic phases. Closer magnifications of these samples are shown in Figure 4.15. The microstructures of these four samples are very comparable, with the grain structure of the samples fired at 1650ºC appearing only slightly coarser. It is apparent that the improvements in powder processing have led to a

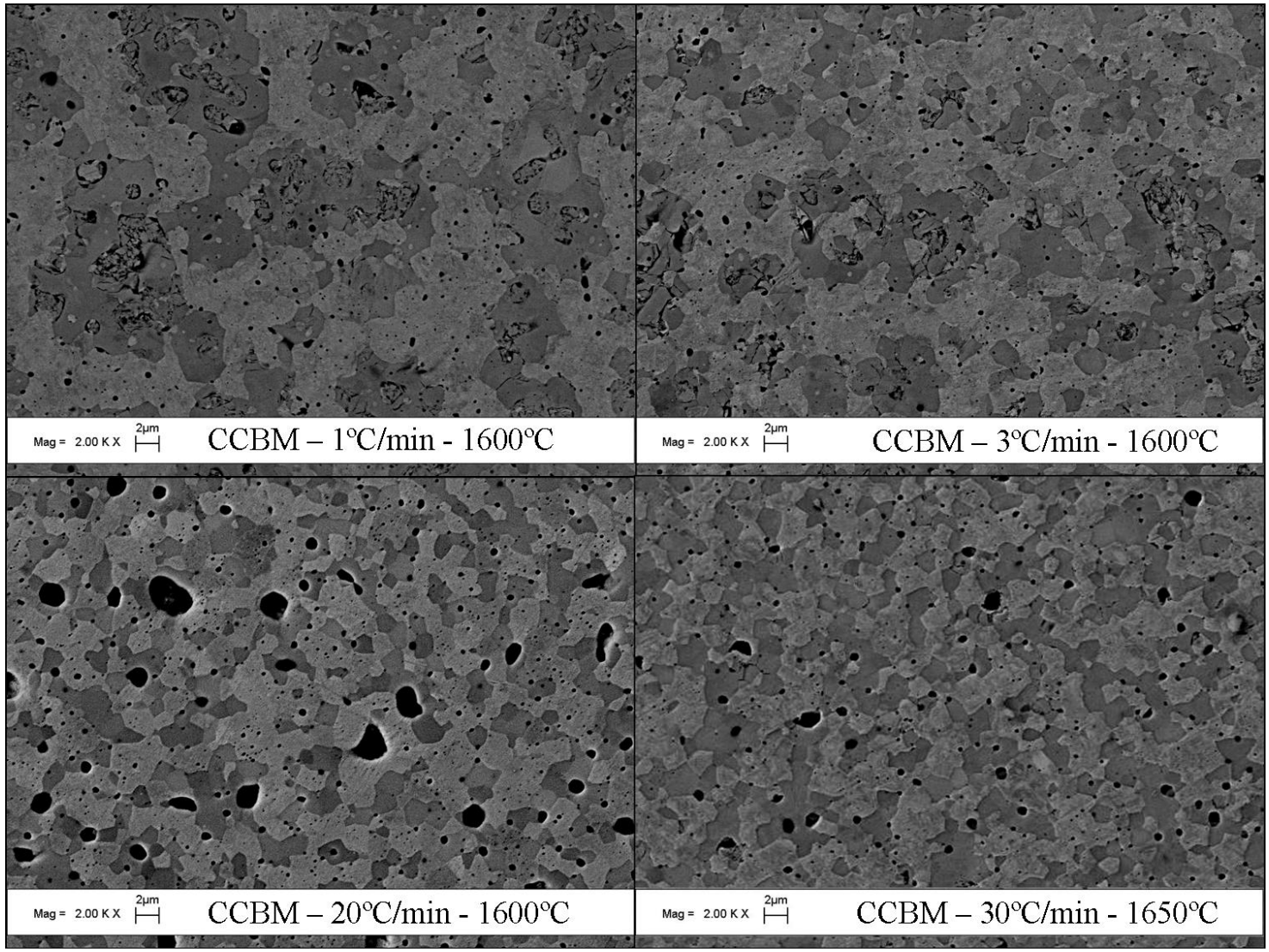


Figure 4.13: Microstructures of Climax-Coarse ball milled samples fired at different heating rates.

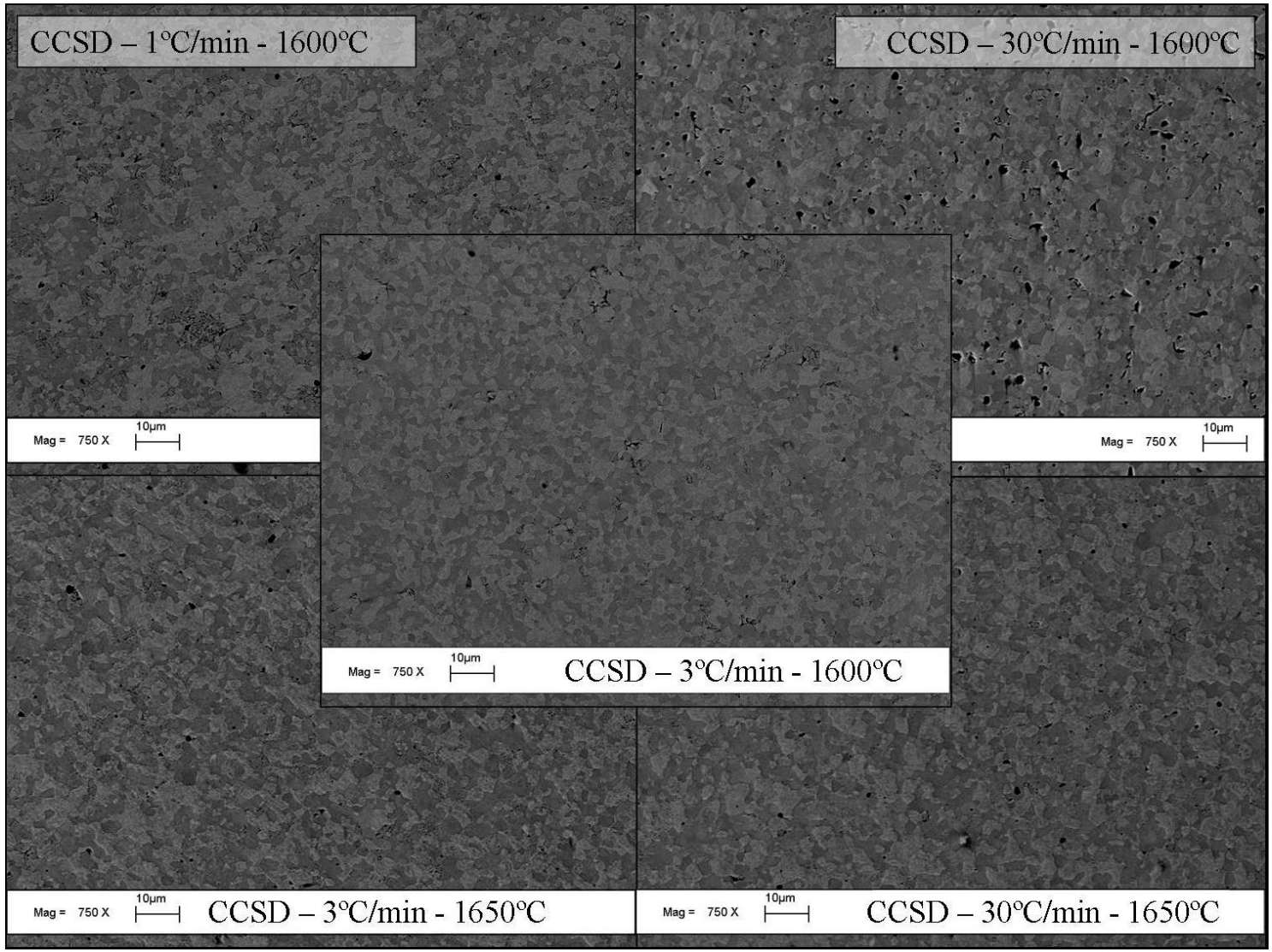


Figure 4.14: Microstructures of Climax-Coarse spray dried samples fired at different heating rates (750X).

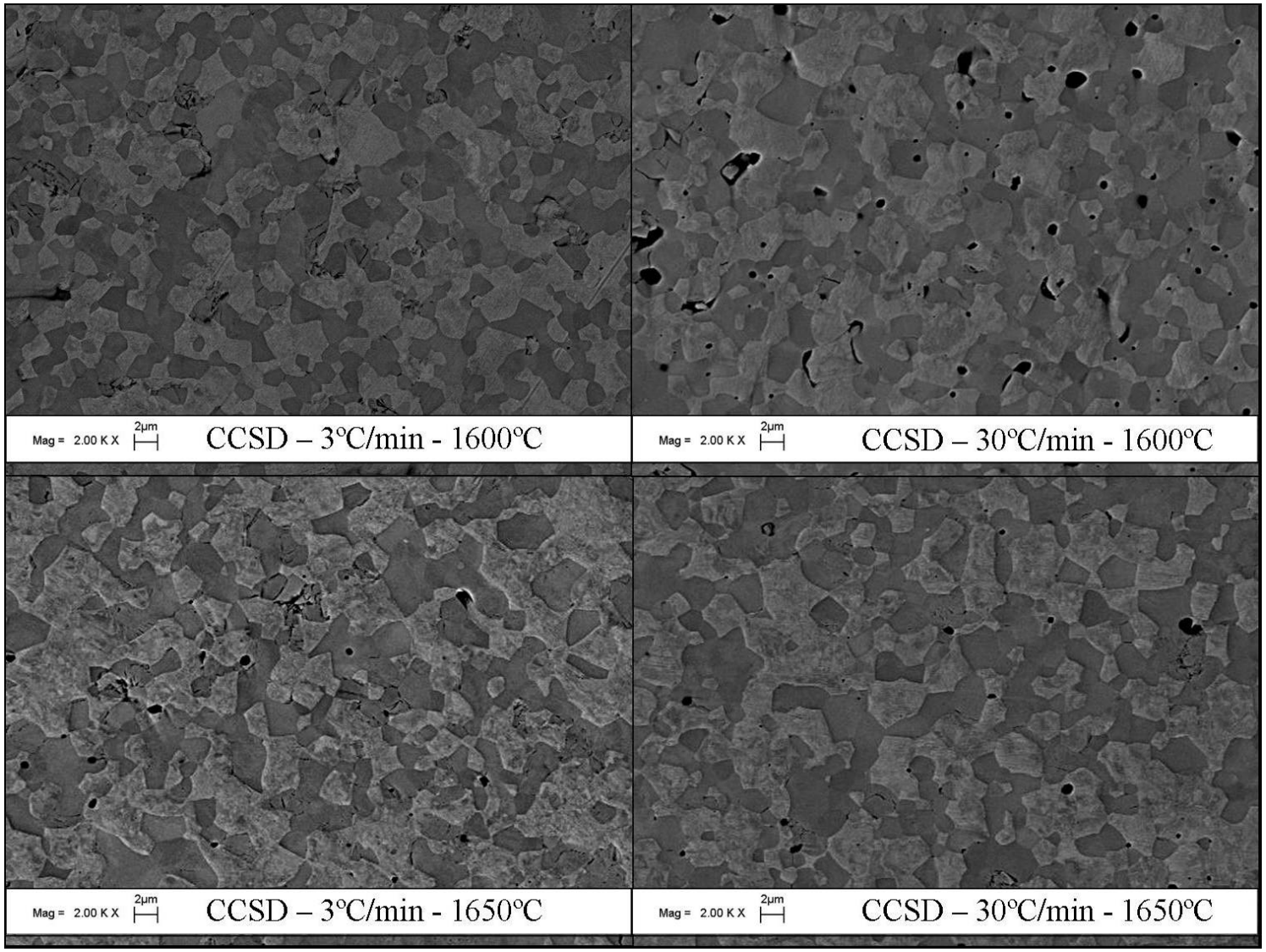


Figure 4.15: Microstructures of Climax-Coarse spray dried samples fired at different heating rates (2000X).

better microstructure. The spray dried powder samples do not show the fine porosity that is found with the ball milled samples and there is less clumping of the intermetallics.

Another set of Climax-Coarse pellets were fired at 3ºC/min to 1500ºC. Their microstructures are compared in Figure 4.16. While the microstructure is not fully dense, the spray dried sample has much smaller pores than the ball milled sample and the 1-2μm grain size of the material is significantly finer than that observed at 1600ºC. It may be possible to obtain fully dense samples and still retain the very fine grain size by processes such as hot pressing and HIPing which can achieve high densities at lower temperatures than conventional sintering.

4.4.3 Climax Molybdenum - Fine Nitrides – Spray Dried

The microstructures of the Climax-Fine spray dried samples fired at different heating rates to 1600ºC and 1650ºC are compared in Figure 4.17. The sample fired at 3ºC/min to 1600ºC has a very discontinuous microstructure with large alternating regions of molybdenum and intermetallic phases. The intermetallic regions are porous and have not sintered well. The sample fired at 3ºC/min to 1650ºC also has a poor microstructure with large pores. These pores are not present in the sample fired at a 1600ºC and appear anomalous. They may have been caused by an experimental error such as insufficient pressing pressure. Looking at the distribution of the phases, the intermetallic grains are also grouped together like the 1600ºC sample. Compared to these two samples, the pellets fired at 30ºC/min have a much more dispersed microstructure. This increase in heating rate was also accompanied by a large jump in density. It is not apparent why increasing the heating rate has such a great effect on these samples as compared to the other powder mixtures fired under the same conditions.

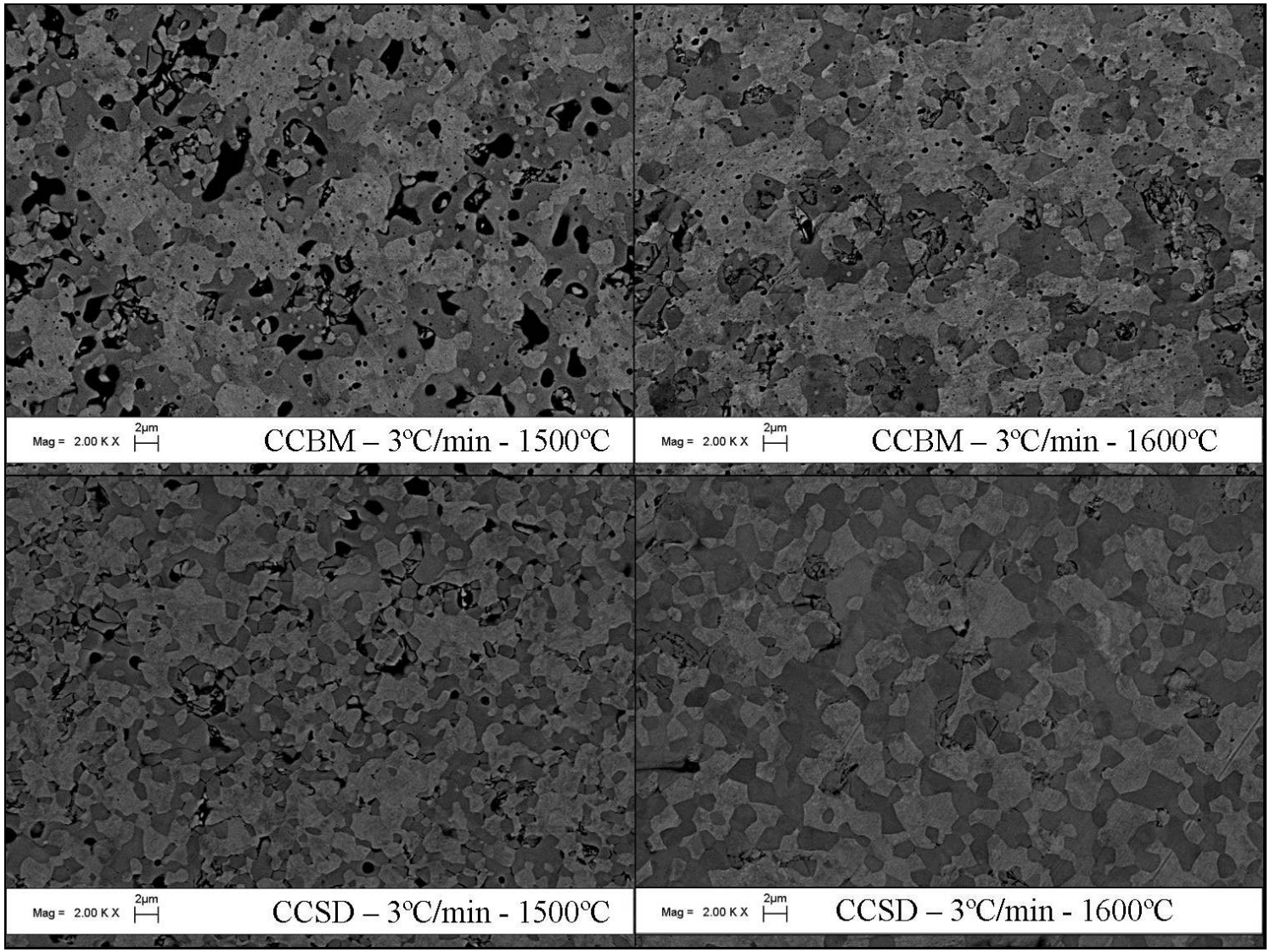


Figure 4.16: Microstructural comparisons of Climax-Coarse ball milled and spray dried samples fired at 1500ºC and 1600ºC.

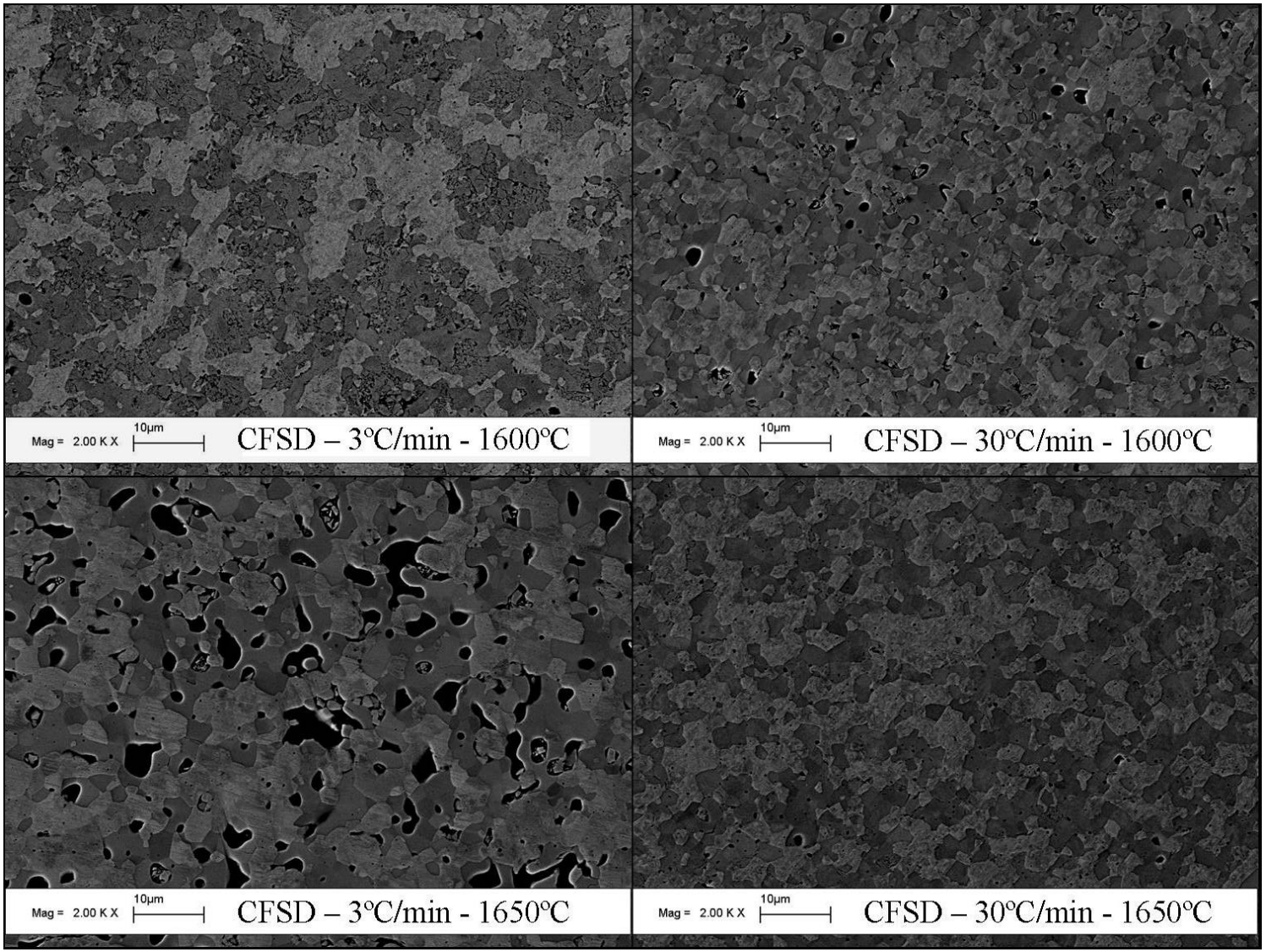


Figure 4.17: Microstructures of Climax-Fine spray dried samples fired at different heating rates.

4.4.4 AEE Molybdenum – Fine Nitrides – Spray Dried

Microstructural comparisons of the AEE-Fine spray dried samples are shown in Figure 4.18. The large pores present in the samples fired to 1600ºC are consistent with the low densities measured for these samples. Examination of the sintering behavior (Section 4.3.1c) showed that due to the coarser grain size of the molybdenum, the AEE mixture still undergoes considerable densification above 1600ºC. Increasing the temperature to 1650ºC significantly improves the microstructure. Large pores are no longer present and the intermetallics are well dispersed. While there was a slight density decrease at 1600ºC for the sample fired at 30ºC/min, it does not appear that the rapid heating rate caused any major changes in the microstructure of these samples.

## 4.5 Comparison of Achieved Microstructures to Other Research

The microstructures obtained using the nitride-based synthesis method developed in this project have a better dispersion of the intermetallics and a finer grain size than has been demonstrated by other researchers. In addition, the experimental methods used in this project are significantly simpler than those used by other researchers. Examining the micrographs presented in Chapter 2, it is clear that this process creates microstructures which are more refined than those obtained from melt casting or by HIPing of pre-alloyed powders. In all of the literature reviewed, the extruded alloy developed by Jéhanno et al. was the closest to the desired microstructure of a fully continuous molybdenum matrix with well dispersed intermetallics[2]. Comparing the micrograph of this alloy to those for the Climax-Coarse spray dried samples at fired 1500ºC and 1600ºC, Figure 4.19, it is apparent that the reaction-based process creates a more uniform dispersion of

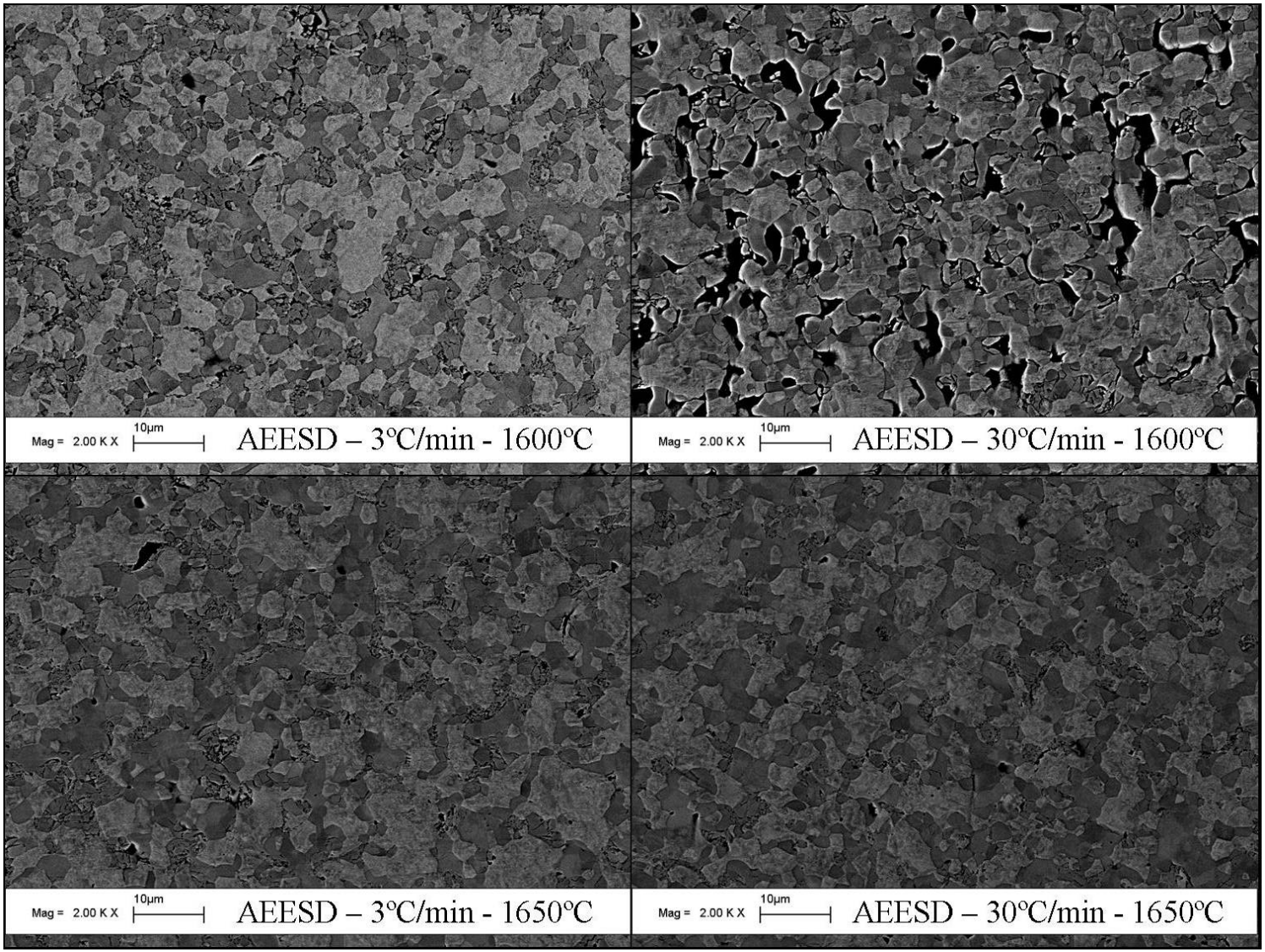


Figure 4.18: Microstructures of AEE-Fine spray dried samples fired at different heating rates.

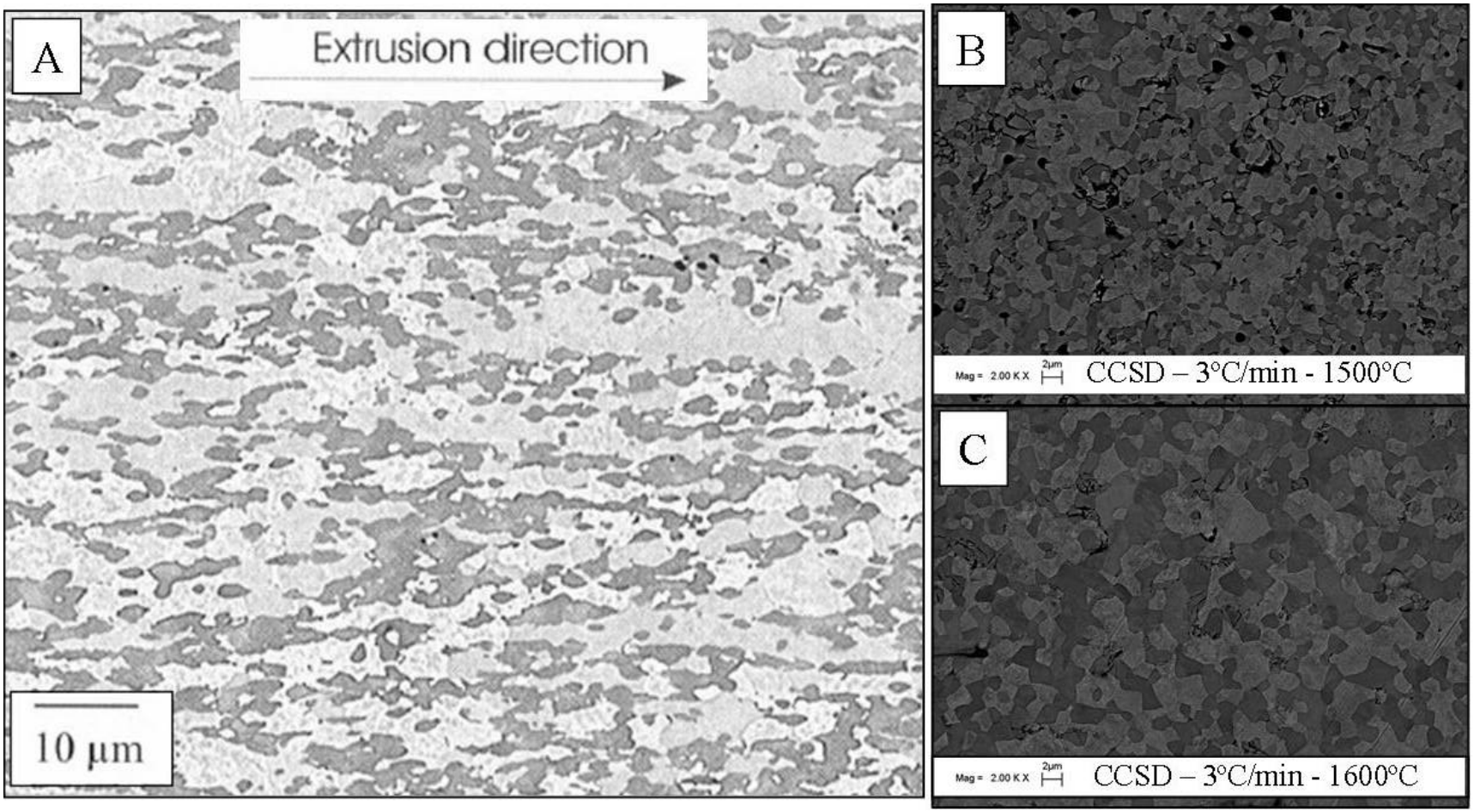


Figure 4.19: Microstructural comparison of an extruded alloy $(A)^2$ and alloys produced by the reaction synthesis method developed in this project: 1500ºC (B) and 1600ºC (C).

intermetallics with a finer grain size. By reducing the intermetallic content of the alloy, it should be possible to create a continuous Mo-matrix with this nitride reaction process.

## 4.6 Skin Formation and Density Discrepancies

There is a consistent discrepancy between the densities measured and that observed in micrographs taken from the center of the samples. For example, the Archimedes density of the Climax-Coarse sample fired at 30ºC/min to 1650ºC is 95% of theoretical, but the microstructure of the material, shown in Figure 4.14, appears almost fully dense. The density discrepancy is apparently caused by a skin effect where this surface layer contains porosity levels of ~20-30%. This is apparent in an edge picture of the sample, Figure 4.20, where a skin thickness of ~110μm is seen. The skin has a high porosity level and surrounds a composite Mo/intermetallic center with little observable porosity. The dimensions of this sample are 3.0mm thick x 7.5mm diameter, therefore this skin represents 13% of the volume of the sample with an estimated 20% porosity level. This contributes 3% of the overall porosity in the sample, accounting for most of the samples porosity. It is therefore feasible in some cases that the actual density of these materials would approach theoretical if the skin effect were removed or eliminated.

In future efforts, the mechanism and kinetics of skin formation should be determined to minimize this effect. Initial assessment of this problem lead to the conclusion that oxygen in the furnace system may be causing this effect. Very small leaks in the gas line connections or at the furnace end caps would allow trace amounts of oxygen into the system. It is possible that the contaminant oxygen diffuses into the porous surface of the pellet and is trapped by subsequent densification which creates a hermetic surface layer. At higher temperatures $SiO_2$ and $B_2O_3$ would form, hence the

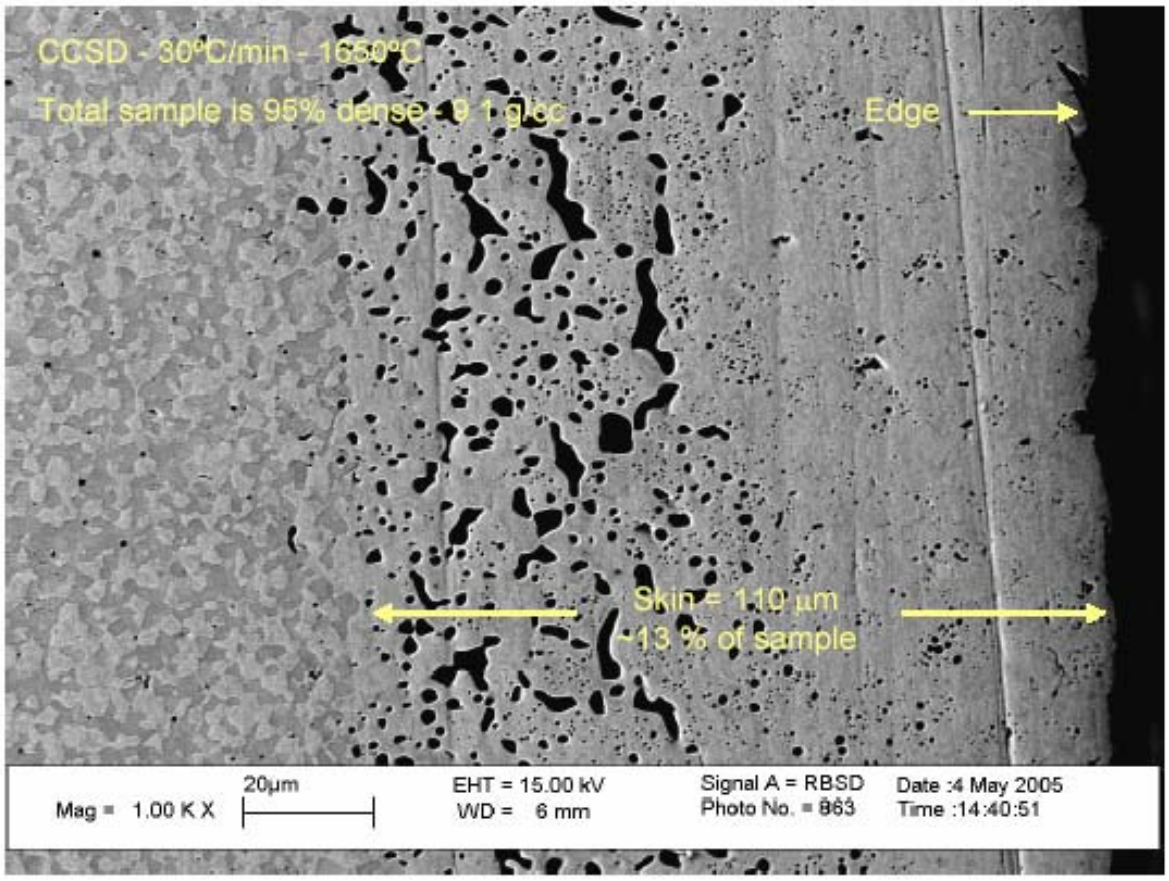


Figure 4.20: Porous skin layer formed on sample surface after firing.

lack of intermetallic phases in the skin layer. The oxidized molybdenum would gasify at high temperatures, forming the porosity.

The thickness of the skin appears to depend on the firing conditions and starting powders for the sample. In Figure 4.21 it is apparent that at slower heating rates a thicker skin is formed. This is likely because it takes longer to reach the temperature at which the hermetic surface barrier forms and prevents further oxygen penetration into the pellet. This may also be the reason that a thinner skin is observed for the Climax samples than for the AEE samples, as seen in Figure 4.22. Because the Climax samples densify at a lower temperature, they may form a protective skin faster, hence having less time for oxygen impurity to penetrate the sample. If oxygen is completely removed from the sintering process by eliminating leaks or by active gettering of the incoming gases, it may be possible to prevent skin formation.

## 4.7 Transient Liquid Sintering

An original hypothesis of the project was that formation of transient liquid silicon would greatly enhance sintering of the material. XRD examination in this study appears to discount this theory for these samples because the reactions between the starting materials have neared completion by the melting point of silicon. Krishnarao reported formation of elemental silicon during the reaction of molybdenum and silicon nitride to form $MoSi_2$.[18] This is may be a non-equilibrium phase caused by slow kinetics of the reaction. $MoSi_2$ is 66at% silicon and decomposition may be occurring before complete reaction of the silicon nitride. Due to the high surface areas of the starting materials and the low silicon content in this study, the reactions may be complete before the temperature required for silicon nitride to spontaneously decompose. Increased heating

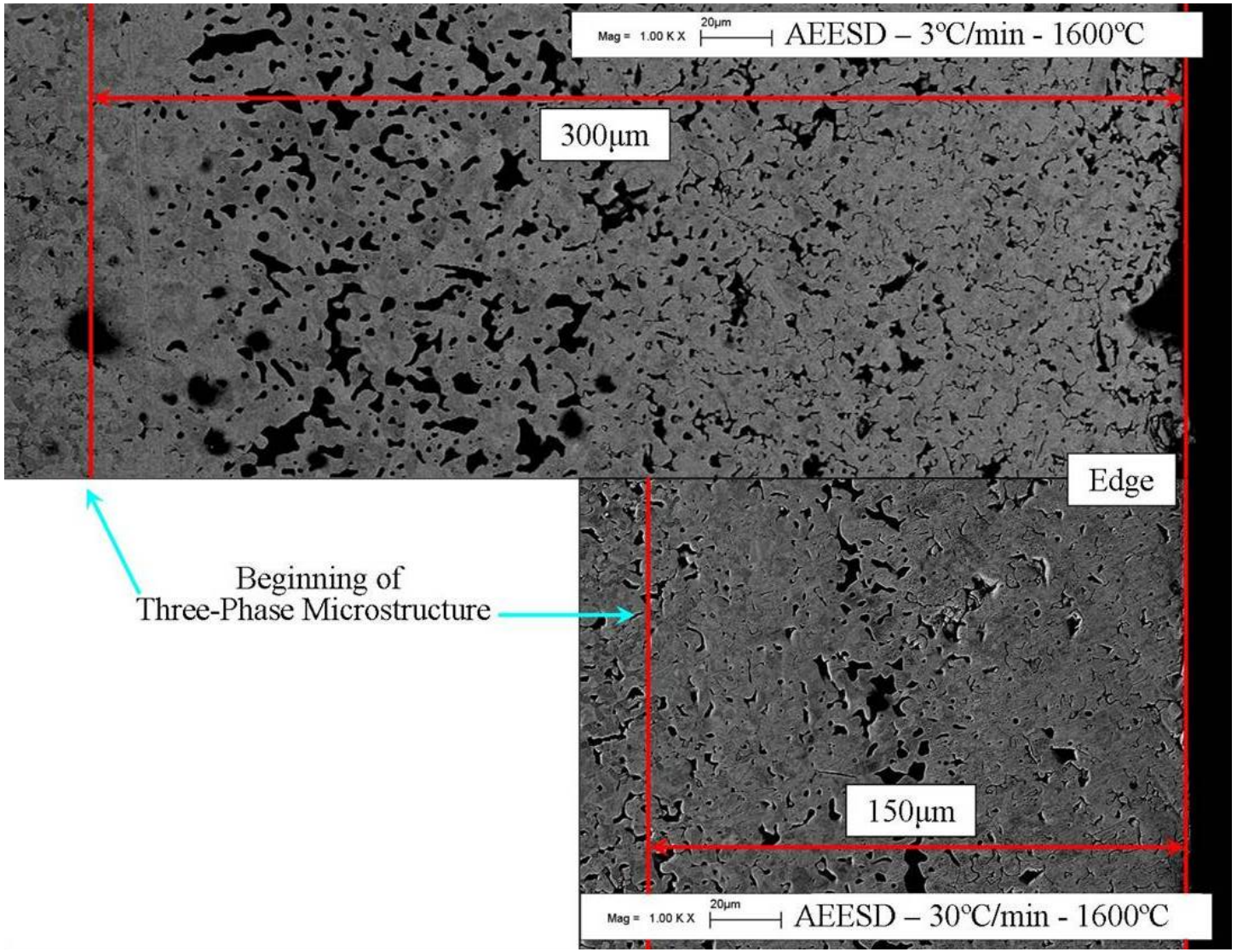


Figure 4.21: Effect of heating rate on porous skin thickness for AEE-Fine samples.

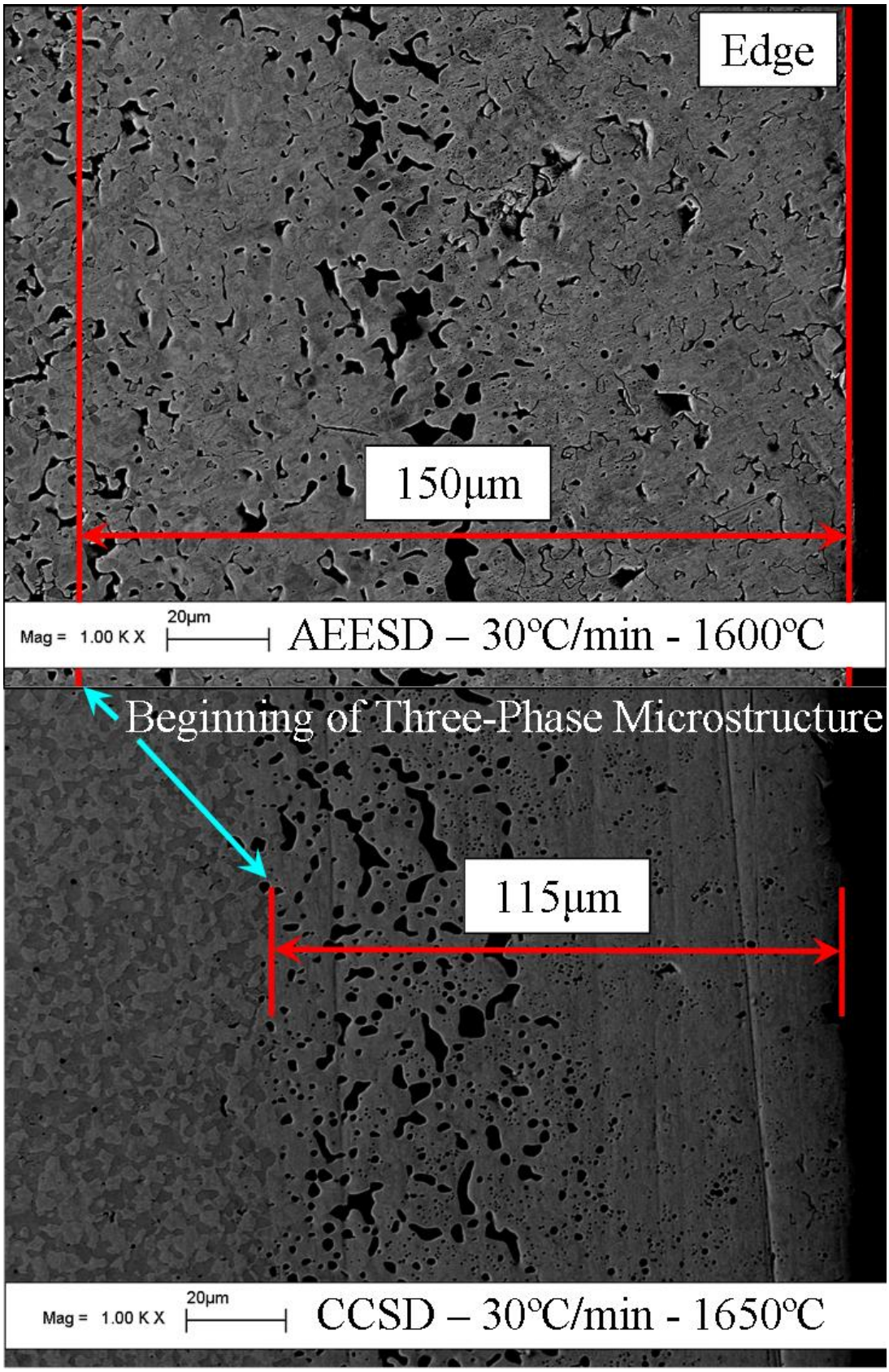


Figure 4.22: Porous skin thickness dependence on the starting materials.

rates were used in an attempt to promote the formation of liquid silicon. Comparison of the microstructures does not provide definitive proof of liquid phase formation. In the case of the Climax-Coarse spray dried samples, increasing the heating rate from 3 to 30ºC/min caused little change in the microstructure. Comparing the Climax-Fine spray dried samples, increasing the heating rate brought a large increase in density and resulted in a much more dispersed microstructure. Further investigation will need to be done to determine if formation of transient liquid silicon is occurring and if so, under what conditions. Future studies could incorporate techniques such as differential thermal analysis which would detect phase changes in the material upon heating.

# CHAPTER VI

## CONCLUSIONS AND RECOMMENDATIONS

Mo-Si-B intermetallic alloys may have the properties required for the next generation of jet turbine engine blades. In order to possess a combination of both oxidation resistance and fracture toughness, the intermetallic phases must be present as fine dispersoids in a continuous molybdenum matrix. Previous research has focused on melt processing methods and HIPing of pre-alloyed powders, which lead to coarse, discontinuous microstructures.

In this project, a $Mo_{ss}$-A15-T2 alloy was produced by the reactive sintering of Mo, $Si_3N_4$ and BN powders. X-ray diffraction analysis was used to examine the formation of the intermetallic phases. A15 and T2 were found to form at 1200ºC and 1300ºC respectively, when fired in a 10:1 mixture of $N_2/H_2$. These phases were determined to form by direct reaction of molybdenum and the nitrides, discounting an initial theory that a transient liquid silicon phase would be created and aid sintering. Attempts were made to promote the formation of liquid silicon by increasing the heating rates from three to 30ºC/min. For some powder mixtures the higher heating rate had little effect, while a drastic jump in density was observed for others. It is unclear whether this is due to the presence of liquid silicon.

The microstructure of the alloy produced by this process has a fine dispersion of the A15 and T2 intermetallics in a semi-continuous molybdenum matrix. With grain

sizes between 1-4μm, this microstructure is more refined than those achieved by other researchers. It was also found that by varying the size of the starting powders and the processing methods used, the final microstructure of the material could be engineered, changing the level of intermetallic dispersion and the continuity of the Mo-matrix. Using a combination of high energy milling and spray drying, powder mixtures were prepared that led to more dispersed microstructures.

After a number of processing improvements, samples with densities of 95% of theoretical were produced. A porous skin layer found on the surface on the pellets was determined to account for most of the remaining porosity in the samples, meaning the density at the center of the sample is likely even higher than measured for the bulk (~99%). Using post-sintering hot-isostatic pressing, it should be possible to eliminate any remaining porosity to achieve fully dense parts.

For further understanding of the discoveries made in this project, the following recommendations are made for future research:

1. Quantitative phase analysis should be used to verify the volume fractions of the phases formed in this reaction. Weight fractions of each phase can be determined by Reitveld analysis of the diffraction patterns using computer programs such as GSAS (General Structure Analysis System). Alternatively, the phase content could be measured by analysis of the SEM images.
2. By changing the firing atmosphere to a 10:1 mixture of $He/H_2$, at 1100ºC it was found that T2 formed prior to A15. A study of the reactions conducted in various nitrogen partial pressures could lead to a better understanding of the formation of the intermetallics.

3. The effect of higher heating rates was shown to increase the density of the samples. It is not understood what mechanism causes this increase. Thermal analysis using equipment such as a differential scanning calorimeter could be used to pinpoint reaction temperatures and determine if high heating rates promote the formation of a liquid phase.

4. A high porosity surface layer was found to form on the surface of the samples. This skin is devoid of the intermetallic phases and likely has poor oxidation resistance. A study should be conducted to understand the conditions that lead to the skin formation so that it can be minimized.

# REFERENCES


[1] J.H. Perepezko, D.M. Dimiduk, "Mo-Si-B Alloys: Developing a Revolutionary Turbine-Engine Material", MRS Bulletin, (2003).

[2] P. Jéhanno, M. Heilmaier, H. Kestler, M. Böning, A. Venskutonis, B. Bewlay, and M. Jackson, "Assessment of a Powder Metallurgical Processing Route for Refractory Metal Silicide Alloys", Metallurgical and Materials Transactions, **35A** (2005) 515-523.

[3] M.K. Meyer, A.J. Thom, and M. Akinc, "Oxide Scale Formation and Isothermal Oxidation Behavior of Mo-Si-B Intermetallics at 600-1000ºC", Intermetallics, **7** (1999) 153-162.

[4] J.J. Petrovic, A.K. Vasudevan, "Key Developments in High Temperature Structural Silicides", Materials Science and Engineering A, **261** (1999) 1-5.

[5] M. Akinc, M.K. Meyer, M.J. Kramer, A.J. Thom, J.J. Huebsch, and B. Cook, "Boron-Doped Molybdenum Silicides for Structural Applications", Materials Science and Engineering A, **261** (1999) 16-23.

[6] C.A. Nunes, R. Sakidja, Z. Dong, and J.H. Perepezko, "Liquidus Projection for the Mo-Rich Portion of the Mo-Si-B Ternary System", Intermetallics, **8** (2000) 327-337.

[7] H. Choe, D. Chen, J.H. Schneibel, and R.O. Ritchie, "Ambient to High Temperature Fracture Toughness and Fatigue-Crack Propagation Behavior in Mo-12Si-8.5B (at%) Intermetallic", Intermetallics, **9** (2001) 319-329.

[8] H.L. Zhao, M.J. Kramer, and M. Akinc, "Thermal Expansion Behavior of Intermetallic Compounds in the Mo-Si-B System", Intermetallics, **12** (2004) 493-498.

[9] P. Jéhanno, M. Heilmaier, and H. Kestler, "Characterization of an Industrially Processed Mo-Based Silicide Alloy", Intermetallics, **12** (2004) 1005-1009.

[10] C.J. Rawn, J.H. Schneibel, C.M. Hoffman, and C.R. Hubbard, "The Crystal Structure and Thermal Expansion of $Mo_5SiB_2$", Intermetallics, **9** (2001) 209-216.

[11] D.M. Berzcik: U.S. Patent No. 5,595,616 (1997).

[12] D.M. Berzcik: U.S. Patent No. 5,693,156 (1997).

[13] H. Choe, J.H. Schneibel, and R.O. Ritchie, "On the Fracture and Fatigue Properties of Mo-$Mo_3Si$-$Mo_5SiB_2$ Refractory Intermetallic Alloys at Ambient to Elevated Temperatures (25ºC to 1300ºC)", Metallurgical and Materials Transactions A, **34A** (2003) 225-239.

[14] J.H. Schneibel, M.J. Kramer, Ö. Ünal, and R.N. Wright, "Processing and Mechanical Properties of a Molybdenum Silicide with the Composition Mo-12Si-8.5B (at%)", Intermetallics, **9** (2001) 25-31.

[15] J.H. Schneibel, M.J. Kramer, and D.S. Easton, "A Mo-Si-B Intermetallic Alloy with a Continuous α-Mo Matrix", Scripta Materialia, **46** (2002) 217-221.

[16] J.J. Kruzic, J.H. Schneibel, and R.O. Ritchie, "Fracture and Fatigue Resistance of Mo-Si-B Alloys for Ultrahigh-Temperature Structural Applications", Scripta Materialia, **50** (2004) 459-464.

[17] R.V. Krishnarao, Y.R. Mahajan, "Studies of the Formation of $MoSi_2$-SiC by Reaction of $Si_3N_4$ with Molybdenum and Carbon", Materials Science and Engineering A, **214** (1996) 161-166.

[18] R.V. Krishnarao, J. Subrahmanyam, "Sintering of $MoSi_2$ by Reacting (Mo+$Si_3N_4$) Compacts", Materials Science and Engineering A, **352** (2003) 340-343.

[19] JANAF Thermochemical Tables, 2nd ed, P.R. Stull, H. Prophet, eds., Journal of Physical and Chemical Reference Data, Washington, DC, 1971.

[20] Thermodynamic properties of 65 Elements – their Oxides, Halides, Carbides, and Nitrides, C.E. Wickes, and F.E. Block, Bureau of Mines Bulletin 605, US Government Printing Office, Washington, DC, 1963.

[21] B.L. Turner-Adomatis, N.N. Thadhani, "Shock-Enhanced Alpha to Beta Phase Transformation in $Si_3N_4$ Powders", Materials Science and Engineering, **A256** (1998) 289-300.